

**EVALUATION OF WWLLN PERFORMANCE
RELATIVE TO THE LIGHTNING IMAGING SENSOR
OF THE INTERNATIONAL SPACE STATION**

MEHDI HASAN RAFI

M.Sc. ENGINEERING THESIS



**DEPARTMENT OF ELECTRICAL, ELECTRONIC AND
COMMUNICATION ENGINEERING
MILITARY INSTITUTE OF SCIENCE AND TECHNOLOGY
DHAKA, BANGLADESH**

MARCH 2023

EVALUATION OF WLLN PERFORMANCE RELATIVE TO THE LIGHTNING IMAGING SENSOR OF THE INTERNATIONAL SPACE STATION

MEHDI HASAN RAFI (SN. 0420160014)

A Thesis Submitted in Partial Fulfillment of the Requirement for the Degree of Master of
Science in Electrical, Electronic and Communication Engineering



DEPARTMENT OF ELECTRICAL, ELECTRONIC AND
COMMUNICATION ENGINEERING
MILITARY INSTITUTE OF SCIENCE AND TECHNOLOGY
DHAKA, BANGLADESH

MARCH 2023

EVALUATION OF WWLLN PERFORMANCE RELATIVE TO THE LIGHTNING IMAGING SENSOR OF THE INTERNATIONAL SPACE STATION

M.Sc. Engineering Thesis

By

MEHDI HASAN RAFI (SN. 0420160014)

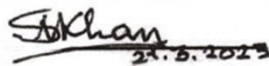
Approved as to style and content by the Board of Examination on 21 March 2023:

Dr. Md Golam Mostafa
Professor
Department of EECE, MIST



Chairman
(Supervisor)

Dr. Robert H. Holzworth
Professor Emeritus
Department of Earth and Space Sciences and Director,
WWLLN, University of Washington, USA



Member
(External)

Dr. Shahidul Islam Khan
Professor
Department of EEE, Brac University

Member
(External)

Lt Col Hussain Md. Abu Nyeem, PhD
Instructor class A
Department of EECE, MIST

Member
(Internal)

Brig Gen Md Mahfuzul Karim Majumder
Dean
Faculty of ECE, MIST

Member
(Ex-Officio)

Department of Electrical, Electronic and Communication Engineering, MIST, Dhaka

EVALUATION OF WLLN PERFORMANCE RELATIVE TO THE LIGHTNING IMAGING SENSOR OF THE INTERNATIONAL SPACE STATION

DECLARATION

I hereby declare that the study reported in this thesis entitled as above is my original work and has not been submitted before anywhere for any other purpose. Further I certify that the intellectual content of this thesis is the product of my own work and all the assistance received in preparing this thesis and sources have been acknowledged and cited in the reference section.

Mehdi Hasan Rafi
Student No. 0420160014

EVALUATION OF WWLLN PERFORMANCE RELATIVE TO THE LIGHTNING IMAGING SENSOR OF THE INTERNATIONAL SPACE STATION

A Thesis

By

Mehdi Hasan Rafi (SN. 0420160014)

DEDICATION

Dedicated to my parents for supporting and
encouraging me to believe in myself.

ABSTRACT

Evaluation of WWLLN Performance Relative to the Lightning Imaging Sensor of the International Space Station

Lightning is a fundamental atmospheric phenomenon that significantly affects the Earth's climatology. This study uncovers intriguing features and demonstrates strong connections with other lightning detection networks and instruments. This study examines the detection efficiency (DE) of World Wide Lightning Location Network (WWLLN) by comparing WWLLN data to Earth Network Total Lightning Network (ENTLN) data within 50km and 100 μ s at 20° S to 70° N latitude and 40° E to 141° E longitude. Additionally, the variation of DE due to ENTLN peak current has also investigated in this study. This study also presents density maps of lightning distribution using 1° by 1° grid boxes and shows a relation with International Space Station (ISS) Lightning Imaging Sensor (LIS). Diurnal differences in WWLLN strokes are analyzed across six global continental regions, and lightning activities over Bangladesh's landmass are assessed. The study employs time series analysis and the Auto Regressive Integrated Moving Average (ARIMA) modelling technique to develop a lightning prediction model for WWLLN stroke energy and ISS-LIS flash radiance data, with standard diagnostic tests evaluating the chosen model's goodness of fit. DE calculations revealed an average DE of 6.54% (June-July) and 16.61% (November-December) with 893,773 and 1,393,031 matching WWLLN and ENTLN CGs, respectively. DE is lowest for peak currents under ± 20 kA, increasing from 40% to 70% above ± 50 kA. The maximum DE is 42% for -80 kA and 71% for 100 kA. The mean positive and negative peak currents for matched ENTLN-WWLLN CG strokes are 48.7 kA and -44.2 kA, respectively. This analysis reveals that about 60% of the total lightning of the globe occurs in the landmass and the rest 40% in the oceans. In summer, lightning maxima align with 30°N, while in winter, they shift towards lower latitudes. The diurnal amplitude variation for land strokes peaks around 20:00 LT in North and South America, 16:00 LT in Europe, Africa, and Australia, and 14:00 LT in Asia. This study further highlights that the lightning stroke density (Strokes per km² year⁻¹) over Bangladesh is significantly high and the months of April, May, and June experiencing the highest lightning activity in the country. Following the necessary diagnostic tests, ARIMA (3, 1, 1) \times (2, 1, 0)₁₂ is selected as the best-fitted model for forecasting WWLLN stroke energy, while ARIMA (2, 1, 2) \times (0, 1, 1)₁₂ is chosen for forecasting ISS-LIS lightning flash radiance.

সারসংক্ষেপ

Evaluation of WWLLN Performance Relative to the Lightning Imaging Sensor of the International Space Station

বজ্রপাত একটি মৌলিক বায়ুমণ্ডলীয় ঘটনা যা পৃথিবীর জলবায়ুবিদ্যাকে উল্লেখযোগ্যভাবে প্রভাবিত করে। এই গবেষণাটি আকর্ষণীয় বৈশিষ্ট্যগুলিকে উন্মোচন করে এবং অন্যান্য বাজ্র সনাক্তকরণ নেটওয়ার্ক এবং যন্ত্রগুলির সাথে শক্তিশালী সংযোগ প্রদর্শন করে। এই গবেষণাটি 20° S থেকে 70° N অক্ষাংশ এবং 40° E থেকে 141° E দ্রাঘিমাংশে 50 কিলোমিটার এবং 100 মাইক্রোসেকেন্ডের মধ্যে ENTLN ডেটার সাথে WWLLN ডেটা তুলনা করে WWLLN এর সনাক্তকরণ দক্ষতা (DE) পরীক্ষা করে। অতিরিক্তভাবে, ENTLN কারেন্টের কারণে DE এর পরিবর্তনও এই গবেষণায় তদন্ত করেছে। এই গবেষণাটি 1° বাই 1° গ্রিড বক্স ব্যবহার করে বজ্র বিতরণের ঘনত্বের মানচিত্রও উপস্থাপন করে এবং আন্তর্জাতিক স্পেস স্টেশন (ISS) লাইটনিং ইমেজিং সেন্সর (LIS) এর সাথে একটি সম্পর্ক দেখায়। WWLLN স্ট্রোকের দৈনিক পার্থক্যগুলি ছয়টি বিশ্ব মহাদেশীয় অঞ্চল জুড়ে বিশ্লেষণ করা হয়, এবং বাংলাদেশের স্থলভাগের উপর বজ্রপাতের ক্রিয়াকলাপগুলি মূল্যায়ন করা হয়। এই গবেষণায় টাইম সিরিজ বিশ্লেষণ এবং ARIMA মডেলিং কৌশল ব্যবহার করে WWLLN স্ট্রোক এনার্জি এবং ISS-LIS ফ্ল্যাশ রেডিয়েন্স ডেটার জন্য একটি বাজ্র ভবিষ্যদ্বাণী মডেল প্রয়োগ করার জন্য, ডায়াগনস্টিক পরীক্ষাগুলির সাথে নির্বাচিত মডেলের উপযুক্ততা মূল্যায়ন করে। DE গণনা থেকে জানা যায় যে WWLLN-এর গড় DE জুন-জুলাই মাসে 6.54% এবং নভেম্বর-ডিসেম্বর মাসে 16.61%। ±20 kA-এর নিচে কারেন্টের জন্য DE সর্বনিম্ন এবং ±50 kA-এর উপরে 40% থেকে 70% পর্যন্ত বৃদ্ধি পায়। -80 kA এর জন্য সর্বাধিক DE 42% এবং 100 kA এর জন্য 71%। এই বিশ্লেষণটি প্রকাশ করে যে পৃথিবীর মোট বজ্রপাতের প্রায় 60% স্থলভাগে এবং বাকি 40% মহাসাগরে ঘটে। গ্রীষ্মকালে, বজ্রপাত 30°N অক্ষাংশের সাথে সারিবদ্ধ হয়, যখন শীতকালে, তারা নিম্ন অক্ষাংশের দিকে সরে যায়। স্থলভাগে বজ্রপাত এর দৈনিক পরিবর্তন উত্তর ও দক্ষিণ আমেরিকায় প্রায় 20:00 LT, ইউরোপ, আফ্রিকা এবং অস্ট্রেলিয়ায় 16:00 LT এবং এশিয়ায় 14:00 LT। এই সমীক্ষাটি আরও দেখায় যে বাংলাদেশে বজ্রপাতের ঘনত্ব (প্রতি বর্গ কিলোমিটার প্রতি বছর) উল্লেখযোগ্যভাবে বেশি এবং এপ্রিল, মে এবং জুন মাসে দেশের সর্বোচ্চ বজ্রপাতের কার্যকলাপের সম্মুখীন হয়। প্রয়োজনীয় পরীক্ষাগুলি অনুসরণ করে, ARIMA (3, 1, 1) × (2, 1, 0)₁₂ কে WWLLN বজ্রপাত শক্তির পূর্বাভাস এবং ARIMA (2, 1, 2) × (0, 1, 1)₁₂ কে ISS-LIS বজ্রপাত ফ্ল্যাশ দীপ্তি পূর্বাভাসের দেওয়ার জন্য সবচেয়ে উপযুক্ত মডেল হিসাবে নির্বাচিত করা হয়েছে।

ACKNOWLEDGMENTS

At the outset, I would like to express my sincere gratitude to my supervisor, Professor Dr. Md. Golam Mostafa, Faculty of Electrical and Computer Engineering, for the valuable comments, remarks, and engagement throughout the learning process of this thesis. I thank him from the core of my heart for his unwavering support and invaluable guidance since I started working with him. It had been a great privilege and honor to work and study under his direct supervision. The door to his office was always open whenever I had questions about my thesis and writing. He has taught the methodology to carry out the thesis and present the work as clearly and precisely as possible. Furthermore, his innovative ideas and prudent guidance have opened new arenas for this thesis. I also feel heartfelt gratitude for his overall technical and logistic support, including administering the official requirements of this research work. Despite his busy schedule and responsibilities, he never felt disturbed or denied giving me time. Besides, this thesis would not have been completed without the guidance and help of a few other people. I would like to extend my heartfelt thanks to Dr. Robert H. Holzworth, Professor Emeritus, Department of Earth and Space Sciences, and Director, WWLLN, University of Washington, USA, for taking the time to delve deeply into my research and provide valuable insights and observations. His expertise and feedback have been tremendously helpful in shaping my research and guiding me towards new avenues of exploration. I am grateful for his generosity and willingness to support my academic pursuits. I must express my profound gratitude Brigadier General A K M Nazrul Islam, PhD, Head, Department of EECE, MIST, Air Commodore Mohammed Hossam-E-Haider, PhD, (Retd), and Major Md Aminul Islam, PhD, EME. I also offer my sincere appreciation for the learning opportunities provided by MIST and acknowledge the support provided by all the MIST office staff. Last but not least, I owe a huge debt of gratitude to my parents and service. Their love and confidence in me have encouraged me to advance in my studies and career. Most importantly, thanks to the Almighty for keeping me physically and mentally well throughout my career.

TABLE OF CONTENTS

Abstract	i
Acknowledgments	iii
LIST OF TABLE	vii
LIST OF FIGURE	viii
LIST OF MAIN NOTATION	xi
LIST OF ABBREVIATIONS	xii
TABLE OF CONTENTS	iv
CHAPTER 1: INTRODUCTION	
1.1 Research Background	01
1.2 Research Motivation	02
1.3 Research Problem	03
1.4 Research Objectives	03
1.5 Thesis Outline	04
CHAPTER 2: LIGHTNING AND ITS DETECTION SYSTEMS	
2.1 The Physical Mechanism of Lightning	05
2.2 Types of Lightning	06
2.2.1 Cloud-to-Ground (CG) Lightning	06
2.2.2 Cloud-to-Cloud (CC) Lightning	07
2.2.3 Cloud-to-Air (CA) Lightning	07
2.2.4 Ground-to-Cloud (GC) Lightning	07
2.2.5 Intra-Cloud (IC) Lightning	07
2.2.6 Transient Luminous Event	08
2.3 Lightning Detection Systems	09
2.4 Global Ground Base Lightning Detection	10
2.4.1 Vaisala Global Lightning Detection Network (GLD360)	10
2.4.1.1 GLD360 instrument description	11
2.4.1.2 Data collection and processing	11
2.4.2 Earth Network Total Lightning Network	11
2.4.2.1 ENTLN data processing	12
2.4.3 World Wide Lightning Location Network	12
2.4.3.1 WLLN network setup	13

2.4.3.2	WWLLN data structure	14
2.5	Satellite based Lightning Detection	16
2.6	Lightning Detection Instruments	17
2.6.1	Lightning Imaging Sensor	17
2.6.2	Optical Transient Detector	18
2.6.3	Global Lightning Mapper	18
2.6.4	Lightning Mapping Arrays	19
2.6.5	OTD/LIS Data Clustering	19
2.7	Differences between Ground-Based and Space-Based Lightning Detection Systems	21
2.8	Literature Review	22
2.8.1	Global Lightning Climatology	22
2.8.2	Analysis of Lightning Phenomena over Bangladesh	27
2.8.3	Detection Efficiency	31
2.8.3.1	WWLLN detection efficiency dependable factor	31
2.8.3.2	Analysis of WWLLN DE compared to other the instruments and networks	73
2.8.3.3	Relative Detection Efficiency	37
2.8.4	WWLLN Lightning Strokes Energy	38
2.8.5	Lightning Prediction	41
2.9	Summary	44
CHAPTER 3: LIGHTNING DETECTION ANALYSIS		
3.1	Introduction	45
3.2	Method of Calculating Detection Efficiency	45
3.3	Contrasting the WWLLN and ENTLN	47
3.4	Time and Location Accuracy	49
3.5	Variation in Detection Efficiency Due to Peak Current	52
3.6	Analysis of Detection Efficiency Using WWLLN APfiles	53
3.7	Summary	54
CHAPTER 4: LIGHTNING CLIMATOLOGY		
4.1	Introduction	55
4.2	Method of Analyzing Global Lightning Climatology	55
4.3	ISS-LIS vs. WWLLN Annual Lightning Climatology	56

4.3.1	Regional Distribution of Lightning	57
4.4	Seasonal Dependence of Lightning Phenomena	59
4.4.1	Lightning Flashes	59
4.4.2	Lightning Strokes	60
4.5	Daily Lightning Cycle	60
4.6	Lightning over Bangladesh	62
4.7	Summary	66
CHAPTER 5: PROPOSED LIGHTNING PREDICTION MODEL		
5.1	Introduction	67
5.2	Method of Performing Time Series Analysis	67
5.3	Time Series Analysis of WWLLN Strokes Energy	69
5.3.1	Analysis of WWLLN Strokes Energy Using Time Series Model	72
5.3.2	Diagnostic Check of the Fitted ARIMA Model for WWLLN Strokes Energy	74
5.3.3	Forecasting the ARIMA Model of WWLLN Strokes Energy	76
5.4	Time Series Analysis of ISS-LIS Lightning Flashes Radiance	77
5.4.1	Analysis of ISS-LIS Lightning Flashes Radiance Using Time Series Model	77
5.4.2	Diagnostic Check of the Fitted ARIMA Model for ISS-LIS Flashes Radiance	80
5.4.3	Forecasting the ARIMA Model of ISS-LIS Lightning Flashes Radiance	81
5.5	Summary	82
CHAPTER 6: CONCLUSION AND FUTURE RECOMMENDATIONS		
6.1	Conclusion	83
6.2	Significant of the Research	83
6.3	Contribution of the Thesis	84
6.4	Future Scope	84
6.5	Summary	85
LIST OF PUBLICATION		86
References		87

LIST OF TABLE

Table 2.1:	WWLLN Data Types	15
Table 2.2:	Comparison of Ground-Based and Space-Based Lightning Detection Systems	21
Table 3.1:	Total number of lightning strokes reported by ENTLN and WWLLN	49
Table 3.2	Total number of lightning strokes reported by WWLLN APfiles	53
Table 4.1:	Global distribution of lightning occurrence in 2020	58
Table 5.1:	AIC Values of Different Models for WWLLN Strokes Energy	74
Table 5.2:	Estimated parameters of the fitted models for WWLLN strokes energy	74
Table 5.3:	AIC Values of Different Models for ISS-LIS flash Radiance	79
Table 5.4:	Estimated Parameters of the Fitted Models for ISS-LIS flash Radiance	79

LIST OF FIGURES

Figure 2.1:	A conceptual model depicts the dispersion of electrical charges within deep convection	06
Figure 2.2:	Different types of lightning	08
Figure 2.3:	Different types of transient luminous events	08
Figure 2.4:	WWLLN VLF receiving station	14
Figure 2.5:	Basic workflow showing the data processing of initial observations at the ISS-LIS	17
Figure 2.6:	Data clustering method of LIS/OTD	20
Figure 2.7:	Annual-mean frequency of occurrence of lightning from (a) LIS/OTD (flashes $\text{km}^{-2} \text{yr}^{-1}$) (b) WWLLN (strokes $\text{km}^{-2} \text{yr}^{-1}$) and (c) Ratio of LIS/OTD flashes to WWLLN strokes	23
Figure 2.8:	Annual cycle of global flash rate, computed from High Resolution Monthly Climatology (HRMC) and from Low Resolution Annual Climatology (LRAC)	24
Figure 2.9:	(a) High-Resolution Flash Climatology (HRFC) mean annual flash rate from combined LIS and OTD on a 0.5° grid. (b) Low-Resolution Flash Climatology (LRFC) mean annual flash rate from combined LIS and OTD on a 2.5° grid	25
Figure 2.10:	The local time peak in lightning flash density estimated by the data from regions (a) N. America, (b) Europe, (c) Asia, (d) S. America, (e) Africa, and (f) Asutralasia	27
Figure 2.11:	Seasonal variation in flash rate density over Bangladesh: a pre-monsoon, b monsoon, c post-monsoon and d winter	28
Figure 2.12:	Daily lightning cycle associated with lightning flash counts over Bangladesh, 1998–2014	29
Figure 2.13:	Seasonal CG stroke density over Bangladesh; a pre-monsoon; b monsoon; c post-monsoon and d winter. District boundaries are superimposed on gridded CG stroke density [82].	30
Figure 2.14:	Variation in the WWLLN CG stroke DE with NZLDN-determined return stroke peak current	33
Figure 2.15:	The relationship between the distribution of NZLDN CG return stroke peak currents and the number of participating WWLLN stations	34

Figure 2.16:	Globally variable WWLLN CG DE estimation based on modelling and comparison to the NZLDN commercial network. Modelling of the ionospheric conditions at 12:00 UT on 16 April 2005	35
Figure 2.17:	Globally varying estimated WWLLN CG DE, for comparison with Fig. 3.3. Modelling undertaken with the ionospheric conditions expected for 00:00 UT on 16 April 2005	35
Figure 2.18:	Ratio of the number of events detected by the Darwin station to the number of events detected at the same range from Darwin network as a whole	36
Figure 2.19:	Daily average relative DE for 15 June 2010. Stations are shown as triangles with operational stations in white, nonoperational in black, and operational for part of the day in grey. The minimum value of DE is set at 5% to prevent unphysical corrections	38
Figure 2.20:	(a) Shows how the WWLLN stroke energy is distributed around the world (in black), the Americas (in blue), Asia (in green), and Africa/Europe (in red). (b) WWLLN worldwide stroke energy distribution for the day (15 June 2010), the hour (9 UTC on 15 June 2010), the year (2010), and the month (June 2010).	39
Figure 2.21:	Distribution of stroke energies for WWLLN data set including the 9 years 2010 to 2018 (blue). The brown colored distribution above 106 J presents the distribution that is call super-bolts [17].	41
Figure 2.22:	Seasonal and yearly meridional mean lightning flash densities for (a) winter, (b) spring, (c) summer, (d) autumn, and (e) the whole year from the LIS/OTD 1995-2010 climatology and the year-long 80-km global simulations from 1999 to 2008. Flashes $\text{km}^{-1} \text{year}^{-1}$ are used to indicate flash densities	43
Figure 3.1:	Locations and hosts of the 111 VLF receiving stations operating in the VLF WWLLN stations as of June–July 2021. The green triangles indicate the stations were functional, while the yellow triangles indicate the stations were weak, and the red triangles indicate the stations were not functional during the period of investigation.	47
Figure 3.2:	Locations and hosts of the 113 VLF receiving stations operating in the VLF WWLLN stations as of June–July 2021. The green triangles	48

indicate the stations were functional, while the yellow triangles indicate the stations were weak, and the red triangles indicate the stations were not functional during the period of investigation. The stations that were newly hosted were shown in blue triangles.

Figure 3.3:	Time difference (ENTLN-WWLLN) between the 893773 matching CG strokes detected by the ENTLN and WWLLN during June-July 2021. The mean (median) time difference is 27.27 μ s (21 μ s).	50
Figure 3.4:	Time difference (ENTLN-WWLLN) between the 1393031 matching CG strokes detected by the ENTLN and WWLLN during November-December 2021. The mean (median) time difference is 35.4 μ s (33 μ s)	50
Figure 3.5:	Location accuracy (ENTLN-WWLLN) between the 8937731 matching CG strokes detected by the ENTLN and WWLLN during June-July 2021. The mean (median) distance is 9.62 km (7.57 km). Red line are the mean accuracy and grey lines are statistical count errors.	51
Figure 3.6:	Location accuracy (ENTLN-WWLLN) between the 1393031 matching CG strokes detected by the ENTLN and WWLLN during November-December 2021. The mean (median) distance is 11.33 km (8.13 km). Red line are the mean accuracy and grey lines are statistical count errors.	51
Figure 3.7:	Variation in the WWLLN CG stroke DE with ENTLN determined return pick current	53
Figure 4.1:	Flow diagram for performing lightning climatology	56
Figure 4.2:	A global map showing the frequency of occurrence of lightning. The spatial distribution of flashes identified by ISS-LIS	56
Figure 4.3:	A global map showing the frequency of occurrence of lightning. The spatial distribution of strokes detected by WWLLN	57
Figure 4.4:	The eleven broad regions used in this study. The thickness of the coastlines shows the size of the coastal region used in the land and ocean study	57
Figure 4.5:	Global distribution of ISS-LIS lightning flash during winter (1st Dec to 29th Feb 2020)	59
Figure 4.6:	Global distribution of ISS-LIS lightning flash during summer (4th May to 3rd August 2020)	59
Figure 4.7:	WWLLN seasonal lightning strokes during winter	60

	(1st Dec to 29th Feb)	
Figure 4.8:	WWLLN seasonal lightning strokes during summer (4th May to 3rd August)	60
Figure 4.9:	Daily lightning cycle depicting the WWLLN lightning stroke count in every 24 hours (Local Time). Data from regions (a) Asia, (b) Europe, (c) Africa, (d) Australia, (e) North America, and (f) South America. Poisson statistics define error bars on the order of the width of the line (gray line).	61
Figure 4.10:	The study area of Bangladesh's landmass (20°34' to 26°38' north latitude and 88°01' to 92°41' east longitude)	63
Figure 4.11:	Spatial variation of lightning strokes density over Bangladesh's landmass detected by WWLLN during 2020	64
Figure 4.12:	Monthly distribution of WWLLN lightning strokes over Bangladesh's landmass during January 2020 to December 2020	65
Figure 4.13:	Diurnal variation of lightning strokes over Bangladesh's landmass detected by WWLLN during 2020.	65
Figure 5.1:	Locations and hosts of the 111 VLF receiving stations operating in the VLF WWLLN stations as of 2020. The green triangles indicate the stations were functional, while the yellow triangles indicate the stations were weak, and the red triangles indicate the stations were not functional during the period of investigation.	68
Figure 5.2:	Flow diagram for performing time series analysis.	69
Figure 5.3:	The time plots of fluctuation in WWLLN strokes energy during the year 2020 at 40° to 141° east longitude and 5° to 50° north latitude (10000×5000 km ² region of Asia). The grey lines are statistical count errors	70
Figure 5.4:	Seasonal first difference plot	71
Figure 5.5:	Auto Correlation Function (ACF) and the Partial Auto Correlation Function (PACF) of the differenced series	73
Figure 5.6:	Standardized residuals, histogram plus density, theoretical quantiles and ACF of the residuals of strokes energy data	75

Figure 5.7:	Model of prediction for some given time span with observed data from January 2020 to December 2020, estimated by the suggested ARIMA model	76
Figure 5.8:	Measured and fitted model of prediction from January 2021 to June 2021, estimated by the suggested ARIMA model	76
Figure 5.9:	The time plots of fluctuation in lightning flashes radiance during the year 2020 around the globe. The grey lines are statistical count errors	77
Figure 5.10:	Auto Correlation Function (ACF) and the Partial Auto Correlation Function (PACF) of the differenced series	78
Figure 5.11:	Standardized residuals, histogram plus density, theoretical quantiles and ACF of the residuals of lightning flashes radiance data	80
Figure 5.12:	Model of prediction for some given time span with observed data from January 2020 to December 2020, estimated by the suggested ARIMA model	81
Figure 5.13:	Measured and fitted model of prediction from January 2021 to June 2021, estimated by the suggested ARIMA model.	82

LIST OF MAIN NOTATION

X_t	Two-valued random process
γ_t	Auto-covariance
σ^2	Variance
μ_t	The first moment independent of time T
Z_t	Uncorrelated white noise
φ_p	The p^{th} degree of autoregressive (AR)
ϑ_q	The q^{th} degree moving average (MA)
B	Back-shift operator
ρ_k	The k^{th} autocorrelation distinct roots

LIST OF ABBREVIATIONS

ACF	Auto Correlation Function
ADF	Augmented Dickey-Fuller
AIC	Akaike's Information Criterion
AR	Auto Regressive
ARIMA	Auto Regressive Integrated Moving Average
BLNET	Beijing Lightning Network
CA	Cloud-to-Air
CC	Cloud-to-Cloud
CG	Cloud-to-ground
CLDN	Canadian Lightning Detection Network
DE	Detection Efficiency
ECMWF	European Centre for Medium-Range Weather Forecasts
EUCLID	European Cooperation for Lightning Detection
ENTLN	Earth Network Total Lightning Network
FORTE	Fast On-orbit Rapid Recording of Transient Events
FOV	Field-of-View
GC	Ground-to-Cloud
GHRC	Global Hydrology Resource Center
GLM	Global Lightning Mapper
GOES	Geostationary Operational Environmental Satellite
GPS	Global Positioning System
HRMC	High Resolution Monthly Climatology
HEO	High Earth Orbit
IC	Intra-cloud
IFS	Integrated Forecasting System
IRIMO	Iranian Meteorological Organization
ISS	International Space Station
JAXA	Japanese Space Agency
LEO	Low-Earth Orbit
LIS	Lightning Imaging Sensor
LMI	Lightning Mapping Imager

LPI	Lightning Potential Index
LRAC	Low Resolution Annual Climatology
MA	Moving Average
MI	Microwave Imaging
NZLDN	New Zealand Lightning Detection Network
OTD	Optical Transient Detector
PA	Precipitation Radar
PACF	Partial Auto Correlation Function
QLL	Quasi-Liquid Layer
RMS	Root Mean Square
RTEP	Real-Time Event Processor
TGF	Terrestrial Gamma-Ray Flashes
TLE	Transient Luminous Events
TOA	Time-of-Arrival
TOGA	Time of Group Arrival
TRMM	Tropical Rainfall Measuring Mission
UTC	Universal Time Coordinated
VLF	Very Low Frequency
WTLN	WeatherBug Total Lightning Network
WRF	Weather Research and Forecasting
WWLLN	World Wide Lightning Location Network

CHAPTER 1

INTRODUCTION

1.1 Research Background

Lightning is a natural phenomenon that can cause significant damage and loss of life. In addition to the direct impacts of lightning stroke, such as starting wildfires and damaging infrastructure, lightning can also affect atmospheric chemistry and contribute to the formation of greenhouse gases. As such, understanding the physics of lightning and developing advance methods for predicting and detecting lightning stroke are critical areas of research.

Lightning detection instruments are essential components of lightning research. Ground-based networks are the most common type of detection system and require a dense network of sensors to accurately detect and locate lightning strikes. Satellite-based systems are an alternative approach to lightning detection and have the advantage of being able to cover large areas. However, satellite-based systems are typically less accurate than ground-based systems and can struggle to detect cloud-to-ground lightning, which is the most dangerous and damaging type of lightning. Developing an effective lightning network is challenging, but the benefits of such a system are immense. A reliable lightning network can provide early warnings of severe weather conditions and help mitigate the negative impacts of lightning strikes. By better understanding the physics of lightning and improving lightning detection and prediction systems, researchers can help protect lives, property, and the environment.

Several research on lightning detection and prediction were made in the past by using different lightning detection instruments and networks [1], [2], [2]–[14]. Among these, World Wide Lightning Location Network (WWLLN) detects, locates and time lightning strokes with ~ 10 km spatial accuracy and ~ 10 μ s temporal accuracy [3], [15]–[17]. It also estimates the VLF energy of the strokes that were emitted into the Earth-ionosphere waveguide [5]. The capability of this network has shown continuous improvement due to the addition of new stations and the upgrade of the detection algorithm. Therefore, periodic difference studies are necessary to assess the current WWLLN detection efficiency. In this research, an attempt to made to compare WWLLN data with the other available datasets for the period not yet investigated by other researchers.

The aim of this thesis is to apply a suitable model that can predict lightning events in the absence of real-time lightning data. In addition, the Detection Efficiency (DE) of the WWLLN relative to the Earth Network Total Lightning Network (ENTLN) was examined in a chosen region. Besides, an updated assessment of the global lightning climatology as detected by different ground-based and space-based lightning detection equipment is carried out.

1.2 Research Motivation

The motivation for this research stems from the need to better understand of global lightning variability. Despite the potential benefits of accurate lightning predictions, no attempt has been made to apply time series forecasting to predict lightning patterns that include WWLLN strokes energy and International Space Station Lightning Imaging Sensor (ISS-LIS) flash radiance. Furthermore, due to the lack of studies on lightning patterns in Bangladesh's landmass and oceanic regions, no climatological study has been attempted using the current dataset. The primary motivation behind this research is to advance our knowledge of lightning detection efficiency, distribution, and variability, as well as to develop more accurate prediction models for lightning stroke energy and flash radiance. Some potential questions that could help motivate this research further include:

- (a) How much has the detection efficiency changed in the region of interest over time?
- (b) What proportion of global lightning strokes would have been undetectable without the participation of the WWLLN Dhaka station?
- (c) Which regions in the world have the most lightning strokes?
- (d) What are the annual, diurnal, and seasonal variations of lightning as observed through WWLLN and ISS-LIS data
- (e) Which portion of the global has more lightning?
- (f) How much lightning occurs in Bangladesh's landmass and ocean compared to the other places in the world?
- (g) Which time series analysis techniques can be applied to identify a suitable model for predicting WWLLN stroke energy and ISS-LIS flash radiance,

By addressing these questions, this study aims to contribute to our understanding of global lightning variability and help improve lightning detection and prediction systems.

1.3 Research Problem

The existing knowledge of spatial and temporal patterns of lightning occurrences has undoubtedly offered valuable insights. However, further research is essential to unravel the factors that impact lightning variability and its evolution over time. Although the climatological study of lightning has been conducted using ground-based and space-based lightning data, it has not been updated recently, indicating a need for further investigation to comprehend the current state of lightning climatology.

Numerous variables, including the number of stations and particular weather conditions, can affect detection efficiency. While numerous researchers have analyzed detection efficiency over the past decade, none have updated the current detection efficiency in light of the significant increase in available stations.

In terms of lightning prediction, the existing models are inadequate. Not only is there a lack of effective prediction models, but no efforts have been made to apply time series forecasting to predict lightning patterns, including WWLLN stroke energy and ISS-LIS flash radiance. Consequently, there is a pressing need for additional research to develop and apply a prediction model capable of forecasting lightning events in the absence of real-time data, using appropriate scientific methodologies.

1.4 Research Objective

The objective of this research is as follows:

- (a) To determine the detection efficiency of WWLLN.
- (b) To develop a global lightning climatology and interpret the differences of observations from different instruments and networks.
- (c) To determine the annual, diurnal and seasonal dependency of the WWLLN data.
- (d) To develop time-series models of WWLLN strokes energy and ISS flash radiance.

This research is significant as it aims to improve our understanding of lightning patterns in both of landmass and oceanic regions, and to develop more accurate lightning prediction models.

1.5 Thesis Outline

To present the research in a clear and coherent manner, the thesis is organized as follows:

Chapter 2: Provides an overview of lightning, discussing the physical mechanisms, types, detection systems, and various instruments used to detect lightning, along with their data descriptions. This chapter also focus on literature review for the thesis, examining references from relevant books, journals, papers, and online resources, while identifying research gaps and expanding on the existing knowledge in this field.

Chapter 3: Focuses primarily on calculating the detection efficiency of WWLLN using two methods: The first approach involved comparing WWLLN data to ENTLN data side by side the variation of detection efficiency due to ENTLN peak current. The second approach involved using the WWLLN APfiles to determine the percentage of detection efficiency has increased by hosting Dhaka station.

Chapter 4: Explores the climatological features of different networks and instruments, presenting global maps that depict the lightning distribution across landmasses and oceanic regions. Side by side the lightning activities over Bangladesh's landmass are assessed in this chapter.

Chapter 5: Introduces time series analysis, providing an overview of the measurement systems and techniques, along with the time series analysis using the second derivative stationary method. This chapter also discusses the construction of time series prediction models using different datasets and covers several diagnostic tests for the fitted models.

Chapter 6: Summarizes the overall research and thesis contributions, and offers recommendations for future work in this specific field.

CHAPTER 2

LIGHTNING AND ITS DETECTION SYSTEMS

2.1 Physical Mechanisms of Lightning

The fundamental scientific knowledge of the charging mechanisms during a thunderstorm has been established based on theory and observations [18], but there is still some debate over the molecular and microphysical processes involved in lightning and how they are triggered. For example, it is widely believed that lightning flashes may occur only when there is a high enough ambient electric field inside the thunderstorms, which is created during the charge separation process. The most widely accepted explanation for the charge separation process is the non-inductive process, which is formed by the stages below [19].

- (a) First, charge separation requires hydrometers such as large graupel particles, ice crystals, and super-cooled water droplets. Supersaturated water vapor over ice particles frequently forms a thin film of the liquid water layer [20]. This layer is referred to as a Quasi-Liquid Layer (QLL).
- (b) Second, bigger graupel particles colliding with ice crystals is essential to non-inductive charge separation. After the collision, QLL mass will be evenly divided between graupel and ice crystals. As a result, the graupel will be net negative and the ice crystal net positive. The ambient temperature and amount of super-cooled water droplets can affect charge transfer direction [21].
- (c) Finally, the existence of convective updrafts in thunderstorms plays a significant role in lifting the lighter (positively charged) ice crystals higher, while the negatively charged rimed particles fall downwards owing to gravity.

A conceptual model depicting the dispersion of electrical charges within deep convection (thunderstorms) are shown in Fig.2.1. There are four major charge zones in the primary updraft (inside and above the red arrow). There are more than four charge zones in the convective region but outside the out draft (in and above the blue arrow).

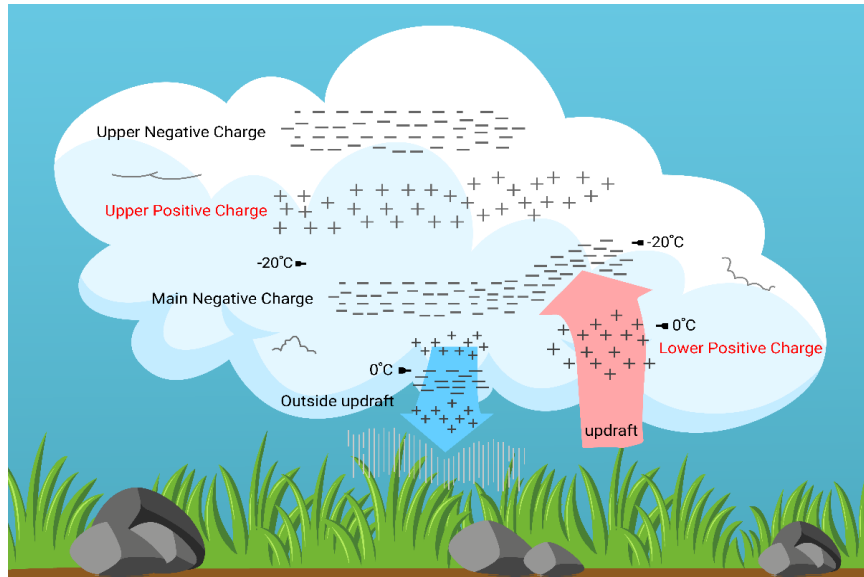


Fig. 2.1: A conceptual model depicts the dispersion of electrical charges within deep convection.

2.2 Types of Lightning

There are several forms of lightning strokes exists even within one family of lightning types. Because each lightning strokes has a different current profile and emits a varied amount of energy. The lightning stroke begin within a thunderstorm and travel through the cloud. It can then remain within the cloud or fly through the open air until it reaches the ground. There are typically 5–10 times as many flashes that remain in the cloud as there are flashes that reach the ground.

2.2.1 Cloud-to-Ground (CG) Lightning

Cloud-to-ground (CG) lightning is the sort of lightning that poses the greatest threat to people's safety. CG lightning strokes establish a conductive conduit between the cloud and the earth because of a potential differential between the two. Along this path, significant current flows. CG lightning is a safety risk due to the huge currents that run between the cloud and the ground, thus people have created lightning detection networks to keep an eye on it. The two primary varieties of CG lightning are the negative and positive varieties. About 90% of CG strokes that are negative, which delivers cloud's negative charge to the ground [22]. CG lightning develops when electrical charges build up in a cloud and on the ground beneath the cloud, respectively. Due to the attraction between opposing electrical charges, the two groupings of charges attempt to combine. A positive current rises up from

the earth to meet a negative current that is flowing downward toward the ground. When the currents combine, a bright lightning flash occurs.

2.2.2 Cloud-to-Cloud (CC) Lightning

Cloud-to-cloud (CC) lightning is the most common type of lightning, occurring between different charge levels within a single cloud or between two separate clouds. Typically, CC lightning is weaker than its counterpart, CG lightning. CC lightning exhibits lower peak currents and transfers smaller amounts of charge across shorter distances. CC lightning flashes exhibit a wide-ranging duration, spanning anywhere from 15 to 660 milliseconds [23]. Because it occurs at higher altitudes and is nearly three times as common as CG lightning, CC lightning might have a large impact on the atmosphere and ionosphere.

2.2.3 Cloud-to-Air (CA) Lightning

Referring to a discharge jumping from a cloud into clear air [24]. Technically speaking, all cloud-to-ground lightning strikes contain 'cloud-to-air' components in the many branches that extend away from the main channel and terminate abruptly in mid-air. However, the most visually dramatic examples of cloud-to-air lightning occur when a long, bright lightning channel jumps out of the side of a cumulonimbus cloud and terminates in the clear air surrounding the storm. Such events are actually failed "bolts from the blue" where the discharge event terminates early before the leader can reach the ground.

2.2.4 Ground-to-Cloud (GC) Lightning

An upward-moving leader starts a discharge between cloud and ground from a ground object [24]. Ground-to-cloud lightning strikes, also known as upward-moving lightning, are prevalent on large buildings and skyscrapers. The polarity of GC lightning can either be positive or negative. A ground-to-cloud flash is indicated by upward branching, while some upward-moving lightning is branchless below the cloud base.

2.2.5 Intra-cloud (IC) Lightning

The most frequent sort of discharge is lightning embedded within a single storm cloud that jumps between various charges locations in the cloud [25]. The two primary varieties of IG lightning are sheet lightning and heat lightning. When a lightning discharge illuminates a cloud, it's referred to as "sheet lightning" since the actual lightning channel is either inside the cloud or below the horizon. It is not just IC lightning, despite the fact that it is frequently

linked with it. Heat lightning is a term that refers to lightning-induced illumination that is too far away for thunder to be heard. Heat lightning gets its name from the fact that it is frequently observed on hot summer evenings when thunderstorms are abundant. Fig 2.2 shows the different types of lightning.

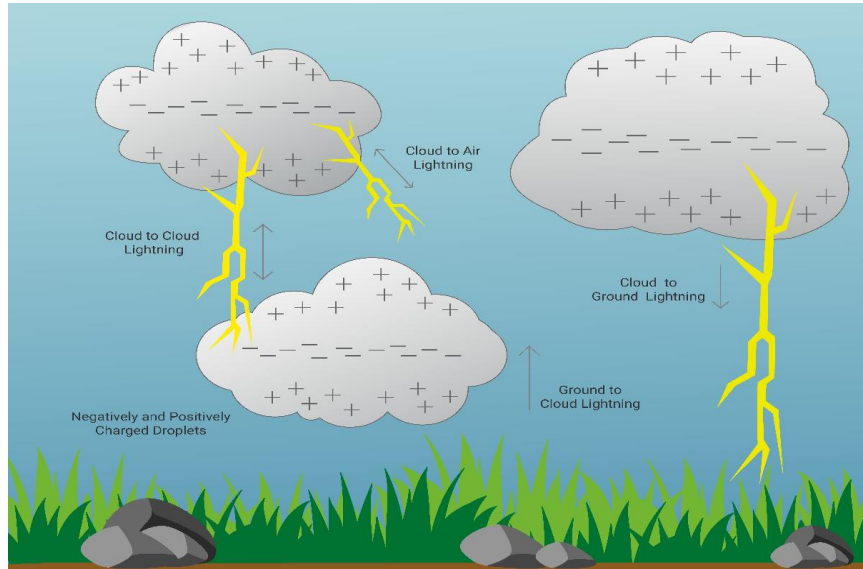


Fig. 2.2: Different types of lightning.

2.2.6 Transient Luminous Events

Large thunderstorms can generate other types of electrical disturbances known as Transient Luminous Events (TLEs) [26], that occur high in the atmosphere. They are hardly seen visually and are poorly understood. Red sprites, blue jets, and elves are the most frequent TLEs [27]. Fig 2.3 shows the different category of transient luminous events with their altitude distance.

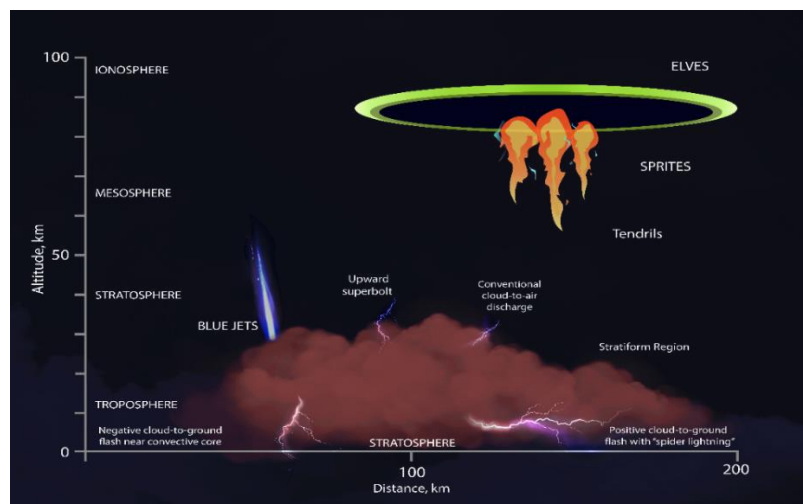


Fig. 2.3: Different types of transient luminous events.

- **Sprites:** Sprites are optical consequences that happen between 40 and 90 km above thunderstorms [28]. Lightning strikes that deliver a significant amount of charge to the ground cause large electrostatic fields, which are linked to sprites. Most of the sprites that have been seen have been connected to positive CG strokes [29], but a few have also been seen with negative CGs. Sprites are usually red and generally last a few seconds (about 10ms). Sprites can only be seen at night since they are not very bright. Since they are rarely visible to the human eye, very sensitive cameras are often used to capture images of them.
- **Blue jets:** Blue jets emerge from the thundercloud's top but are not related with cloud-to-ground lightning. They rise as narrow cones that spread out and disappear at altitudes between 25 and 35 miles [30]. Jets appear to accelerate at around 100 km/s and reach terminal heights of 40–50 km.
- **Elves:** Elves are quickly spreading, disk-shaped, up to 300-mile-wide zones of glowing light [13]. They endure less than a thousandth of a second, and occur over areas of active cloud to ground lightning. Elves result when an intense electromagnetic pulse stretches up into the ionosphere and it is now known that they are related with Terrestrial Gamma-Ray Flashes (TGFs).
- **Terrestrial Gamma-Ray (TGFs) Flashes:** TGFs are transient gamma-ray emissions from lightning caused by electrons accelerated to relativistic energy by electric fields. TGFs are ultra-violet and optical emissions stimulated in the lower ionosphere by electromagnetic waves emitted by the lightning current pulse. TGF, sometimes known as dark lightning, is a gamma-ray flash created in the Earth's atmosphere. In the past five years, substantial progress has been achieved in this area of lightning physics, which is a relatively new field. The BATSE satellite, which was built to examine gamma rays from the sun and beyond [31], made the first unexpected discovery of TGFs.

2.3 Lightning Detection Systems

To detect cloud-to-ground lightning strokes, many lightning networks of different types (local, regional or global) are formed. A few examples of the local networks are: the Canadian Lightning Detection Network (CLDN), Beijing Lightning Network (BLNET), New Zealand Lightning Detection Network (NZLDN), etc. A few examples of the regional networks are: North American Lightning Detection Network (NALDN), European

Cooperation for Lightning Detection (EUCLID), etc. On the other hand, World Wide Lightning Location Networks (WWLLN), Earth Network Total Lightning Network (ENTLN) and Vaisala's Global Lightning Dataset (GLD360) are global network. Space-based detectors on satellite can be used to locate lightning range, bearing and flash intensity by direct observation. A few examples are: The Tropical Rainfall Measuring Mission (TRMM) satellite, The International Space Station (ISS), The FY-4A geostationary satellite, GOES-16, etc.

2.4 Global Ground Based Lightning Detection

The GLD360, ENTLN and the WWLLN are ground-based global lightning detection networks that operate in a number of countries around the world. The use of these lightning detection networks is expanding quickly in a variety of meteorological applications, including severe storm predicting and lightning monitoring. The dependability of these meteorological applications is linked to a knowledge of these lightning networks' capabilities. The lightning detection technology has improved, and the number of stations in both networks has expanded in recent years.

2.4.1 Vaisala Global Lightning Detection Network

The GLD360 was launched in September 2009 [32]. GLD360 is the first ground-based lightning detection network capable of providing both global coverage and consistent, high performance without significant detection discrepancies between day and nighttime conditions. GLD360's DE and median location accuracy were projected to be 70% [32] cloud-to-ground flash DE and 5-10 km median cloud-to-ground stroke location accuracy. The Vaisala GLD360 global lightning dataset is generated by a long-range network that employs both Time of Arrival (TOA) and Magnetic Direction Finding (MDF) technologies at each sensor to geo-locate individual lightning flashes. The sensors, sensitive to the Very Low Frequency range (VLF; ~500 Hz--~50 kHz) [33], use a waveform recognition algorithm to identify specific features in radio atmospherics generated by individual lightning discharges. A propagation correction is applied to the time delay of each feature in order to recover a more consistent arrival time across a wide range of distances and propagation conditions. An attenuation model is also applied to the amplitude of the waveform, which is used to recover an estimate of peak current.

2.4.1.1 GLD360 instrument description

The sensors in the underlying long-range network detect the horizontal magnetic field vector between about 300 Hz and about 48 kHz using orthogonally oriented air-core magnetic loop antennas [34]. In order to partly eliminate nearby power line noise and numerous anthropogenic narrowband noise sources in the VLF band, broadband data collected at 100 KSamples/second are processed. Using a locally stored waveform bank, each individual impulsive waveform produced by radio atmospheric from lightning discharges is examined in order to locate a low time variance feature that may be used by the central analyzer.

2.4.1.2 Data collection and processing

The central analyzer processes sensor data to determine the location, time, and peak current and polarity estimates for individual lightning strokes. Each reported event corresponds to a single return stroke, which can be one of many within a CG flash. However, the stroke order information is not provided. Some reported events pertain to cloud pulses, which are large discharges within clouds that generate VLF-range pulses. For these events, GLD360 assigns an effective peak current based on sensor-amplitude data, even though peak current validation is only applicable for CG strokes. Event types (CG stroke or cloud pulse) are not reported.

Key performance metrics for lightning detection networks include location accuracy, detection efficiency (DE), and peak current and polarity accuracy. These factors depend on sensor locations relative to storm locations, propagation conditions (including ionospheric state), and each sensor's local noise environment. GLD360 aims for a global 70% CG flash DE, median location accuracy of 2-5 km, peak current estimation error of 20%, and over 90% polarity determination accuracy. However, performance may vary based on sensor availability and propagation factors. Currently, there is no separate database for performance correction factors to calibrate statistical measurements. The network's methodology is detailed in [35].

2.4.2 Earth Network Total Lightning Network

The ENTLN, formerly WeatherBug Total Lightning Network (WTLN) [36] is a network of more than 1800 sensors spread over more than 100 countries that are used to record IC and CG lightning [37]. The ENTLN monitors total lightning activity using wideband

sensors with detection frequencies ranging from 1 Hz to 12 MHz (i.e., VLF to HF). The Time-of-Arrival (TOA) technique is used to implement the geolocation of lightning in real-time as the central processor receives the electric field signals continuously recorded by the sensors. The ENTLN records 50 lightning strikes per second globally on average. The ENTLN reports the time, geolocation, event type, and peak current for each instance of lightning. All ENTLN sensors raw electric field waveforms are permanently archived, allowing for future processing or usage in scientific research.

2.4.2.1 ENTLN data processing

The ENTLN's processor (data processing algorithms, including those for locating and classification) was upgraded multiple times over its lifetime to enhance DE, classification accuracy, and location accuracy. The performance of the ENTLN was tested after each upgrade using independent datasets such as high-speed video records, rocket-triggered lightning measurements [38], and satellite-based optical lightning observations [39]. The ENTLN detects the components of both IC and CG flashes, and algorithms use waveform shapes to differentiate between the IC and CG pulses. The IC and CG pulses are combined (grouped) into IC (cloud) and CG flashes using space (10 km) and time (0.7 sec) criteria. ENTLN pulse and flash density grids simply report the pulse/flash counts within grid cells of various sizes over various periods of time.

2.4.3 World Wide Lightning Location Network

Initially patented as Time of Group Arrival (TOGA) network (Dowden, R. L. and J.B. Brundell, Improvements relating to the location of lightning discharges, Australian Patent Office, patent number AU 200071483 A1, Publication date:2001.05.17), it was later renamed the “World Wide Lightning Location Network” and made operational in 2004. The WWLLN is a network that operates on the ground and covers the entire globe and provides real-time, quality lightning data. This network detects VLF up to 3–30 kHz radio wave receivers distributed around the globe to identify the TOGA for individual lightning sferics [40]. The WWLLN network consists of 80 sensors around the globe that observe VLF radio waves for lightning strikes. The network locates lightning within 5 km and 10 microseconds approach on the observed sferic waveforms. WWLLN receives the low frequency data from hundreds of ENTLN sensors and processes those waveforms, thus expanding the VLF capability for seeing the world. The data set that WWLLN processes (WWLLN-only data combined with the VLF data we get from ENTLN sensors), is

delivered in real time, stroke by stroke, back to Earth Networks, where it is combined with ENTLN to form ENGLN (Earth Networks Global Lightning Network) VLF sferics from lightning propagate nearly around the world with little attenuation. The peak energy of lightning is around 10-13 kHz, so the VLF band is ideal for detecting global lightning with a relatively small number of sensors.

2.4.3.1 WWLLN network setup

The components within the dotted line are stored in a building, whilst the antenna and preamp are outdoors. The VLF antennae are often installed atop ferroconcrete structures. These buildings shield the antenna from man-made noise in the area. Also, the vertical electric field from strong CG lightning is stronger than the noise from the power lines. Because of these things, WWLLN receivers are free of noise as much as other long-range lightning location methods [41]. In the VLF band (1-24 kHz), lightning discharges emit radio wave pulses known as sferics. Lightning waves in this frequency range may reach hundreds of kilometers in the Earth-ionosphere waveguide because to minimal attenuation and a high power spectral density [42]. The antenna's electric field signal gains 10 from the preamp. The Service Unit isolates the signal using an audio transformer and transfers it to the computer sound card through a lengthy connection within a building. The Service Unit powers the preamplifier. Global Positioning System (GPS) pulses every second. Computer sound card accepts stereo waveforms (Left and Right) channel, one of which is the VLF waveform with the lightning sferics, and the other is the Pulse Per Second (PPS) from the GPS engine. Thus both waveforms (L and R) are digitized (at 48,000 s/s) and the samples are organized within each second by the GPS time pulse. The correct second is determined by syncing to NTP (Network Time Protocol). The GPS antenna sends a serial port-connected NMEA signal to the computer indicating the station's location. Fig. 2.4 shows WWLLN VLF receiving station with their necessary antennas and instruments.

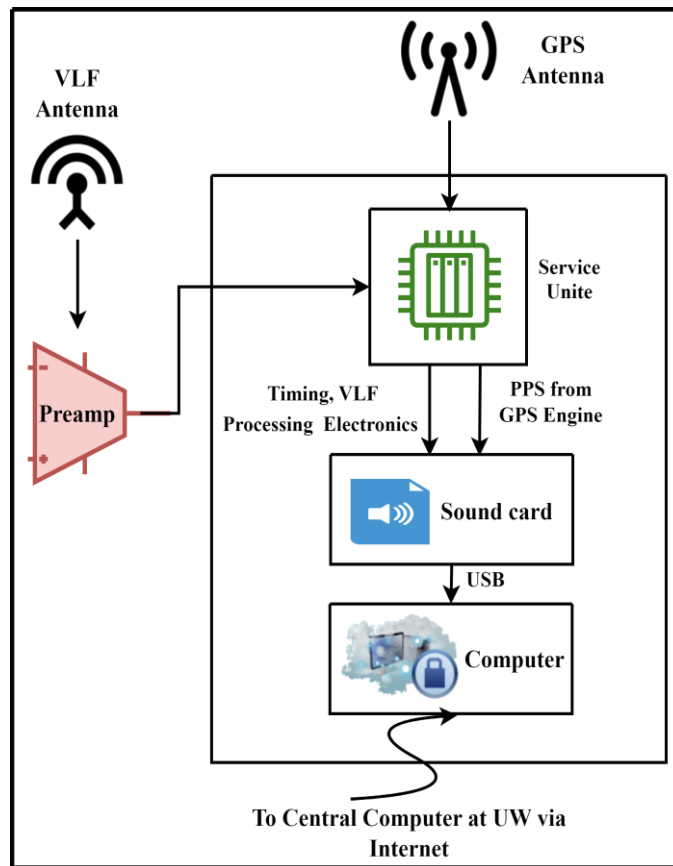


Fig. 2.4: WWLLN VLF receiving station.

2.4.3.2 WWLLN data structure

Table 2.1 lists all of the different types of WWLLN data files. The file names in the table are examples for January 1, 2020, at 12:00 UTC. Except for WB-files, most file types can be found on the flashfile on wd1/wwlln. Except for R-files, each type of file has its own area, with names like "Afiles," "AEfiles," and so on. R-files are split into yearly and monthly groups because there are so many of them: Rfiles/R [YYYY]/R [YYYY] [MM]. Some of the WWLLN data file folders were copied to the other flashes, but not all of them. This was done based on what was needed, so the other flashes shouldn't be thought of as a backup of the flashfile dataset.

Below are descriptions of each file and an example line from the R, A, AP, and AE files.

The simplest files are Rfiles, which have three fields on each line:

```
12 500.14903 2335
```

The first number represents the station ID, the second represents the passing time since the hour began, and the third is the station's root integrated square electric field in uncalibrated sound card units. Every line in an A-file looks like this:

```
2020/01/01,12:00:01.103460,9.0621,-117.8276,19.9,9
```

The first six digits represent the date (YYYY/MM/DD) and the stroke's UTC time (hh,mm,ss). The latitude and longitude of the stroke, in degrees north and east, are the following two. The number of WWLLN stations that participated in the stroke location, and timing uncertainty in microseconds. APfiles are like Afiles, but they have more information after the stroke position.

2020/01/01,12:00:01.142335,-10.4622, 20.0863, 13.4, 5, 17, 600, 19, 2084, 26, 453, 53, 225, 64, 226

The station ID 17 and the field strength 600 in sound card units, which is the same value as in the Rfiles, are given by pairs of integers starting at 17,600.

Table 2.1: WWLLN Data Types

File Type	File Name	Description
Rfiles	R20200101051000	Raw packets transmitted by stations
Afiles	A20200101.loc	Locations of lightning emitted in real time
AEfiles	AE20200101.loc	Bootstrap generated daily stroke energy and location data
APfiles	AP20200101.loc	Location data for each stroke solution, including station E-field data
DEfiles	DE20200101.mat	Matlab data for relative DE maps
Sfiles	S202001010510.loc	Waveform information for strokes near a certain location
WBfiles	WB202001010510.mat	production of continuous wideband field data using toga -r
Tfiles	T20200101_single.dat	TCurrent station packet count record.dat is the most recent running total

Finally, AEfiles are identical to Afiles but include three more numbers:

2020/01/01,12:00:07.142335, -10.4622, 020.0863, 13.4, 5, 448.86, 114.87, 4

The final three values are the radiated VLF stroke energy in joules (448.86), the median absolute deviation of the energy value in joules (114.87), and the number of stations that participated in the energy value answer (a subset of the stations). 4. T-files keep track of how many packets a station sent to flash4 over the course of WWLLN's history. It is not made automatically like the other files. Instead, it is written anytime the TfileUpdater.m

script in the functions.git repository is modified. Each line shows the date in days since January 1, 2000, as well as the counts for each station, with column 2 corresponding to station 0.

2.5 Satellite Based Lightning System

Tropical Rainfall Measuring Mission (TRMM) satellite, the Geostationary Operational Environmental Satellite (GOES-16), the FengYun-4A series (FY-4A) and International Space Station (ISS) have given a significant global coverage of average lightning incidence over the previous decade.

On November 27, 1997, The Japanese Space Agency (JAXA) launched the TRMM satellite aboard an H-II rocket from Tanegashima Space Center [43]. The TRMM was designed to be a low-Earth orbit (LEO) satellite stationed between 35°N and 35°S. It has a 350 km altitude distance with a 35° inclination angle [43]. The TRMM satellite combines many equipment's, including Precipitation Radar (PA), Microwave Imaging (MI), Lightning Imaging Sensor (LIS) and Optical Transient Detector (OTD) to detect precipitation and observing lightning activates which contributes to a better knowledge of climate and weather. After the spacecraft ran out of fuel on April 15, 2015, TRMM was officially over. On June 15, 2015, TRMM was turned off and sent back to Earth.

The ISS-LIS adds greatly to our understanding of these complex interrelationships by providing worldwide total lightning observations with high spatial and temporal accuracy. This optically based lightning detection sensor was sent to the ISS in February 2017 [44] and has been operating satisfactorily with minimal downtime since then. Because of its accessibility, adequate space, power, and data bandwidth, and capacity to process during the diurnal cycle, the ISS, which is in a Low-Earth Orbit (LEO) inclined approximately 55° [44], has been increasingly employed as a home for a variety of Earth-observing devices.

In November 2016, GOES-16 (formerly GOES-R) was sent into orbit. After a period of dedicated satellite and sensor spin-up, Global Lightning Mapper (GLM) started running in March 2017. The use of a geographic orbit increases the lead time for severe storm warnings, earlier detection of approaching ground-level lightning strikes, and overall lightning detection with virtually uniform spatial coverage of 10 km [45]. The GOES-16 is located at the GOES East position at 75.2°W and an altitude distance of 35,786 kilometers.

The FY-4A geostationary meteorological satellite is a Chinese geostationary meteorological satellite of the second generation. It has a new Lightning Mapping Imager (LMI) instrument for complete lightning detection. On December 11, 2016, the FY-4A satellite with LMI was launched, capable of detecting complete lightning throughout the day and night [46].

2.6 Lightning Detection Instrument

Optical Transient Detector (OTD), Lightning Imaging Sensor (LIS), Global Lightning Mapper (GLM), Lightning Mapping Arrays (LMA) are used to capture lightning during the day as well as at night.

2.6.1 Lightning Imaging Sensor

When a lightning strike occurs, the ISS-LIS equipment records the time, measures the radiated energy, and estimate the location during day and night. Like TRMM-LIS, the ISS-LIS has a spatial resolution of around 4 km for resolving lightning; although it can cover a broader range of latitudes up to 55° due to its 51.6° inclination [44]. TRMM-LIS and ISS-LIS data are available from November 1997 to 2015 and March 2017 to October 2020 respectively. Optical pulse-to-flash and flash-to-cell collecting techniques integrate individual lightning occurrences into events, groups, flashes, and areas. An optical “group” is defined by spatially contiguous light occurrences inside a 2-ms frame. A 5.5-km geographical constraint and a 330-ms temporal constraint are employed to identify whether groups are part of the same optical “flash” [47]. Fig. 2.5 shows a basic workflow of data processing of initial observations at the ISS-LIS.

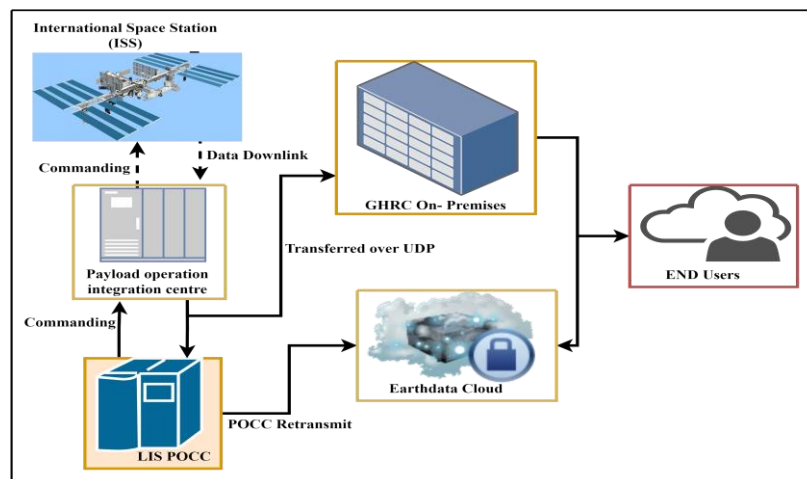


Fig. 2.5: Basic workflow of the data processing of initial observations at the ISS-LIS.

The NASA Global Hydrology Resource Center (GHRC) Distributed Active Archive Center (DAAC) produces and disseminates ISS LIS products, which may be found on the GHRC website for ISS-LIS, the NASA Earth-data Search tool, and the GHRC Hydrology Data Search Tool.

2.6.2. Optical Transient Detector

The OTD is a mix of optical and electrical components that is extremely compact. OTD refers to the device's capacity to detect the transient changes in an optical scene that signal the existence of lightning. The OTD instrument is a significant improvement above prior technologies in that it can collect lightning data during the day as well as at night. The Microlab-1 satellite launched the OTD in 1995 at $\pm 70^\circ$ inclination. The field of view of OTD was 1300×1300 km [48]. By comparing the luminance of adjacent frames of OTD optical data, "flashes" are identified. If the difference exceeds a certain threshold, a "event" is recorded. As a "group," one or more nearby occurrences within the same 2ms time range are recorded. A "flash" is characterized by the presence of one or more groups during a sufficiently brief timeframe. These are classified as "areas" if they are adequately isolated from existing areas. Depending on environmental factors such as glint and radiation, the OTD detects lightning flashes in both daylight and nighttime with a DE from 40% to 65% [49].

2.6.3 Global Lightning Mapper

A single-channel, near-infrared OTD called GLM is capable of spotting brief alterations in an optical landscape that signify the incidence of lightning. GLM will continually record total lightning movement with a spatial resolution of 8km at Nadir, and up to 15 km or more at the edges of the field of view. To identify the intensification of potentially severe storms, which are frequently accompanied by increasing lightning activity, the equipment will gather data such as the frequency and location of lightning incidents. The GLM captures transient light events at a rate of 500 frames per second, equating to a frame exposure time of 2 milliseconds (GOES-R Data Book). The sensor is a 1372×1300 pixel nadir-pointed single-channel near-IR CCD focal plane with a 14-bit dynamic range of optical intensity digitization. The mapping precision is approximately 5 km, which corresponds to the inaccuracy in latitude and longitude location at the pixel center. The spectral pass band is just 1.1 nm broad and is focused on the O I triplet of atomic lines at

777.4 nm. This is to assure that lightning can be seen against the light daytime cloud background [45], in conjunction with spatial and temporal filtering.

2.6.4 Lightning Mapping Arrays

The Lightning Mapping Array (LMA) measures the total lightning activity of a storm. This includes both lightning that occurs within the clouds (CC) and lightning that reaches the ground (CG); although typically not the actual point at which the flash comes to ground. The system is able to determine the location and time of lightning discharge based on the time it takes the very high frequency (VHF) signal radiated by the discharge to arrive at the various antenna stations. The LMA produces detailed 3-dimensional images both of individual lightning discharges and of the overall lightning activity of electrically active storms. The discharges are imaged by locating the sources of impulsive radio signals in an unused VHF television channel (typically 60-66 MHz, U.S. Channel 3) [50]. The radiation events are located by measuring their time of arrival at a network of measurement stations, usually including about 10 receivers spaced by 10 to 50 km. A Lightning Mapping Array (LMA) is a network of antennas, GPS receivers, and processing systems that detect total lightning. The LMAs are operated in many locations but each covers lightning only in a small region (maybe 100 -200 km across) but they see and record every little spark in the cloud and track the evolution of lightning strokes in their region of operation. These LMAs have been used to test the DE of all the other systems for lightning that occurs in the LMA field of view, and it is found that, for instance, the space based optical sensors tend to miss a lot of strokes that occur between mid-level clouds and indeed, cloud to ground strokes – because the light from low level or CG strokes often comes out of the cloud near the bottom and never reaches up vertically to the satellites. The LMA was patterned after the Lightning Detection and Ranging (LDAR) system developed at the NASA Kennedy Space Center [51]. More detailed descriptions of the system operation and results have been given by [52], [53].

2.6.5 OTD/LIS Data Clustering

The LIS/OTD clustering approach is based on a tree or parent-child connection between the different levels of the clustering [54]. Each item at the lower cluster level is only connected to a single parent (upper) item; yet, as shown in Fig. 2.6, each parent item may be associated with numerous child or lower level items.

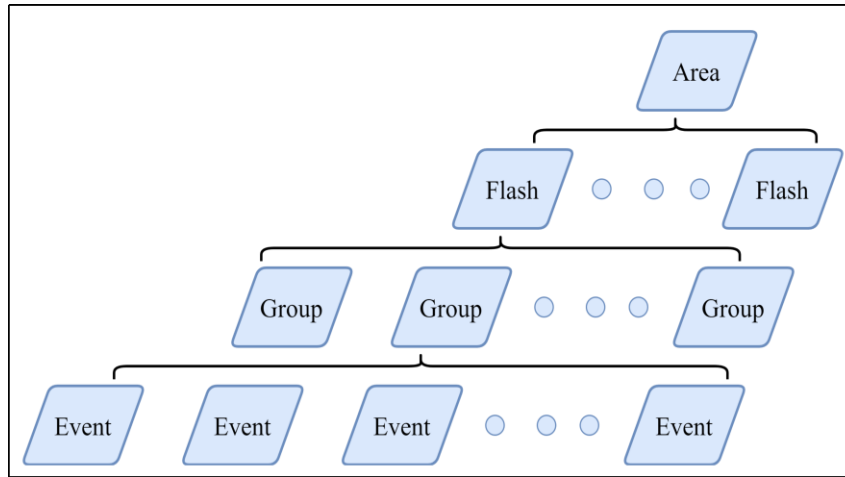


Fig. 2.6: Data clustering method of LIS/OTD.

- **Events:** The basic unit of LIS/OTD data is the event. A single pixel surpassing the background threshold within a single frame is classified as it. In other words, each pixel created by the onboard instrument hardware and software results in a distinct event. Although an event is often conceived of as a single optical pulse triggered by lightning, numerous pulses occurring inside the 2-ms frame may contribute to an event.
- **Groups:** In pixel space, the event-to-group clustering is carried out. A lightning discharge often illuminates more than one LIS/OTD pixel in a single frame. When many events are adjacent to each other, they are grouped together. A group is defined as one or more simultaneous events (events that occur in the same time-integration frame) that register in adjacent pixels in the focal plane array.
- **Flashes:** A lightning flash will generate one to several optical pulses within a certain temporal and geographical range. In a restricted geographical and temporal range, a LIS/OTD flash equates to several related groups. A flash might consist of as few as one group with a single event or as many as multiple groups with multiple events together.
- **Areas:** Areas are formed when many flashes occur within a certain distance of each other. An area are described as a relatively close location on the Earth's surface that has generated lightning during a single LIS or OTD orbit. A designated region is made up of a string of flashes that are no more than 16.5 km apart from one another in space. A region may have several flashes made up of multiple groups and events, or its region may have several flashes made up of multiple groups and events, or it

may contain only one event. Because, as previously stated, the LIS and OTD viewing durations are substantially shorter than a storm life cycle, no inter-flash or absolute time-limit limitation is placed on the area definition.

2.7 Differences between Ground and Space Based Lightning Detection Systems

There have some fundamental differences between ground-based lightning detection system and space-based optical lightning detection systems. These differences are listed in Table 2.2.

Table 2.2: Comparison of Ground-Based and Space-Based Lightning Detection Systems.

Parameter	Ground-Based Systems (WWLLN, ENGLN, GLD360)	Space-Based Systems (TRMM/LIS, ISS-LIS, GLM-16, GLM-17, GLM-18)
Spatial Resolution	4-5 km, better than space-based systems	8 km, not as precise as ground-based systems
Temporal Resolution	1 μ s, faster than space-based systems	2 milliseconds, slower than ground-based systems
Global Coverage	Real-time coverage of the whole globe.	Limited coverage (up to $\sim 70^\circ$) and revisit rate. Only see a small region (~ 400 km across) just below the satellite for about 1 minute or so
Distinguishing Lightning Types (IC vs. CG)	Can distinguish with some limitations	Unable to distinguish between IC and CG strokes
Tracking Storm Development	Capable of tracking storm development	Hindered by limited observation time. Only see a storm for a minute or two, then not again for 2 to 3 days later.
Global Lightning Detection	Detects global lightning	Incomplete detection due to coverage limitations (even with multiple GLMs)
Lightning Warning Systems	Provides worldwide warnings	Limited to satellite's field of view (up to $\sim 65^\circ$ latitude)
Total Strokes Detected	Detects orders of magnitude more strokes	Limited by low altitude and coverage, detecting fewer strokes

2.8 Literature Review

The climatological study of lightning have done by the several researcher [4], [7], [9], [55]–[62], by using both of ground-based and space-based observation. The climatological study and risk analysis over Bangladesh are investigated in [63]–[68]. Several attempts have been made to study the DE of WWLLN [1], [12], [12], [16], [55], [69]–[72], compared to other instruments and networks in the period of 2006 to 2018. The WWLLN has been upgraded to monitor radiated VLF stroke energy. Many attempts have been made to study the lightning strokes energy [5], [17], [22], [73], in different time period using several stations and equipment. The lightning prediction has gained increasing attention by developing several prediction models [74]–[78], using both space-based and ground-based data during the past decade.

2.8.1 Global Lightning Climatology

The climatological features of lightning strokes are divided into two aspects: those that are global and those that differ by climatic location. Global lightning climatology investigations have consistently revealed that lightning activity is greater over continents than over ocean [9]. K.S. Virts et al. [4] highlights a global lightning climatology by analyzing four years (2008-2011) of lightning strokes data obtained from WWLLN. Side by side, the TRMM precipitation data are investigated to determine the annual mean, seasonal variation, and diurnal cycle. This study reveals that the lightning concentrated over the major tropical continents of Africa, Southeast Asia, Australasia, and Central and South America that are shown in Fig. 2.7. The lightning strokes over the maritime continents are mostly occurred in afternoon and early evening [4]. Similar observation has been found in Lay et al. [79]. Where authors demonstrate that every region has similar trends of what happens during the day. But the peak amplitudes on land and in the ocean do not happen at the same LT in each place.

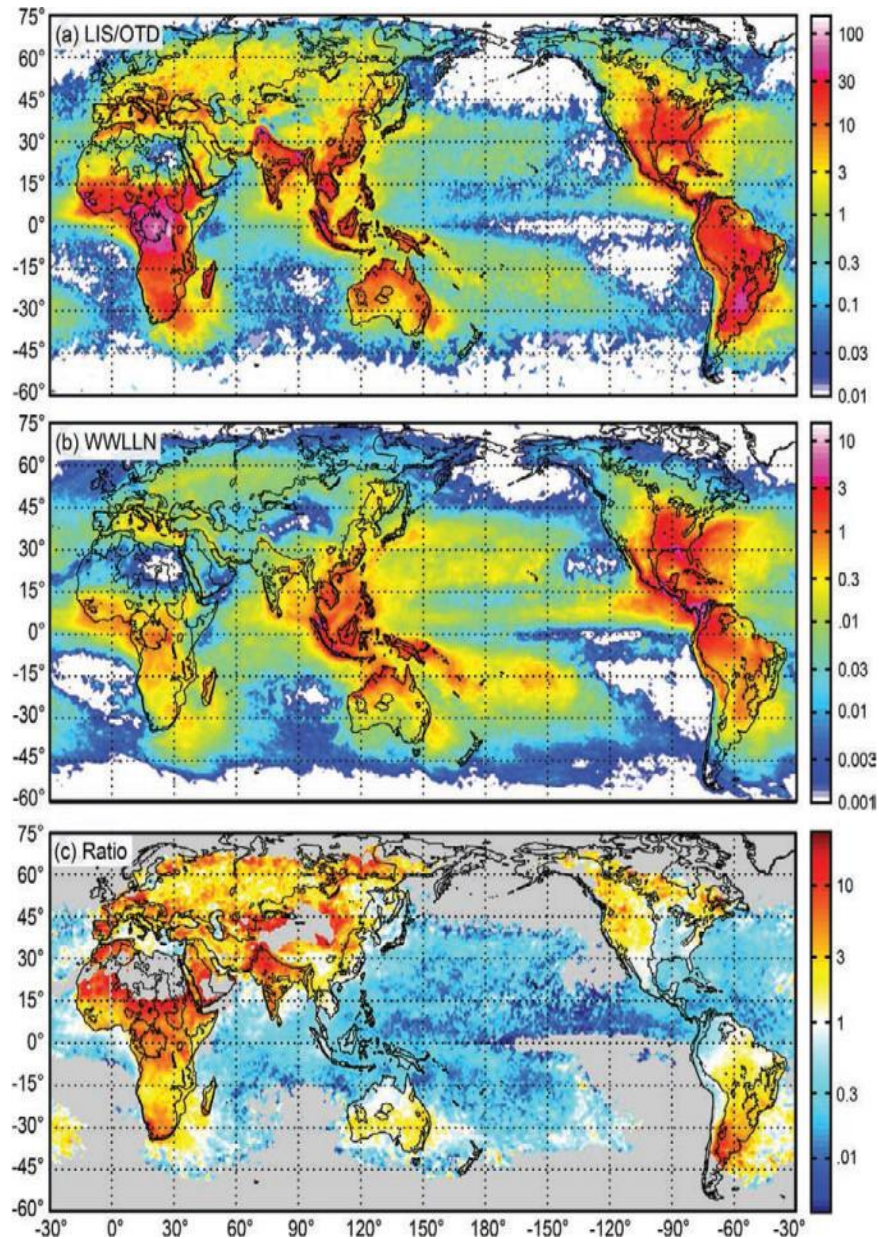


Fig. 2.7: Annual-mean frequency of occurrence of lightning from (a) LIS/OTD (flashes $\text{km}^{-2} \text{yr}^{-1}$) (b) WWLLN (strokes $\text{km}^{-2} \text{yr}^{-1}$) and (c) Ratio of LIS/OTD flashes to WWLLN strokes [4].

The Fig. 2.7a and 2.7b are chosen to emphasize the similarities between the LIS/OTD and WWLLN lightning climatologies. Differences between these two climatologies are illustrated in Fig. 2.7c, which displays the point-wise ratio of lightning frequency reported by LIS/OTD and WWLLN. For visualization purposes, this ratio is multiplied by a scaling factor—the global-mean WWLLN lightning frequency divided by the global-mean LIS/OTD lightning frequency, so that values below 1 indicate proportionally more WWLLN lightning and vice versa, relative to their respective global means. With a few

notable exceptions, such as over the Maritime Continent and southeastern United States, LIS/OTD reports proportionally more lightning over land and less over the oceans compared to WWLLN. The land-sea comparisons in Fig. 2.7c may represent a propensity for lightning strokes over the seas to be more powerful than those over land, since WWLLN's DE is greater for lightning strokes with larger peak currents [71]. In an examination of the mean peak currents in negative cloud-to-ground flashes recorded by the NLDN, Rudlosky et al. [80] already identified this pattern. According to M.L. Hutchins et al. [16], when WWLLN's DE is smaller, Fig. 2.7c, the LIS lightning climatology lays substantially larger emphasis on the maxima in lightning frequency in locations like Africa and the Himalayas. The study of lightning stroke energy is still being done, especially over the eastern United States.

A gridded lightning climatology from TRMM-LIS and OTD is presented in [7]. This study investigates thirteen years of lightning data observed by the OTD and LIS to determine the total lightning flash rate during the period 1998 to 2010. This study evaluated that the average global flash rate was 46 flashes/s (shown in Fig. 2.8) and it varied from 35 flashes/s to 60 flashes/s in February to August.

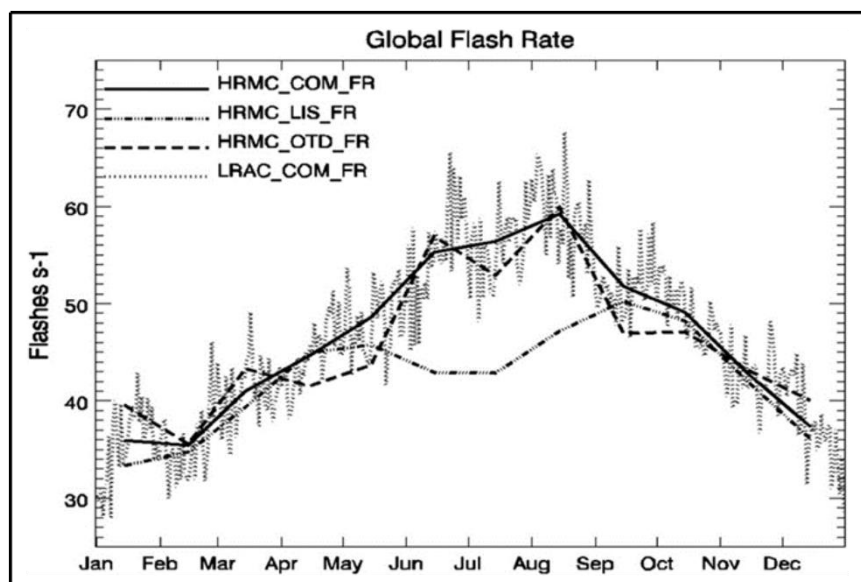


Fig. 2.8: Annual cycle of global flash rate, computed from high resolution monthly climatology (HRMC) and from low resolution annual climatology (LRAC) [7].

Fig. 2.8 displays the product of the flash rates in High Resolution Monthly Climatology (HRMC) and Low Resolution Annual Climatology (LRAC) multiplied by the corresponding grid box sizes and sums all grid boxes to estimate the annual cycle of the global flash rate. The combined OTD-LIS HRMC product estimates a minimum global flash rate of 35 flashes per second in February and a maximum of 60 flashes per second in August. From October to April, the estimate from LIS is within a few percent of the combined estimate, even though LIS does not observe high latitudes. Apart from during the boreal summer, the LIS domain encompasses the majority of global lightning. This LIS estimate is likely somewhat too high because the high flash rates near the edge of the LIS domain in northern Argentina and southern Africa.

It is noted that the vast majority of time the satellite does not see current lightning. So this number of 35-60 flashes/sec is highly model dependent, and not based on actual global data or anywhere near that rate. The mean annual flash rate from combined LIS and OTD, 0.5° grid are reported in Fig. 2.9.

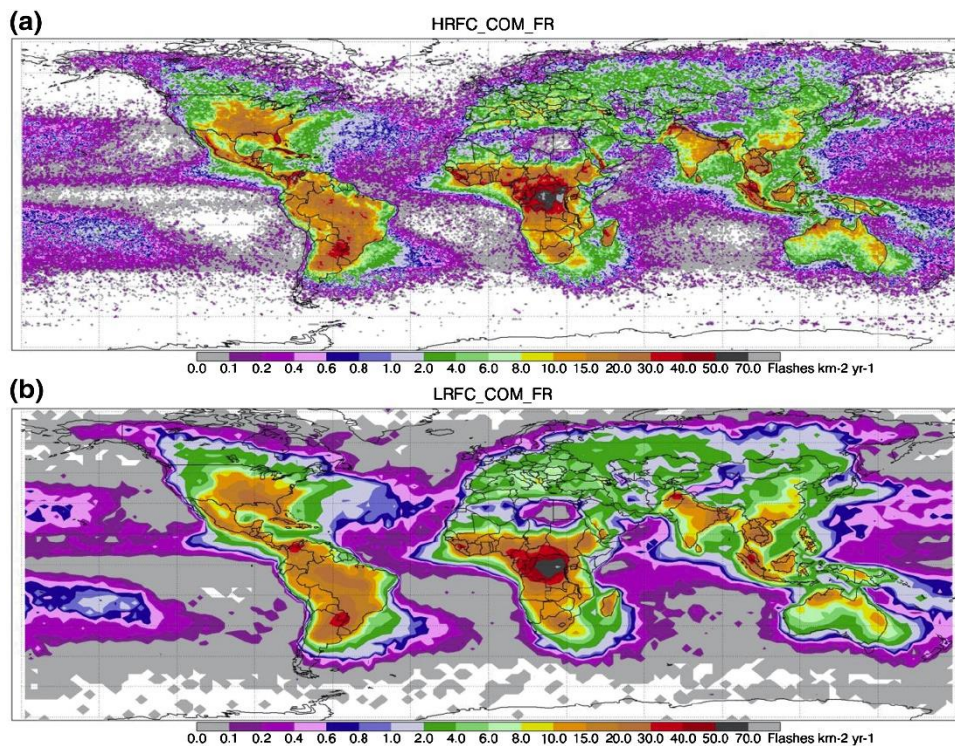


Fig. 2.9: (a) High-Resolution Flash Climatology (HRFC) mean annual flash rate from combined LIS and OTD on a 0.5° grid. (b) Low-Resolution Flash Climatology (LRFC) mean annual flash rate from combined LIS and OTD on a 2.5° grid.[7].

In certain areas with low flash rates (primarily oceans and arid regions) or at high latitudes with limited OTD-only sampling, the High-Resolution Flash Climatology (HRFC) data may appear slightly noisy (Fig. 2.9a) due to insufficient sampling for such high resolution. Conversely, the Low-Resolution Flash Climatology (LRFC) (Fig. 2.9b) seems smoother than necessary over land, particularly in the tropics. By providing data at both resolutions, users can apply the most suitable smoothing for their specific application. In some tropical locations, where high flash rates are associated with topographic features, even finer resolution might be appropriate in Albrecht et al. [81].

View-times are allocated to 1-hour (local solar time) $\times 2.5^\circ \times 2.5^\circ$ bins during each orbit accumulation. The flash rate for the Low-Resolution Diurnal Climatology (LRDC) is stored in units of flashes per hour per square kilometer. The diurnal cycle's amplitude is considerably stronger over land than the ocean, peaking between 1500 and 1700 LST. The Low-Resolution Annual Climatology (LRAC) assigns flashes and view-times to bins of one day $\times 2.5^\circ \times 2.5^\circ$, and the LRAC flash rate is stored in units of flashes per day per square kilometer. Both HRFC and LRDC's hourly binning and LRAC's daily binning result in sample sizes that are not robust enough, leaving users to choose the appropriate smoothing.

Using data from the WWLLN and Fast On-orbit Rapid Recording of Transient Events (FORTE) satellites, Lay et al. [79] examined the local temporal variation in land/ocean lightning flash density. This study has been found that the peak lightning flash density varies by up to 5 hours in local time for different continents. Fig. 2.10 shows the contribution six different region makes to the position of the local time peak in lightning flash density. Given that the WWLLN measures lightning strokes with large peak currents, the variation in local time of WWLLN-detected strokes is suggested to indicate a similar variation in local time of transient luminous events (e.g., elves) and their impact on the lower ionosphere.

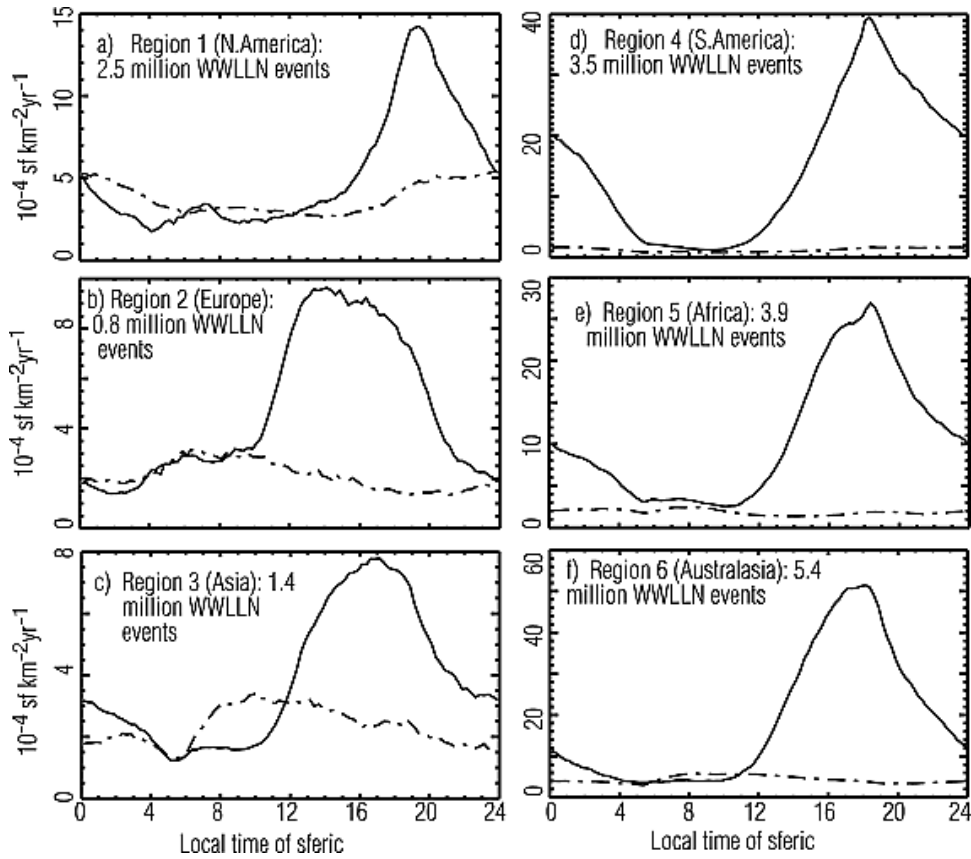


Fig. 2.10: The local time peak in lightning flash density estimated by the data from regions (a) N. America, (b) Europe, (c) Asia, (d) S. America, (e) Africa, and (f) Asutralasia.

Each area has similar trends at 20 LT which happened during the day. But the peak amplitudes on land and in the ocean do not happen at the same LT in each place. The size of an error bar in Poisson statistics is based on the width of the line. The largest percentage error occurs in Fig. 2.10b where, the error at 1400 LT is $\pm 0.084 \times 10^{-4}$ sf km² yr⁻¹.

2.8.2 Analysis of Lightning Phenomena over Bangladesh

Bangladesh region is vulnerable to severe convective systems during the hot period of pre-monsoon season. A database of lightning-related deaths and injuries in Bangladesh was developed from 1990 to mid-2016. The annual averages for Bangladesh are 114 fatalities and 89 injuries over the entire period [63]. A. Dewan et al. [67], used TRMM-LIS data to try to analyze the geographical and temporal patterns of a 17-year lightning climatology over Bangladesh. This study shows that, across the landmass of Bangladesh, the pre-monsoon season has the highest percentage of lightning flash counts (69.2%), followed by the monsoon (24.1%), post-monsoon (4.6%), and winter (2.1%). The flash density hotspots

in Bangladesh were mainly found in the north and north-eastern regions, with a maximum of 72 flash km⁻² year⁻¹. Fig. 2.11 shows the spatial distribution of seasonal lightning activity over Bangladesh during of 1998–2014.

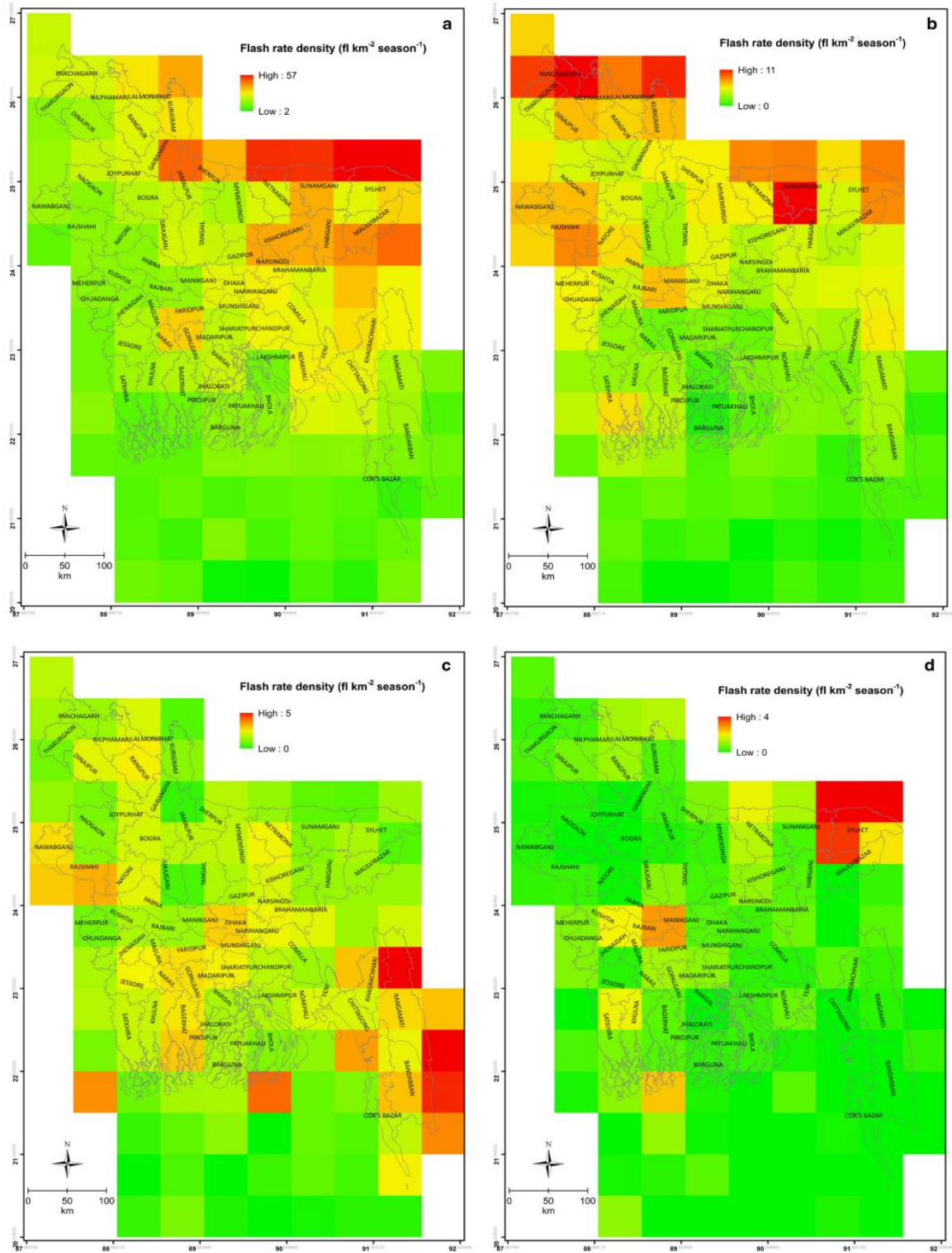


Fig. 2.11: Seasonal variation in flash rate density over Bangladesh: a pre-monsoon, b monsoon, c post-monsoon and d winter [67].

The above figure shows that the highest lightning activity was found in pre-monsoon season ($57 \text{ flash km}^{-2} \text{ season}^{-1}$) and the lowest highest lightning activity was found in winter season ($4 \text{ flash km}^{-2} \text{ season}^{-1}$). This study also reveals the daily lightning cycle over Bangladesh that shows in Fig. 2.12.

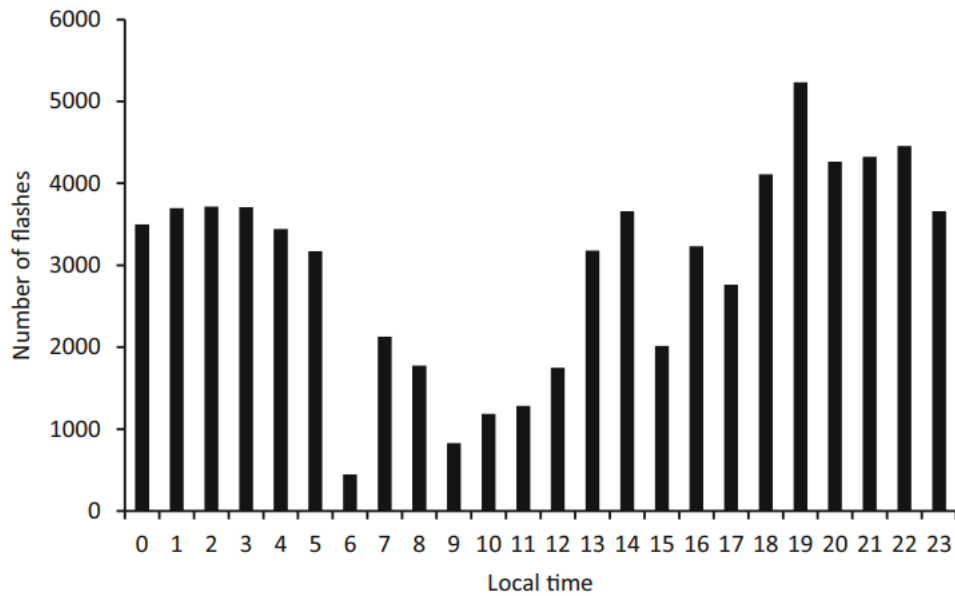


Fig. 2.12: Daily lightning cycle associated with lightning flash counts over Bangladesh, 1998–2014 [67].

The above figure shows the daily lightning cycle between 1998 and 2014. The diurnal variation of lightning flashes in Bangladesh revealed two unique maxima. The first peak occurs between 1:00 and 3:00 LST, and the second between 18:00 and 22:00 LST. A muted peak is also evident around 14:00 LST (Fig. 2.12). Lightning activity is often stronger in the early evening hours and decreases from morning to afternoon, with an afternoon-evening maximum trend. An examination of the 24-hour lightning activity distribution, separated into 6-hour intervals, reveals the following pattern: Early morning (00:00 to 5:59 LST) accounts for 29.68%, late morning (06:00 to 11:59 LST) accounts for 10.69%, afternoon (12:00 to 17:59 LST) accounts for 23.20%, and evening (18:00 to 23:55 LST) accounts for 36.41%. This pattern illustrates that lightning activity in Bangladesh is characterized by maximums in the early morning and late evening.

The spatial pattern and land surface features associated with CG lightning in Bangladesh has been attempted by A. Dewan et al. [82].

In order to explain the seasonal lightning climatology, GLD360 data from 2015 to 2020 were employed. All land surface characteristics that may be linked with CG lightning occurrence were analyzed using elevation, land use and land cover, vegetation, and surface heat flux data [82]. A logarithmic scale was employed to generate the stroke density maps which is shown in Fig. 2.13.

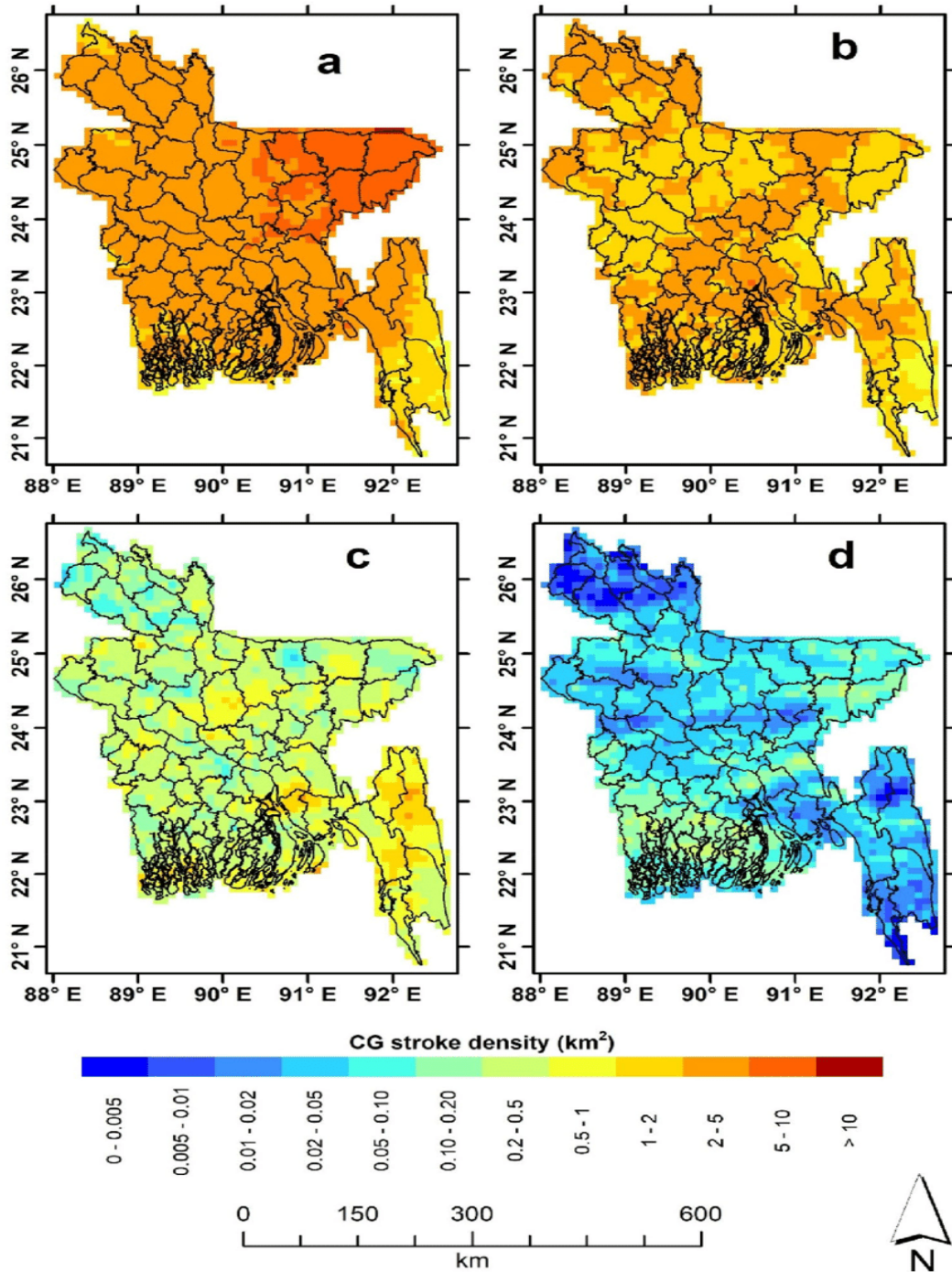


Fig. 2.13: Seasonal CG stroke density over Bangladesh; a pre-monsoon; b monsoon; c post-monsoon and d winter. District boundaries are superimposed on gridded CG stroke density [82].

The analysis, normalized by season length, shows that lightning density (strokes per km² per season) varies across seasons, with pre-monsoon (MAM) having the highest density (Fig. 2.13a). In pre-monsoon months, cloud-to-ground (CG) strokes occur throughout the country, with the highest concentrations (>10) in four eastern districts (Sunamganj, Sylhet, Habiganj, and Maulvibazar). During the monsoon period (JJAS), lightning density decreases nationwide, with the highest density primarily in Sunamganj and Shariatpur districts (Fig. 2.13b). The maximum CG strokes in MAM also decrease in JJAS for the two eastern districts (Mouvbazar and Sylhet). As the post-monsoon (ON) period begins, stroke numbers significantly decrease, with densities not exceeding 1.0 stroke per km² (Fig. 2.13c). Chittagong Hill Tract (CHT) districts and the central coastal region have the highest stroke density during ON. In the winter season, there is a substantial reduction in CG stroke density, with the southwest and central coastal districts experiencing a maximum density of 1.0 stroke per km² (Fig. 2.13d).

2.8.3 Detection Efficiency

The DE of a network is difficult to quantify precisely, as it can vary based on a number of factors, including the location and orientation of the sensor, the atmospheric conditions, peak current, minimum detectable energy, station outage effect, detection range of station, triggering threshold, VLF propagation and the characteristics of the lightning discharge being detected [1], [16], [15]. It's also can vary depending on the location and time of day. The WWLLN network is designed to provide reliable lightning detection coverage around the world, and its sensors are continuously monitored and maintained to ensure accurate and timely lightning location data. But the WWLLN hasn't seen lightning everywhere with the same DE. This is due to the shifting WWLLN station coverage as well as the significant impact of surface electric conductivity and ionospheric conditions on VLF radio transmission along a wave's great circle course [16]. Several comparative investigations have been conducted between WWLLN and other ground-based networks or satellite observations. Some refer to it as relative DE while others refer to it as absolute DE. However, accurately determining the absolute DE of a networks has been a challenging task, as no network can detect every single lightning event that occurs on Earth.

2.8.3.1 WWLLN detection efficiency dependable factor

Comparing the WWLLN network's observations with those from MF/HF lightning detection networks in Australia, Brazil, and America has allowed researchers to assess the

location accuracy and regional DE of the network (e.g., Lay et al., 2004 [83]; Rodger et al., 2004 [84]; Jacobson et al., 2006 [85]). These studies showed that WWLLN does identify strong lightning discharges in different parts of the Earth. They also made estimates for the global location accuracy and confirmed that the DE is low, with only a few percent of global lightning activity being picked up (e.g., Rodger et al., 2005 [15]).

Past work by Rodger et al. [15], the mean lightning rate reported by the network can give you a rough idea of the WWLLN area DE. In contrast, the mean “high quality” WWLLN lightning rate in 2004 was 0.63 per second, indicating that the WWLLN detected very roughly 1.5% of the global total lightning. Taking into account the point in [15], about how IC and CG discharges are found, this means that in 2004, WWLLN reported good locations for about 2.3% of global CG activity. By comparing the regional maximums on the Carnegie curves to the WWLLN data, it is possible to get a rough idea of how WWLLN DE changes in different parts of the country [15]. This study found that the WWLLN DE changed a lot from place to place. For example, the DE in the Maritime Continent was about three times bigger than in the Americas.

As noted by Rodger et al. [1], analyzed the DE of the WWLLN by comparing the data obtained from the New Zealand lightning location network (NZLDN) in April 2006 with 25 WWLLN operational stations. This research demonstrates that WWLLN likes high peak current return stroke lightning discharges, and in 2005, the network will have identified around 12% of the world's elve-producing lightning. Keep in mind that the absence of a lower peak current threshold in the NZLDN data has an impact on this DE. Fig. 2.14, showing the variation in the WWLLN CG stroke DE against NZLDN-determined return stroke peak current using 10 kA bins. This tendency was also reported by Abreu et al. [3], the study has been attempted to analysis the performance of WWLLN via compared with Canadian Lightning Detection Network (CLDN). A similar approach was taken in the comparison of lightning observations between the Los Alamos Sferic Array and WWLLN [85]. Even though the average WWLLN DE for all CG discharges reported to NZLDN is only 3%, it is much higher for the bigger peak currents, at 9%–10% for return stroke peak currents >50 kA. Beyond 80 kA, there aren't many people, so it's hard to get good data, but the 10% relationship seems to hold.

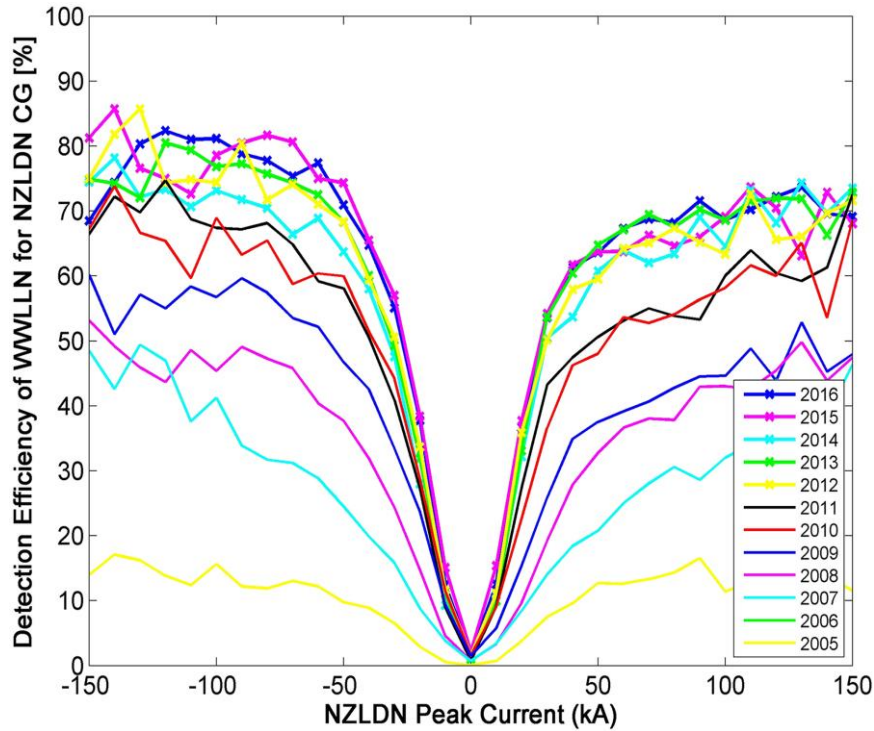


Fig. 2.14: Variation in the WWLLN CG stroke DE with NZLDN-determined return stroke peak current [1].

Rodger et al. [1] said that as the WWLLN network grew, so did its DE. Abarca et al. [2] compared WWLLN's DE with the U.S. National Lightning Detection Network (NLDN) and found that WWLLN's 28–38 world stations caught 10.3% of all cloud-to-ground strokes and 4.8% of all in-cloud strokes. About the same time, Abreu et al. [3] compared the 2008 WWLLN DE to the CLDN near Toronto and found similar results for 2008. They saw that the WWLLN DE for strokes with peak currents above 50 kA was over 50%, which was the same as Fig. 2.14 for that year.

Between 2010 and 2018, as the WWLLN network grew, the number of strokes that could be found went from 139 million to 233 million. This is a 67% increase over the study time. In the Rudlosky and Shea et al. [69], which compared WWLLN and TRMM-LIS data for 2009-2012 flashes, a DE of 9.2% was found in 2012, with the WWLLN DE rising to 17.3% over water and 6.4% over land. During the mid-data period for this study, between 2012 and 2014, Burgess et al. [55], compared WWLLN DE to TRMM/LIS and found that more than one stroke was found by WWLLN during a TRMM/LIS flash. This is called a 1.5 times multiplicity. This means that WWLLN picked up almost all of the TRMM/LIS flashes, while TRMM/LIS only picked up about 70% of the WWLLN strokes in the

TRMM/LIS field of view, which said that below the expected DE for the TRMM/LIS instrument.

These studies, which compared lightning monitors on the ground and in space, suggest that the WWLLN's DE for strong lightning strokes during this superbolt study [17] ranged from about 50% to over 80% of all strokes with peak currents of more than 50 kA. Also, WWLLN's DE is likely to be two to three times higher over the seas than it is over land. In Fig. 2.15 [1], the relationship between the number of WWLLN stations involved in location finding and the peak current of CG return stroke determined by NZLDN is shown.

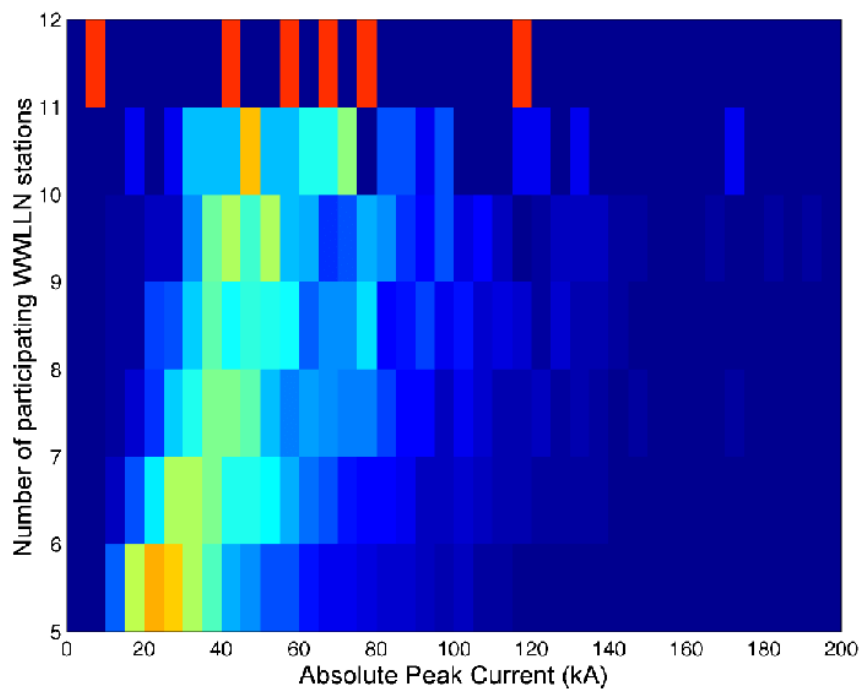


Fig. 2.15: The relationship between the distribution of NZLDN CG return stroke peak currents and the number of participating WWLLN stations [1].

As more stations participate, there is a shift towards higher peak currents, indicating a correlation between peak current strength and spheric amplitude triggering more WWLLN stations. The color scale denotes the number of stations participating, with hotter colors indicating more stations.

The WWLLN DE is shown in Fig. 2.16 taking this into consideration. Be aware that this results in extremely differing detection efficiencies in Australia and New Zealand. Only over half of the DE for South-Eastern Australia recorded for a single day of lightning

sightings in January 2004 was calculated [15]. This apparent decrease is likely due to the variable character of the network and the diminishing efficiency of the current TOGA combination algorithm as the number of global stations increases.

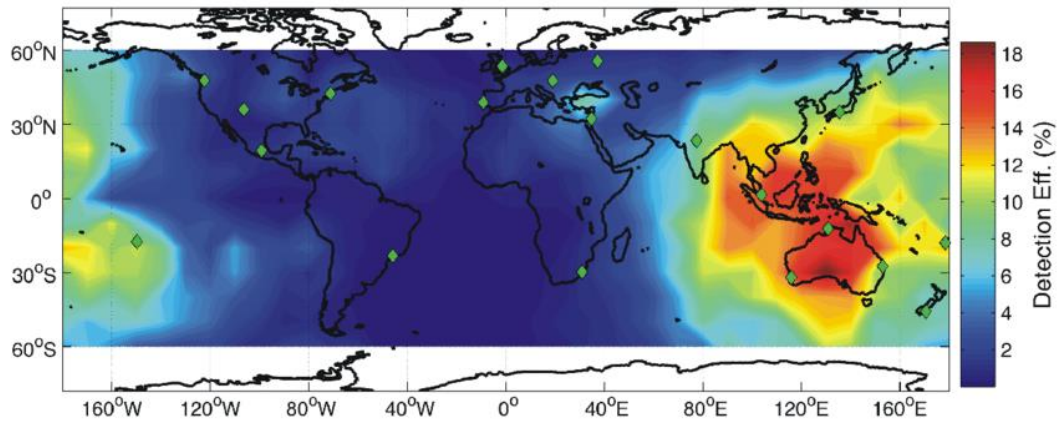


Fig. 2.16: Globally variable WWLLN CG DE estimation based on modelling and comparison to the NZLDN commercial network. Modelling of the ionospheric conditions at 12:00 UT on 16 April 2005[1].

As WWLLN relies upon propagation of the VLF spheric beneath the ionosphere, WWLLN detection efficiencies will depend on the changing nature of the ionospheric D-region. Rodger [1], repeated the LWPC calculations for global ionospheric conditions on two specific dates: 00:00 UT on 16 April and 12:00 UT on 16 October. Fig. 2.16 shows the WWLLN DE for 00:00 UT on 16 April, which displays the largest differences in VLF propagation compared to Fig. 2.17.

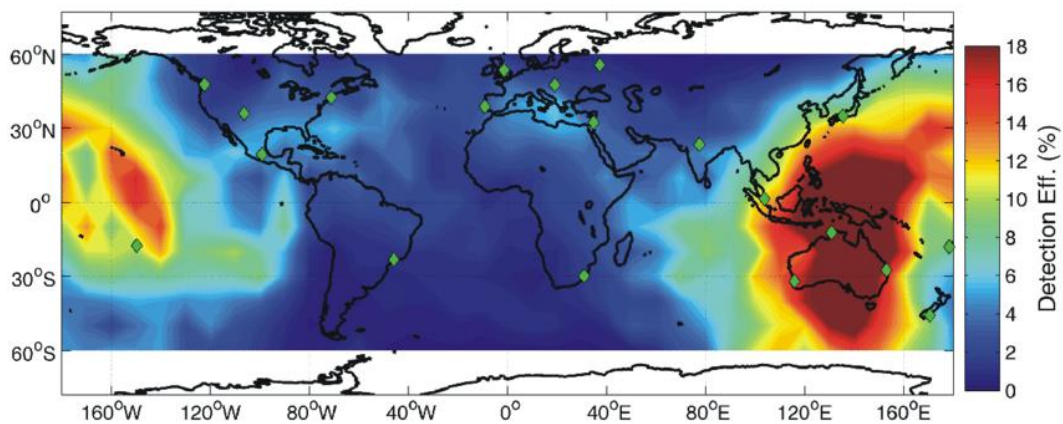


Fig. 2.17: Globally varying estimated WWLLN CG DE, for comparison with Fig. 3.3. Modelling undertaken with the ionospheric conditions expected for 00:00 UT on 16 April 2005 [1].

The Maritime Continent has significant increases in estimated DE due to less attenuation of VLF beneath the nighttime D-region. In Europe and the Americas, the dominant factor determining the DE of WWLLN is station locations and thresholding. In Australia, there is a slight increase in DE by 3-5%, while the largest improvement of 10% occurs for locations near Papua New Guinea. The change near Papua New Guinea corresponds to a significant increase in DE by approximately 25%, indicating the importance of diurnal cycles in VLF propagation for the WWLLN DE. However, the differences between April and October are negligible, with no DE differences larger than 1%. Fig. 2.18 illustrated the behavior of a typical WWLLN station, showing two distinct patterns of participation.

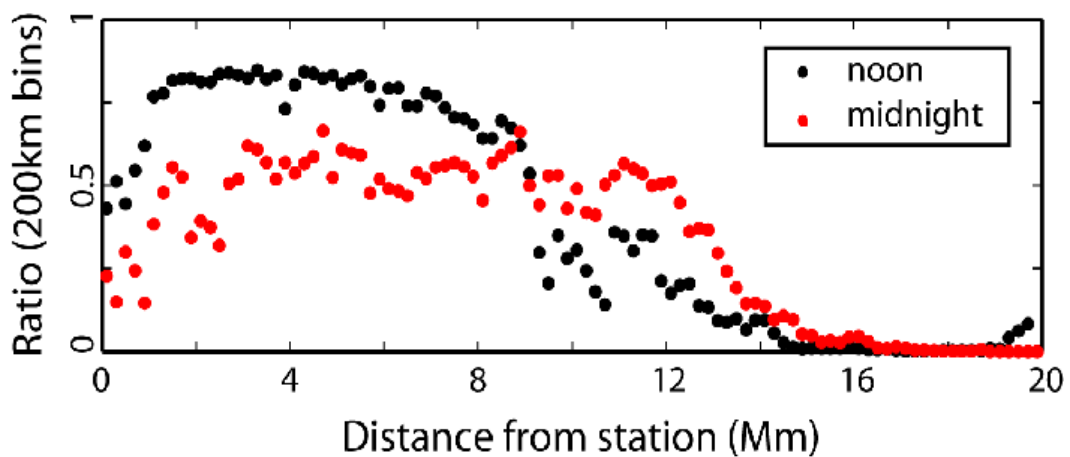


Fig. 2.18: Ratio of the number of events detected by the Darwin station to the number of events detected at the same range from Darwin network as a whole. [1].

The black dots from Fig. 2.18, shows this ratio for ± 2 h around local noon, while the red dots are for ± 2 h around local midnight. During the day (black), the station detects lightning stroke up to a distance of approximately 8,000 to 10,000 km, which is about one-quarter of the circumference of the Earth. At night (red), the station can detect lightning stroke up to a distance of 12,000 to 13,000 km. The participation of a typical station is roughly constant at these distances during both the day and night. However, the Fig. 2.18 also showed that the DE decreases for stroke that occur closer to the station than 500 km. This decrease in efficiency is due to the fact that as lightning signals propagate in the Earth's ionosphere waveguide, the higher modes are attenuated more strongly than the lower modes, causing the signal to be distorted. Therefore, each WWLLN station uses a simple VLF waveform with a $1/\sqrt{f}$ dependence to analyze the signal and obtain the location of the lightning stroke.

2.8.3.2 Analysis of WWLLN DE compared to other the instruments and networks

Current DE of WWLLN in comparison to another ground based network is up to 80% for strokes over 40 kAmp's, as shown by R.H. Holzworth et al. [17]. Another study has been done by S. Rudlosky et al. [69], which attempted to determine the DE of WWLLN by evaluating 4 years (2009–2012) of WWLLN data relative to the TRMM-LIS. In this study, flashes detected by LIS were matched with strokes detected by WWLLN. To determine the DE of WWLLN relative to LIS. The authors found an improvement from 6% in 2009 to 9.2% in 2012 in the Western Hemisphere between 38°N and 38°S. Kasereka et al. [12] estimated the DE of WWLLN in the Congo Basin by comparing its data with LIS data from 2005 to 2013. This comparison demonstrates that the relative DE of the WWLLN in the 2500 km² region grows from roughly 1.70% at the start of the period to 5.90% in 2013, which is consistent with earlier results from other parts of the world. M.L. Hutchins et al. [70], calculated the absolute DE of WWLLN by comparing to the ENTLN over the continental United States and examined the relationship between the ENTLN peak current and the WWLLN radiated power per stroke data at many geographical and temporal scales. In this study, strokes detected by WWLLN were matched with strokes detected by ENTLN within 0.1° and 100µs.

2.8.3.3 Relative detection efficiency

The relative DE of WWLLN determines how effectively a certain area of the network is being observed in comparison to the network's best region. Understanding the variation of WWLLN DE across different locations and over time is important. M.L. Hutchins et al. (2012) [16], developed a method to correct for relative DE variations. WWLLN regularly publishes global relative DE data on a 1° × 1° global grid (available at <http://wwlln.net/deMaps>), which allows comparison of stroke density at different locations. After applying these corrections, the WWLLN data can be compared around the world as if DE were nearly constant everywhere. Over time, the relative DE corrections have become closer to 1.0 for most locations (typically ranging from 0.90 to 0.99), so they have little effect on the overall WWLLN data set. This means that WWLLN has relatively smooth DE on a daily basis around the world. However, these studies were conducted using the entire WWLLN data set, not just the high-energy population being studied. Therefore, further verification of the data set is necessary by comparing it one-to-one with other networks. In Fig. 2.19, a collection of four hourly maps from 15 June 2010 depicting the networks' relative DE every six hours from 00 UTC to 18 UTC are displayed.

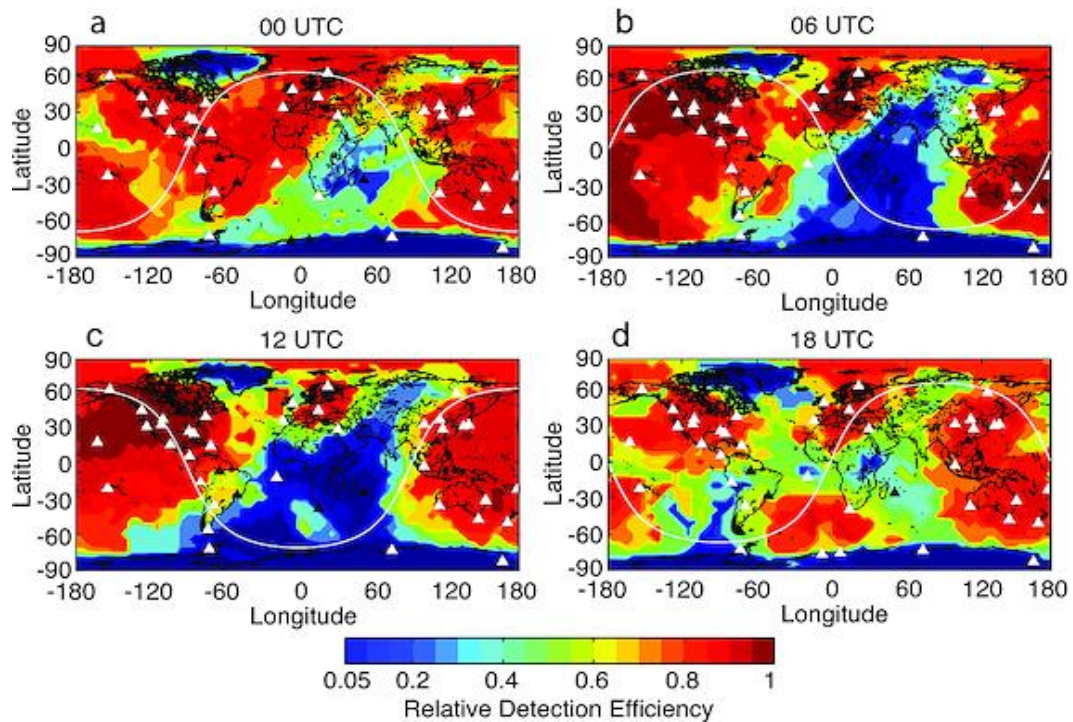


Fig. 2.19: Daily average relative DE for 15 June 2010. Stations are shown as triangles with operational stations in white, nonoperational in black, and operational for part of the day in grey. The minimum value of DE is set at 5% to prevent unphysical corrections [16].

In the above image, white dots represent operational stations during the hour shown, while black dots represent non-operational stations (defined as triggering over 500 strokes per hour). Four main factors affect the DE of these stations: local stroke activity, station density, and station performance, as well as the day/night terminator effect. From 00 UTC (Fig. 2.14a) until 18 UTC (Fig. 2.19d), the day/night terminator effect may be seen. An increase in local stroke activity during North American afternoon (Fig. 2.19a) leads to decreased DE as nearby stations raise their triggering thresholds. Station density and performance are interconnected, as poorly performing stations have a similar effect as removing them altogether.

2.8.4 WWLLN Lightning Strokes Energy

The WWLLN has been upgraded to monitor radiated VLF stroke energy as well as stroke locations. The network's capacity to monitor stroke energy, as well as its global coverage, enables a global comparison of stroke energies over land and ocean. Several investigations have been conducted on radiated electromagnetic energy of lightning strokes detected by

WWLLN. The median of far-field radiated electromagnetic energy of lightning strokes in the frequency band from 6 to 18 kHz is about 1000 J [5]. WWLLN recorded a global median stroke energy of 629 J in 2010, with a 25% average error in measured energy [16]. Fig. 2.20 depicts the global and regional distribution of energy, 97% of the strokes observed had equivalent energy levels.

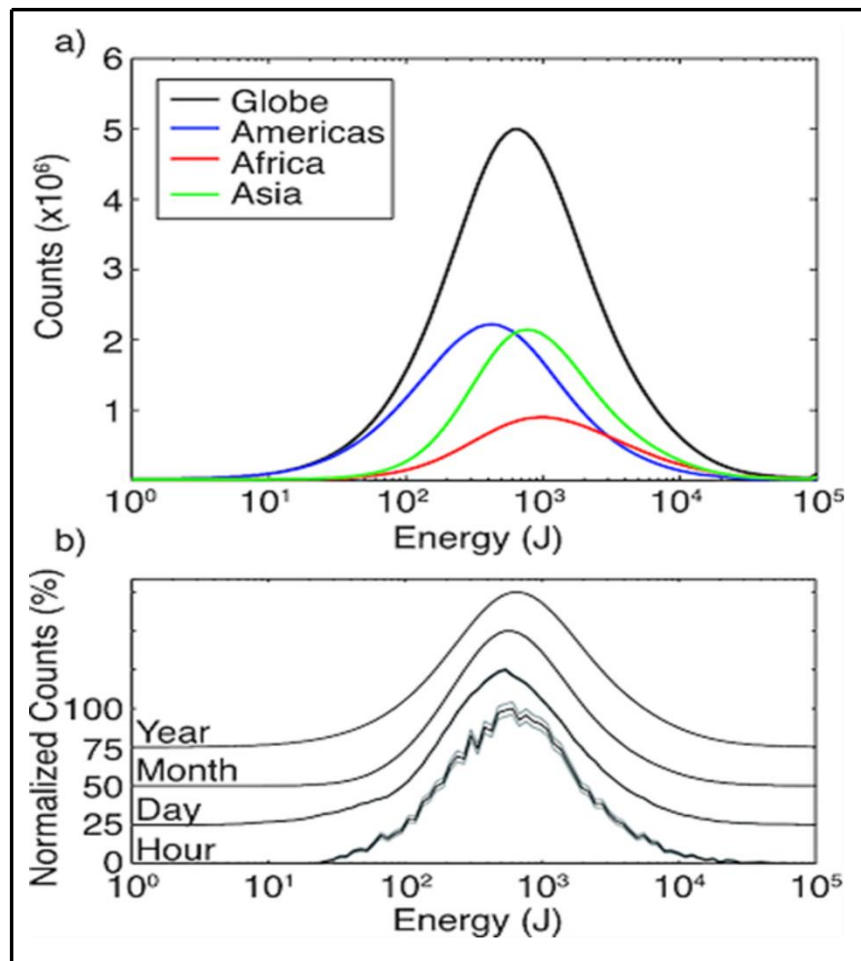


Fig. 2.20: (a) Shows how the WWLLN stroke energy is distributed around the world (in black), the Americas (in blue), Asia (in green), and Africa/Europe (in red). (b) WWLLN worldwide stroke energy distribution for the day (15 June 2010), the hour (9 UTC on 15 June 2010), the year (2010), and the month (June 2010). [16].

In Fig. 20a, the error bars (Poisson statistics) are omitted because they would be of the same magnitude or smaller than the line width. It is important to note that the distribution of strokes in each region follows a lognormal pattern [16], with the major differences between the Americas (-1800 E to -600 E), Africa (-600 E to 600 E), and Asia (600 E to 1800 E)

being the total strokes detected and the median energy, which are 399 J, 1101 J, and 798 J, respectively. The overall lower DE over Africa, particularly for low-energy strokes, results in a higher median energy than in other regions. Additionally, the energy distribution is lognormal within each region, from an hourly timescale to the annual distribution. In Fig. 20b, the annual lognormal distribution is displayed alongside the monthly, daily, and hourly distributions. It is only at the hourly distribution level that the errors become noticeable, while the distribution still remains fairly lognormal.

R.H. Holzworth et al. [17] showed the global distribution of super-bolts. This research looks at nine years of data from the WWLLN, which includes 2×10^9 detected lightning strokes from 2010-2018. This study reveals that the global mean of lightning strokes energy is 1000 J (shown in Fig. 2.21) and if the energy per stroke is more than 10^6 J, it is called super-bolts. M.L. Hutchins showed that the peak for any given subset in time and place can change from about 400 to 2,500 J, but it stayed in this range during their first study [5], [16], [73], which is in line with the current data shown in Fig. 2.21. M.L. Hutchins et al. [16] found that the distribution of energy on Earth still falls within this range, with the mean and median being close to 10^3 J.

As was already said, the dataset has more than 10^9 strokes, and all strokes with amplitudes above 106 J (brown shading in Fig. 2.21) have been looked at. To make sure that the big stroke sample is not tainted by wrong data, these criteria were used: the standard error of the energy fit is less than 30% of the energy for that stroke, and at least seven WWLLN stations identify the stroke. Rodger et al. [1], showed that there is a strong link between peak current and the number of WWLLN sites that pick up a stroke. In [16], authors found that there is a steady link between peak current and stroke energy. So, needing seven or more stations to be a part of this study doesn't limit the kinds of high-energy strokes that can be used. Instead, it gets rid of strokes where the energy could be hard to figure out because there weren't enough stations involved. Fig. 2.21 shows, however, that the high-energy part of the distribution used in this study (brown shading) is an extension of the whole world energy distribution and is the top of the log-normal energy distribution.

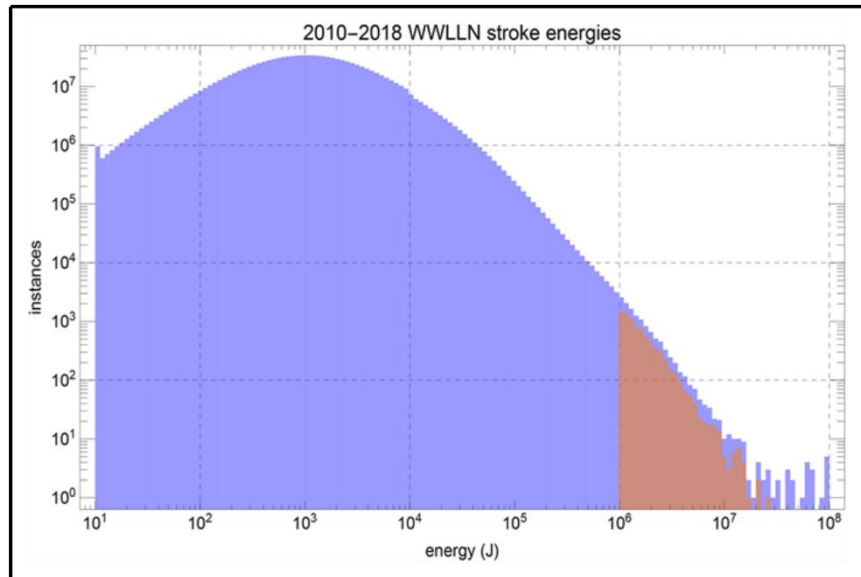


Fig. 2.21: Distribution of stroke energies for WWLLN data set including the 9 years 2010 to 2018 (blue). The brown colored distribution above 10^6 J presents the distribution that is call super-bolts [17].

Another study has been done by M.L. Hutchins et al. [73], in this study, WWLLN data from May 2009 through May 2012 is investigated to determine the global distribution of lightning strokes energy and developed a linear regression technique to take into consideration its temporal and spatial fluctuation. The authors came to the conclusion that there is a significant energetic difference between landmass and ocean lightning, which leads to a higher fraction of more powerful strokes over the oceans. They supported their findings with data from the LIS, the OTD, and the ENTLN. Turman et al. [86] identified the strokes optical energy using optical strokes data detected by Vela satellite that is 100 times more powerful than usual lightning and discovered 20 strokes in the super-bolts category. Kolmasova et al. [58] depicted lightning activity across northern Europe during a severe winter in 2008–2017. During the colder months (Dec, Jan and Feb), the mean energy of recorded strokes was two orders of magnitude higher than the global mean stroke energy of 1 kJ. For the first time, their investigation found that winter super-bolts with stroke energy over 1 MJ occurred at night and early morning.

2.8.5 Lightning Prediction

For both research and forecasting purposes, it is crucial to describe lightning activity in various geographic locations. Strong evidence suggests to a link between flash rate and other thunderstorm characteristics, such as precipitation rate [87], [88]. In addition, there is

a growing interest in studying the modulation of lightning distribution and frequency by inter-annual phenomena, such as regional variations, as well as the impact of climate change on lightning activity [89]. The unavailability of long-term time series data is one of the primary difficulties to this type of study. However, the lightning prediction has gained increasing attention during the past decade by developing several prediction models using both space-based and ground-based data.

The lightning forecasts are based on the work of McCaul et al. [74], who determined the statistical link between the model-derived graupel flux in convective clouds and the overall ice content to determine the total lightning flash density. Yair et al. [75], describe the development and use of the Lightning Potential Index (LPI), obtained from the output of a Weather Research and Forecasting (WRF) model. Lynn et al. [76], developed statistical method for estimating cloud-to-ground and overall lightning flash density with the WRF model. As with previous statistical techniques, the lightning prediction schemes of [74], [76], assume that the quantity of lightning flashes depends on certain temporal and geographical averages of parameters derived from model fields. M. Gharaylou et al [77], developed another prediction scheme based on WRF-ELEC model. The severity, frequency, and certain physical and dynamic features of lightning strokes from 2004 to 2014 are examined. The observational data from the Iranian Meteorological Organization (IRIMO), ground-based lightning data from the WWLLN, and satellite-based lightning data from the TRMM-LIS were used in the study. The results show that there is a good agreement between the simulated time-averaged horizontal patterns of the Lightning Potential Index (LPI) obtained from the locations of lightning occurrence of WWLLN data as well as LIS observations. A general lightning data assimilation technique is developed and tested with observations from the WWLLN is shown in [90], where author's used WWLLN data ingested into the WRF weather prediction model, to show that predictions were greatly improved in both precipitation and timing predictions with the inclusion of the WWLLN data. This approach is applied to both deterministic and ensemble forecasts of the 29 June 2012 derecho event over the eastern United States and a deterministic forecast of the 17 November 2013 convective event over the Midwest using the WRF Model run at a convection-permitting resolution.

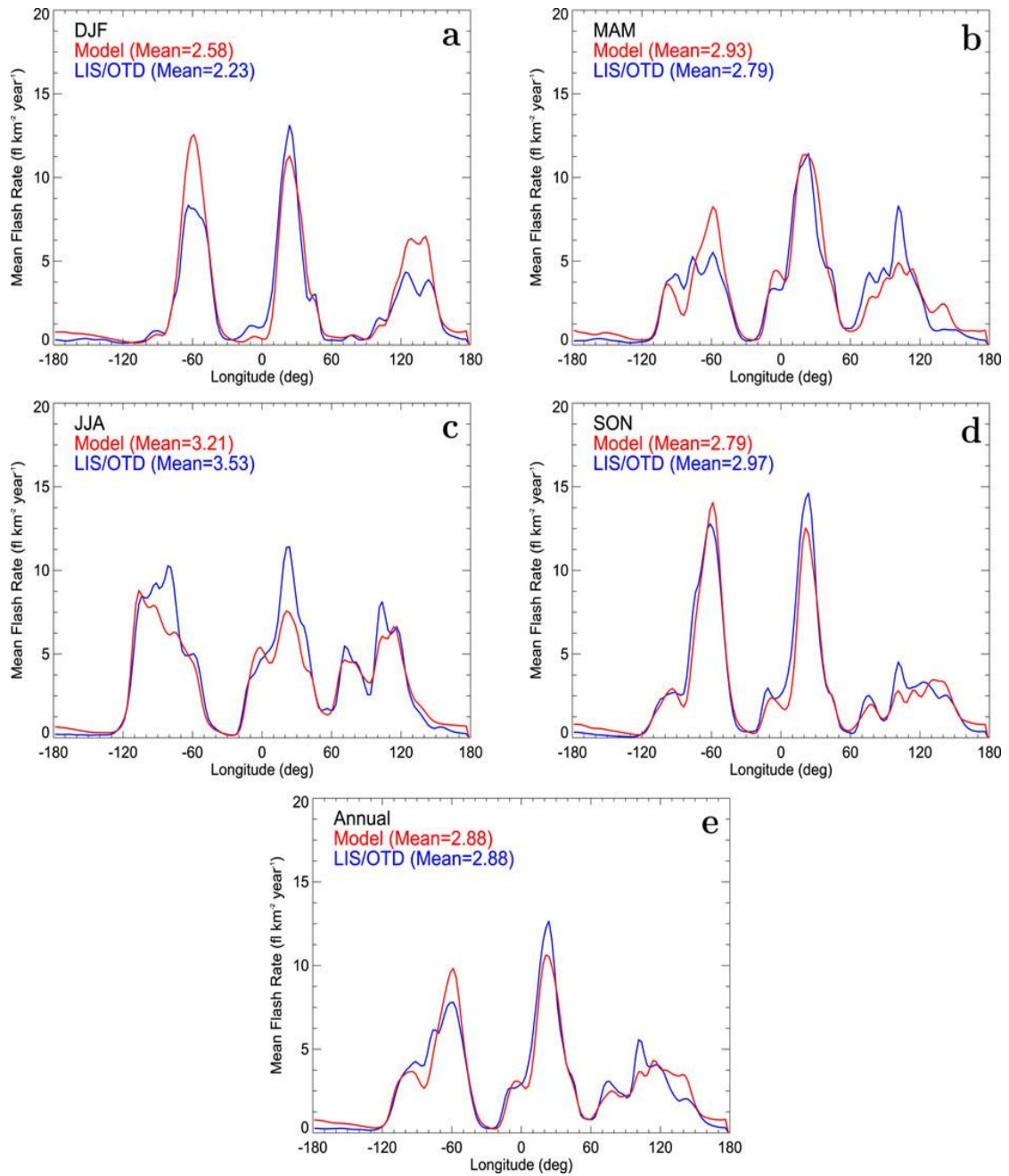


Fig. 2.22: Seasonal and yearly meridional mean lightning flash densities for (a) winter, (b) spring, (c) summer, (d) autumn, and (e) the whole year from the LIS/OTD 1995-2010 climatology and the year-long 80-km global simulations from 1999 to 2008. Flashes $\text{km}^{-1} \text{year}^{-1}$ are used to indicate flash densities. [78].

Philippe Lopez et al. [78] introduced a new parameterization to diagnose lightning flash densities for the European Centre for Medium-Range Weather Forecasts (ECMWF) Integrated Forecasting System (IFS), including its tangent-linear and adjoint versions. They conducted a decade-long experiment to calibrate the yearly mean global flash density

against the LIS/OTD climatological value. The lightning concentration predictions were found to be mostly independent of the model's horizontal resolution.

Fig. 2.22 displays a comparison between the meridional mean lightning flash densities from the model and LIS/OTD data for each season and the entire year. Overall, the pairs of curves show excellent agreement, with some overestimation in the simulations over the Americas and Asia during winter (Fig. 2.22a) and underestimation over the Americas and Africa during summer (Fig. 2.22c).

2.9 Summary

This chapter provides a comprehensive overview of lightning, exploring the scientific principles behind charging mechanisms in thunderstorms and various forms of lightning, including intra-cloud, cloud-to-ground, and cloud-to-cloud. Transient luminous events, such as sprites, elves, and blue jets, are also discussed. The chapter examines lightning detection systems, comparing ground-based and space-based systems, and their respective advantages and limitations. The chapter also concludes by presenting a literature review for the thesis, examining sources that address lightning DE, climatology, energy, and location and time accuracy. The literature review helps identify research gaps and opportunities for the thesis. The next chapter will outline the methods of analysis used to investigate research questions and achieve thesis objectives. The next chapter will focus on determining the DE of WWLLN at a specific geographic location, considering a 10,000 km radius around Dhaka station.

CHAPTER 3

LIGHTNING DETECTION ANALYSIS

3.1 Introduction

The ENTLN and the WWLLN are ground-based lightning detection networks operating in a number of countries all over the globe. The lightning detection technology has been improved and the numbers of sensors/ stations in both networks have been increased in the past few years. The ENTLN is a total lightning network utilizing 1800 wide-band sensors (1 Hz to 12 MHz) [37]. The WWLLN network does not always record lightning with the same DE. If a location has maximum number of station, that's mean these location detects maximum number of strokes and the DE of WWLLN for this location will be maximum. The concern of this chapter is to determine the DE of WWLLN at 20°S to 70°N and 40°E to 141°E (10,000 km center of Dhaka station).

3.2 Method of Calculation Detection Efficiency

In this study, the DE of the WWLLN relative to the ENTLN was examined in a chosen region, using two different approaches. M.L. Hutchins et al. [70], compared WWLLN to the ENTLN to determine the DE over the continental United States of America (25°N to 50°N and 120°W to 70°W) and detected 2.1×10^7 strokes and 2.9×10^8 strokes respectively and identify lightning matched strokes that occurred within a 0.1° and 100 microsecond range of each other. The first approach of this study involved analyzing ENTLN and WWLLN data to identify lightning matched strokes that occurred within a 50 km and 100 microsecond range of each other. This study performed this calculation for four months, two months when the Dhaka station was fully active (November- December, 2021) and another two months when the Dhaka station was not yet established (June- July, 2021).

This analysis provides valuable insights into the impact of adding the Dhaka station to the WWLLN network on stroke DE also accounted for others WWLLN stations that are new or go on and off during the period of investigation. Additionally, it is known that the DE of WWLLN does not change significantly over the year. Therefore, the analysis for these four months can provide a reasonable estimate of the changing DE of WWLLN on a yearly basis. The DE of WWLLN relative to ENTLN was then calculated based on the number of matched strokes detected by each network. The ENTLN data could be limited to CG strokes, which are known to pose a greater risk to human life. The DE of WWLLN relative to ENTLN for CG strokes could be reported separately. Previous studies on the WWLLN

have suggested that the network can also detect intra-cloud (IC) lightning discharges. Rodger et al. [1] showed that, there were 7536 WWLLN discharges reported that did not matched with the NZLDN cloud to ground (CG) strokes. However, 190 of these discharges occurred within ± 0.5 ms of NZLDN reported ICs, suggesting that about 1% of the NZLDN reported ICs were also detected by WWLLN. On the other hand, there were 7346 WWLLN locations that did not correspond to any reported CG or IC strokes by NZLDN. An analysis of the Los Alamos Sferic Array [91] suggests that the majority of these "missing" WWLLN locations are likely IC discharges that NZLDN did not report [85]. Since WWLLN does not determine stroke type, only ENTLN CG strokes would be analyzed, and any matches with WWLLN data would indicate that the stroke was detected by both networks. This study focused on developing a CG DE model based on the well-known distribution of CG return stroke peak currents. In addition, this study also investigated the relationship between the time and location accuracy of lightning stroke detections by the two networks.

The second approach involved analyzing the AP data (WWLLN AP-file) to identify lightning strokes that used information from the Dhaka station. The number of stations for each stroke will then be determined, with a focus on those strokes with exactly 5 total stations participating. These strokes would not have been detected by WWLLN without Dhaka, so the number of strokes with Dhaka data will be compared to the total number of 5-station strokes to determine the percentage that are now possible because of the addition of Dhaka. All WWLLN data will be used for this calculation, not just strokes in the region of Bangladesh. As noted by Rodger et al. [1], to produce a good observation, at least 5 WWLLN stations are required. While only 4 stations are needed for a distinct location, using 5 provides better elimination of multi-packet sets, resulting in higher quality locations. To determine the 5 stations with the largest changes in the VLF waveform received at the WWLLN stations, which are caused by lightning discharges. These 5 stations are the bare minimum required for producing a high-quality location. Based on the electric field change thresholds required for all five stations to activate, the WWLLN can determine the minimum return stroke peak current required to detect lightning at a given location. This method provides valuable insights into the impact of adding a new station to the ENTLN network and can be used to improve lightning detection systems in the region.

3.3 Contrasting the WWLLN and ENTLN

Both ENTLN and WWLLN locations were limited to a spatial window around Asia with specific longitude and latitude limits. The spatial window covered longitudes from 40° E to 141° E and latitudes from 20° S to 70° N, which included all areas of high DE for ENTLN. A total of 13656342 ENTLN CG strokes were detected in June-July and 8386049 ENTLN CG strokes in November-December, while 9353828 WWLLN strokes were detected in June-July and 7694767 WWLLN strokes in November-December, indicating that ENTLN detected approximately 1.45 times more lightning strokes in June-July and 1.1 times more in November-December than WWLLN. Fig. 3.1 and Fig. 3.2 depict the number of WWLLN stations that are new or intermittent during the months of June-July and November-December, respectively.

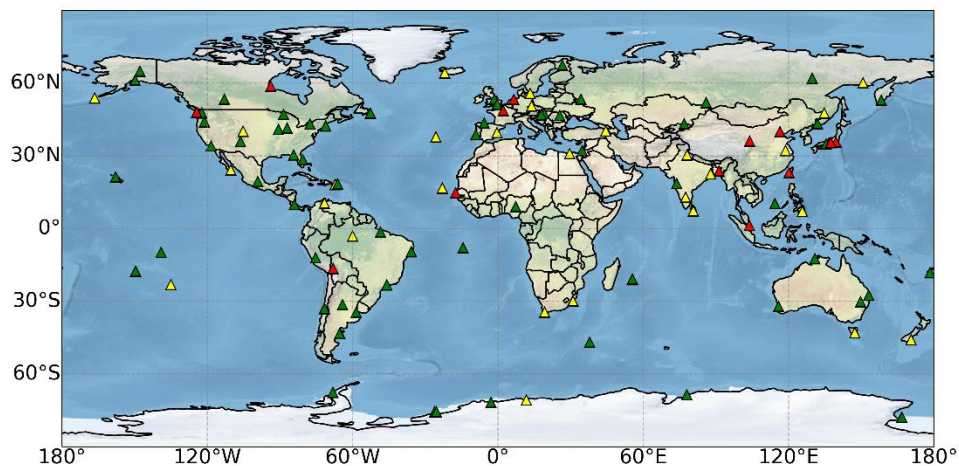


Fig. 3.1: Locations and hosts of the 111 VLF receiving stations operating in the VLF WWLLN stations as of June–July 2021. The green triangles indicate the stations were functional, while the yellow triangles indicate the stations were weak, and the red triangles indicate the stations were not functional during the period of investigation.

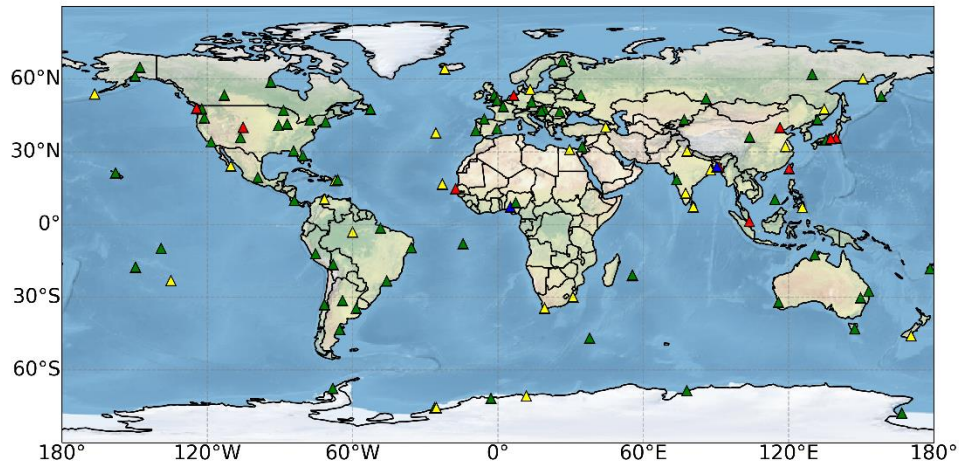


Fig. 3.2: Locations and hosts of the 113 VLF receiving stations operating in the VLF WWLLN stations as of June–July 2021. The green triangles indicate the stations were functional, while the yellow triangles indicate the stations were weak, and the red triangles indicate the stations were not functional during the period of investigation. The stations that were newly hosted were shown in blue triangles.

Unlike previous studies, the NZLDN lightning locations offered nanosecond time resolution, while WWLLN data provided $1\mu\text{s}$ resolution, which is sufficient for DE requirements. To compare the location estimates for CG lightning discharges between ENTLN and WWLLN, events within $100\mu\text{s}$ time resolution and 50km spatial separation of an ENTLN-detected lightning event were selected in the chosen region. The time difference and spatial separation limits differ from those used in earlier studies [15], [83], [84]. Nonetheless, the high time resolution of ENTLN and WWLLN data should be adequate to determine all matching events.

Under these constraints, 893,773 WWLLN lightning discharges matched ENTLN CGs, yielding an average DE of 6.54% for June-July, while 1,393,031 WWLLN discharges matched ENTLN CGs, resulting in an average DE of 16.61% for November-December. Table 3.1 displays the number of detected strokes by both networks over the selected period and region.

Table 3.1: Total number of lightning strokes reported by ENTLN and WWLLN

Date	ENTLN	WWLLN	Matched	DE (%) (CG Strokes)
June-July 2021	13656342	9353828	893773	6.54
Nov-Dec 2021	8386049	7694767	1393031	16.61

The DE is increased from 6% to 16% by adding Dhaka (23.81° N, 90.41° E) and Nigeria (7.29° N, 5.13° E) station in WWLLN. Note that there were four stations such as Kingston (42.98° S, 147.29° E), Valencia (39.51° N, -0.42° W), Milesovka (50.55° N, 13.93° E) and Paris (48.71° N, 2.23° E) which was remain weak in June-July 2021 but make functional in November- December. Also two station like La Paz (-16.53° S, -68.06° W) and Chili (33.02° S, -71.63° W) which was remain off in June-July 2021 but make functional in November-December. So the DE could be influenced by adding these station also influenced by the stations which was make functional in month of November- December but not operated on June-July. M.L. Hutchins et al [16], described that the overall performance of the network trends along with the total number of stations, the effects a single station turning on or off can have an effect on a large region of the global but only small effect on the network as a whole.

3.4 Time and Location Accuracy

Prior comparisons between WWLLN and other regional lightning detection networks utilized various criteria to define shared strokes. Lay et al. [83] and Rodger et al. [84] required strokes to be within 3 ms and 50 km, Jacobson et al. [85] demanded strokes be within 1 ms and 100 km, and Rodger et al. [1] set a limit of 0.5 ms. Rodger et al. [1] highlighted the microsecond resolution of WWLLN data, suggesting a time criterion alone should suffice for characterizing shared events. Following this criterion, Rodger et al. [1] found a mean time difference of 32 μ s for shared events (WWLLN - NZLDN), while Abreu et al. [3] observed a mean time difference of 35 μ s for shared events (WWLLN - CLDN). In Fig. 3.3 and Fig. 3.4 shows the mean (median) time difference between ENTLN and WWLLN for matching CG strokes during June-July and November-December respectively.

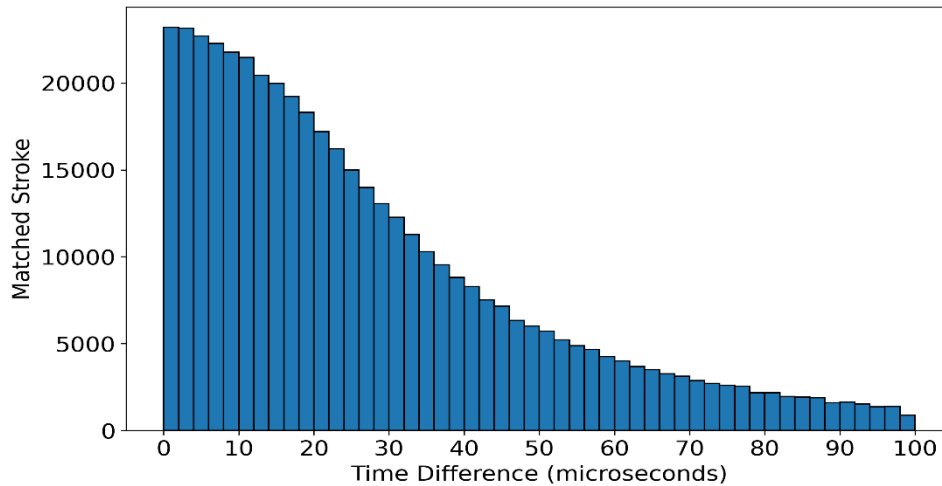


Fig. 3.3: Time difference (ENTLN-WWLLN) between the 893773 matching CG strokes detected by the ENTLN and WWLLN during June-July 2021. The mean (median) time difference is 27.27 μs (21 μs).

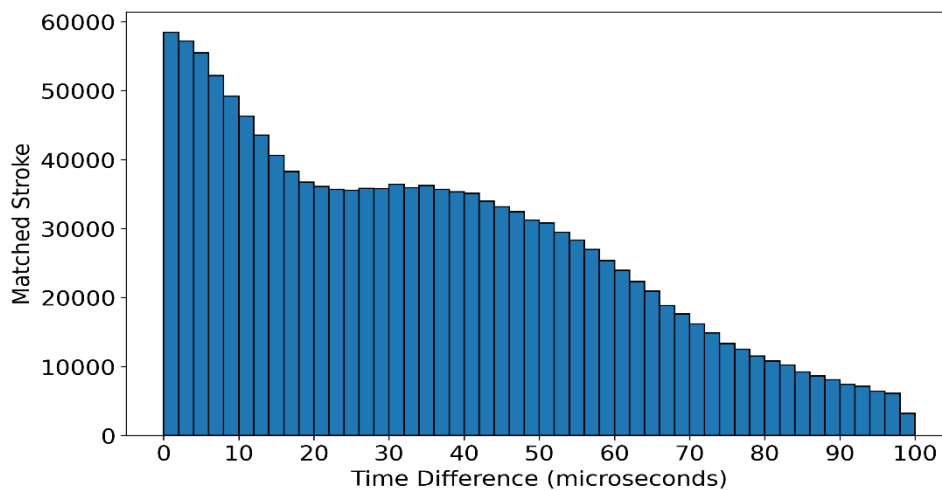


Fig. 3.4: Time difference (ENTLN-WWLLN) between the 1393031 matching CG strokes detected by the ENTLN and WWLLN during November-December 2021. The mean (median) time difference is 35.4 μs (33 μs).

By following through with this criterion, this study has found the mean (median) time difference between ENTLN and WWLLN for matching CG strokes was 27.27 μs (21 μs) during June-July 2021. During November-December 2021, the mean (median) time difference between ENTLN and WWLLN for matching CG strokes was 35.4 μs (33 μs). After plotting the matched strokes count at the function of location difference the mean (Median) accuracy has determined. The Fig. 3.5 and Fig. 3.6 shows the number of matched

strokes with respect to location difference. The statistical error bars (Poisson statistics) are plotted as they would be on the order (gray line), or smaller than, the line width.

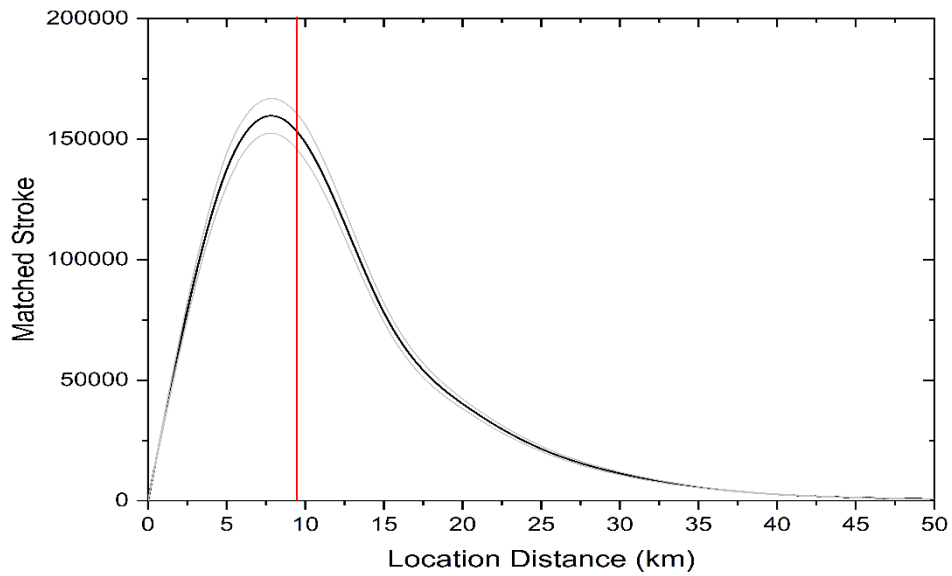


Fig. 3.5: Location accuracy (ENTLN-WWLLN) between the 8937731 matching CG strokes detected by the ENTLN and WWLLN during June-July 2021. The mean (median) distance is 9.62 km (7.57 km). Red line are the mean accuracy and grey lines are statistical count errors.

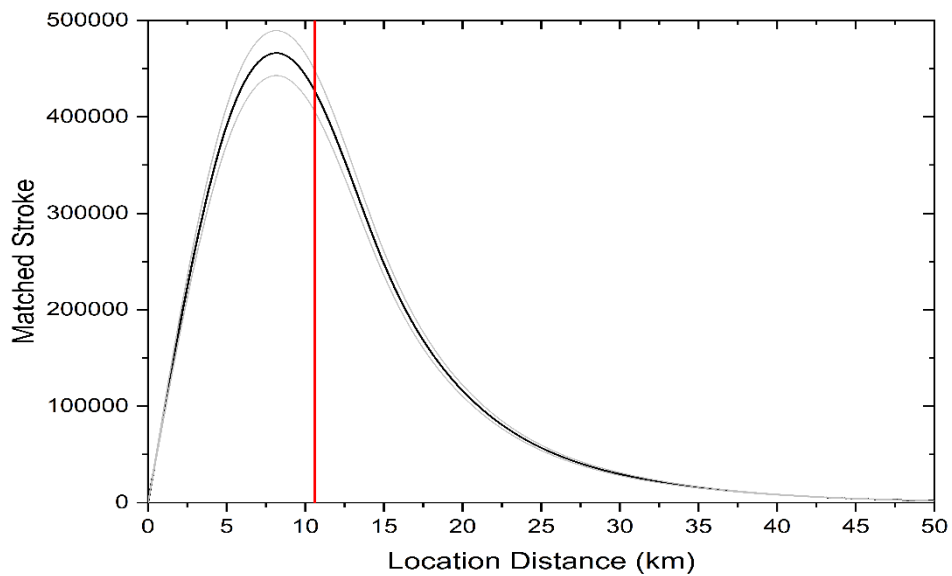


Fig. 3.6: Location accuracy (ENTLN-WWLLN) between the 1393031 matching CG strokes detected by the ENTLN and WWLLN during November-December 2021. The mean (median) distance is 11.33 km (8.13 km). Red line are the mean accuracy and grey lines are statistical count errors.

The mean absolute location accuracy was assessed in Abreu et al. [3], represented by the mean of the distances between shared strokes, yielding a value of 7.24 km with a standard deviation of 6.34 km. The first study to evaluate the absolute location accuracy of WWLLN was conducted by Lay et al. [83], which reported a value of 20.25 ± 13.5 km. In this study, the mean (median) location accuracy for matching CG strokes detected by ENTLN and WWLLN was found to be 9.62 km (7.57 km) during June-July 2021 and 11.33 km (8.13 km) during November-December 2021.

3.5 Variation in Detection Efficiency Due to Peak Current

The DE could be influenced by the peak current threshold, as previously described in section 2.8.3. In [3], noted that DE is negligible for peak currents below approximately 20 kA, but it ranges between 60% and 85% for higher peak currents, The DE was reaching around 70% at ± 120 kA. The mean positive peak current for shared strokes was 59.2 kA, while the mean negative peak current was -46.7 kA [3]. In an earlier study [1], the average WWLLN DE was only around 3% for all NZLDN-reported CG discharges, but it was considerably higher for stronger peak currents, being approximately 9-10% for return stroke peak currents greater than 50 kA. The mean absolute peak current for the CG strokes observed by both NZLDN and WWLLN was 46.2 kA, with a median of 37.5 kA. Another study comparing ground-based and space-borne lightning monitors suggested that the WWLLN's DE for strong lightning strokes during the super-bolt study [17] ranged from about 50% to over 80% for all strokes with peak currents exceeding 50 kA. This study also showed the variation of WWLLN DE due to ENTLN peak current. Fig. 3.7 shows the DE of the WWLLN relative to the ENTLN, as a function of peak current in 5-kA bins.

Fig. 3.7 indicates that DE is at its lowest for peak currents below approximately ± 20 kA for both negative and positive peak currents. As peak currents surpass ± 50 kA, the DE increases from 40% to 70%. The maximum DE reaches 42% for -80 kA negative peak current, while it exceeds 71% for 100 kA positive peak current. The mean positive peak current for ENTLN-WWLLN matched CG strokes was 48.7 kA, and the mean negative peak current was -44.2 kA.

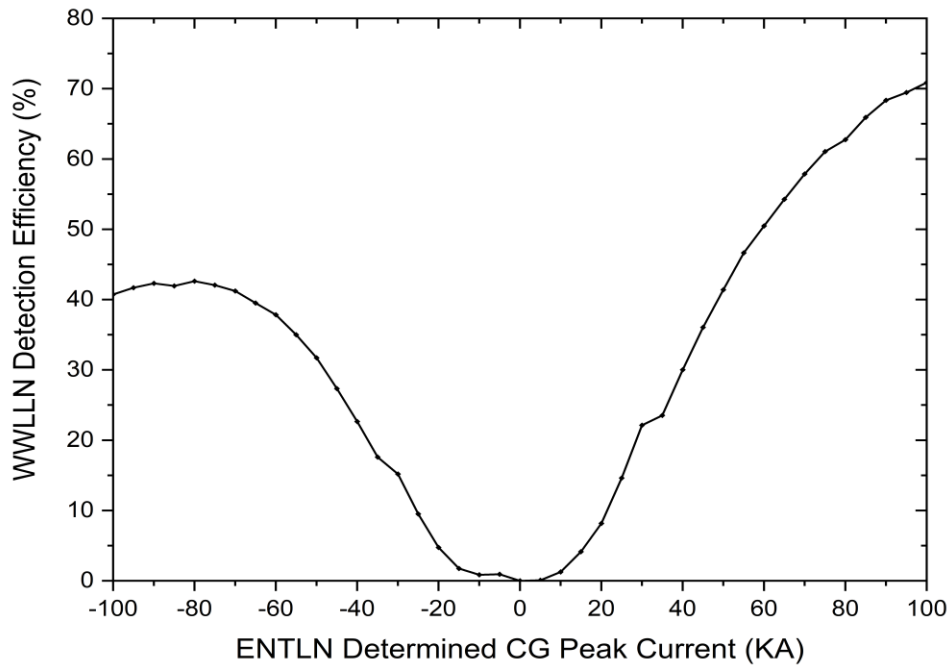


Fig. 3.7: Variation in the WWLLN CG stroke DE with ENTLN determined return pick current.

3.6 Analysis of Detection Efficiency Using WWLLN APfiles

The DE has also been calculated using WWLLN APfiles in this study. It determined the strokes that would not have been detected by WWLLN without the Dhaka station and quantified the increase in DE resulting from the addition of the new Dhaka station. Table 3.2 presents the total number of lightning strokes reported by WWLLN globally during November-December 2021, as well as the total number of lightning strokes detected by the WWLLN Dhaka Station during the same period.

Table 3.2: Total number of lightning strokes reported by WWLLN APfiles.

Duration	Total WWLLN Strokes	Total number of 5-station strokes	The strokes detected by WWLLN Dhaka Station	Detection Efficiency (%)
November-December 2021	38954740	13190462	596623	4.52

Table 3.2 presents the lightning stroke data collected during November-December 2021, emphasizing the significant contribution of the Dhaka station. Within the specified time period, the WWLLN network reported a total of 38,954,740 lightning strokes worldwide. Total number of 5-station strokes was 13190462. The strokes that would not have been detected by WWLLN without Dhaka station was 596623. The percentage increase in DE resulting from the addition of the Dhaka station 4.52%. This study effectively demonstrates the positive impact of the Dhaka station on the overall DE of the WWLLN network during November-December 2021.

3.7 Summary

In this chapter, the WWLLN data is analyzed alongside the ENTLN data to assess the DE over Bangladesh's landmass and to investigate the location accuracy relationship between ENTLN and WWLLN strokes. During the period under investigation, the DE of WWLLN improved from 3.96% to 4.37% over Bangladesh's landmass (as discussed in Section 5.2). The mean (median) accuracy was found to be 3.94 km (3.44 km) between October 2020 and September 2021, and 4.99 km (4.75 km) between October 2021 and September 2022 (also described in Section 5.2). The following chapter presents an examination of the characteristics of worldwide lightning climatology based on WWLLN lightning stroke data and ISS-LIS data, providing a broader context for the research findings.

CHAPTER 4

LIGHTNING CLIMATOLOGY

4.1 Introduction

Data from WWLLN for the year 2020 is examined to calculate the total number of lightning strokes globally. Concurrently, ISS-LIS data is investigated to determine the total number of flashes during the same time period. The chapter presents the features of worldwide lightning climatology based on both WWLLN lightning stroke data and ISS-LIS data, comparing the annual-mean lightning climatology of ISS-LIS and WWLLN. Additionally, this study showcases global maps using 1° by 1° grid box that depict the distribution of WWLLN lightning strokes in relation to ISS-LIS, covering both landmasses and oceanic regions. Seasonal and diurnal variations in lightning activity are also explored and described within this chapter, offering a comprehensive analysis of lightning patterns around the world.

4.2 Method of Analyzing Global Lightning Climatology

In this study, one year's worth of WWLLN data (2020) was examined to calculate totals of 214404020 lightning strokes. Side by side, the ISS-LIS data is investigated to calculate the total of 9942424 flashes in the same duration. These data are further distributed by landmass and oceanic region. The total number of strokes and flashes detected by WWLLN and ISS-LIS respectively over Bangladesh's landmass and Bay-of-Bengal has identified to calculate the flash density. The flash density is determined by the number of flashes/strokes per square kilometer per year. For seasonal variation two season has taken which is winter (1st Dec to 29th Feb) and summer (4th May to 3rd August). The summer is determined by identifying a large number of strokes/flashes and getting maximum number of lightning from 4th May to 3rd August. To determine the diurnal variation 24 hour local time are used. Fig. 4.1 shows the flow diagram for stages of the work done.

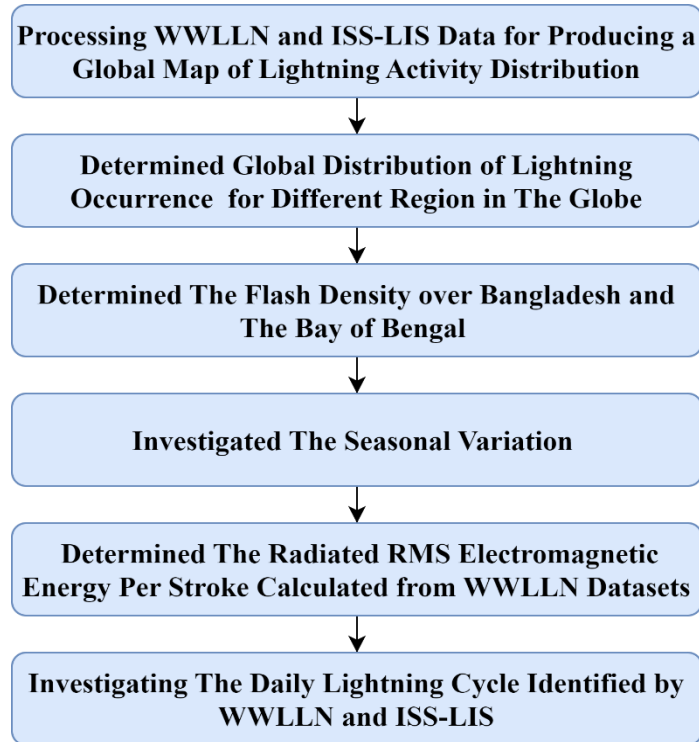


Fig. 4.1: Flow diagram for performing lightning climatology.

4.3 ISS-LIS vs. WWLLN Annual Lightning Climatology

The global distribution of lightning flashes identified by ISS-LIS during 2020 are shown in Fig. 4.2 and strokes identified by WWLLN during 2020 are shown in Fig. 4.3.

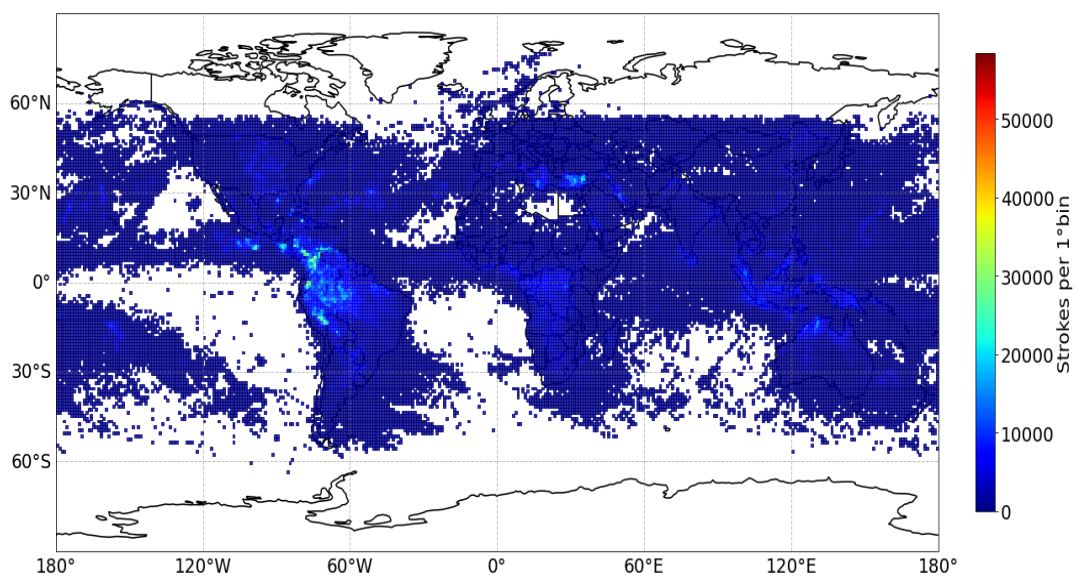


Fig. 4.2: A global map showing the frequency of occurrence of lightning. The spatial distribution of flashes identified by ISS-LIS.

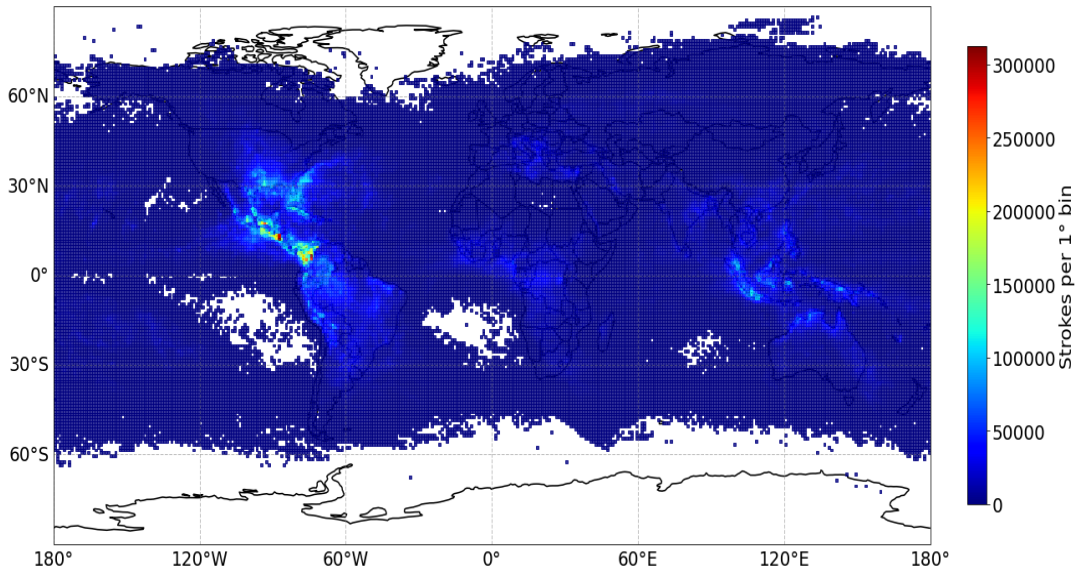


Fig. 4.3: A global map showing the frequency of occurrence of lightning. The spatial distribution of strokes detected by WWLLN.

Both the maps indicate concentration of lightning across major tropical continents (North America, South America, middle of Africa and maritime continent) with strong gradients near the coastlines and confirms the finding of [4]. The color bar of Fig. 4.2 and Fig. 4.3 indicates the number of flashes per 1° bin detected by ISS-LIS and the number of strokes per 1° bin detected by WWLLN respectively.

4.3.1 Regional Distribution of Lightning

To investigate regional differences in lightning distribution, the events are divided into the eleven global regions illustrated in Fig. 4.4.

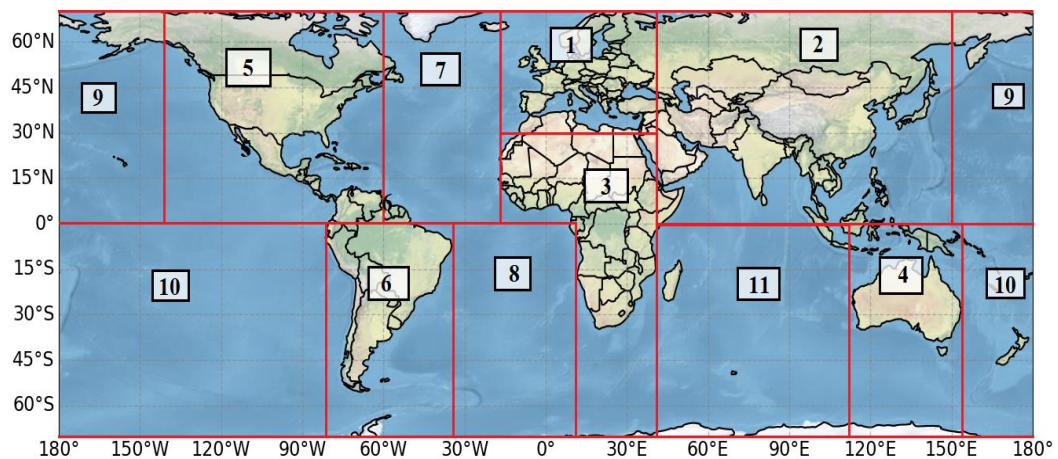


Fig. 4.4: The eleven broad regions used in this study. The thickness of the coastlines shows the size of the coastal region used in the land and ocean study.

The categorization results are presented in Table 4.1, with data organized into three columns corresponding to the following regions of interest: Region-1 (Europe), Region-2 (Asia), Region-3 (Africa), Region-4 (Australia), Region-5 (North America), Region-6 (South America), Region-7 (North Atlantic Ocean), Region-8 (South Atlantic Ocean), Region-9 (North Pacific Ocean), Region-10 (South Pacific Ocean), Region-11 (Indian Ocean).

Table 4.1: Global distribution of lightning occurrence in 2020

Region		Number of Strokes detected by WWLLN	Number of Flashes detected by ISS-LIS
Landmass	Region-1 Europe	4554624	130156
	Region-2 Asia	31685325	1040362
	Region-3 Africa	14910166	1426302
	Region-4 Australia	5758115	68602
	Region-5 North America	46892218	2058884
	Region-6 South America	27287291	511504
Ocean	Region-7 North Atlantic Ocean	12650247	1507779
	Region-8 South Atlantic Ocean	6051114	539562
	Region-9 North Pacific Ocean	15484255	893443
	Region-10 South Pacific Ocean	11889218	358428
	Region-11 Indian Ocean	37241447	1407402

According to the WWLLN strokes count, out of 214404020 detected strokes over the globe in 2020, 83316282 were detected over the ocean (region-7 to region-11) and 131087738 strokes over the landmass (region-1 to region-6), which is 40% and 60% respectively of total strokes around the globe in 2020. Table 4.1 shows the continent wise distribution of lightning occurrence detected by WWLLN and ISS-LIS. According to the ISS-LIS flash count, out of 9942424 detected flashes over the globe in 2020. Among these, 2047341 were detected across in the Atlantic Ocean (region-7 and region-8), 1251871 were detected in

the Pacific Ocean (region-9 and region-10) and 1407403 in the Indian Ocean (region-11). Which is 12.54%, 20.59% and 14.15% respectively of total strokes over the globe in 2020.

4.4 Seasonal Dependence of Lightning Phenomena

In 2020, the summer is determined by identifying a large number of strokes/ashes from 4th May to 3rd August. The months of December, January and February is considered as winter.

4.4.1 Lightning Flashes

The global distribution of lightning flashes detected by ISS-LIS during the winter and the summer are shown in Fig. 4.5 and Fig. 4.6 respectively. During summer, the lightning maxima lie along 30°N, Which was also observed in [4]. During winter, the lightning maxima shifts towards the low latitude region.

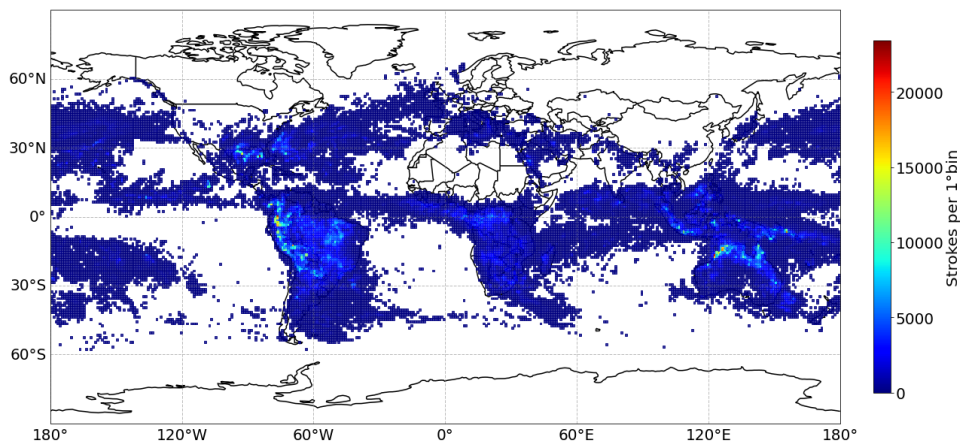


Fig. 4.5: Global distribution of ISS-LIS lightning flash during winter (1st Dec to 29th Feb 2020).

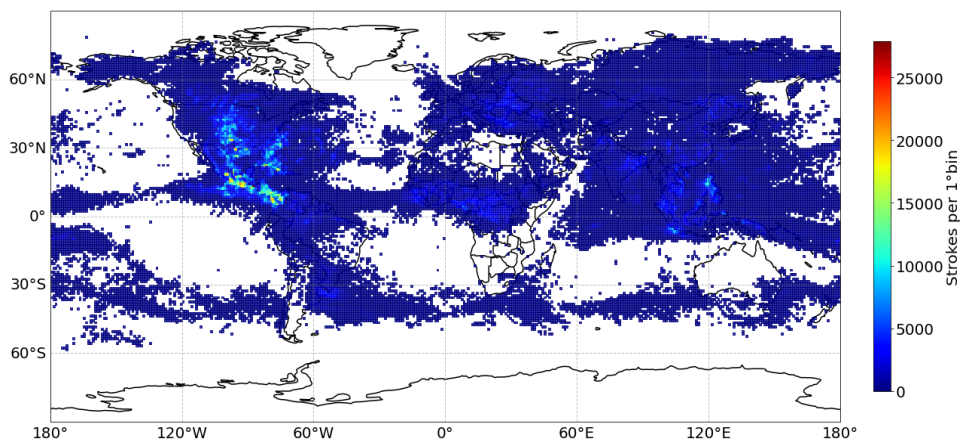


Fig. 4.6: Global distribution of ISS-LIS lightning flash during summer (4th May to 3rd August 2020).

4.4.2 Lightning Strokes

The concentration of lightning strokes detected by WWLLN during winter and summer, respectively are shown in Fig. 4.7 and Fig. 4.8. The lightning strokes concentration shows the similar pattern as of flashes concentration detected by ISS-LIS. During winter, lightning densities are higher in oceans than on land that was also observed in [4].

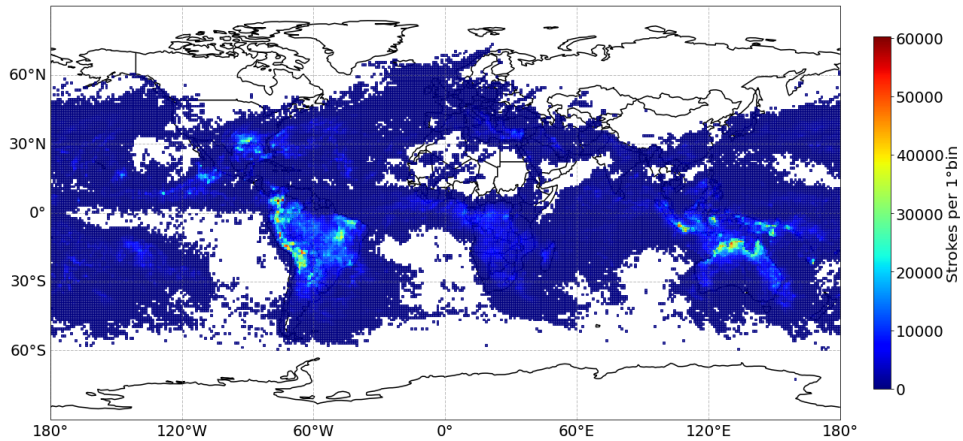


Fig. 4.7: WWLLN seasonal lightning strokes during winter (1st Dec to 29th Feb).

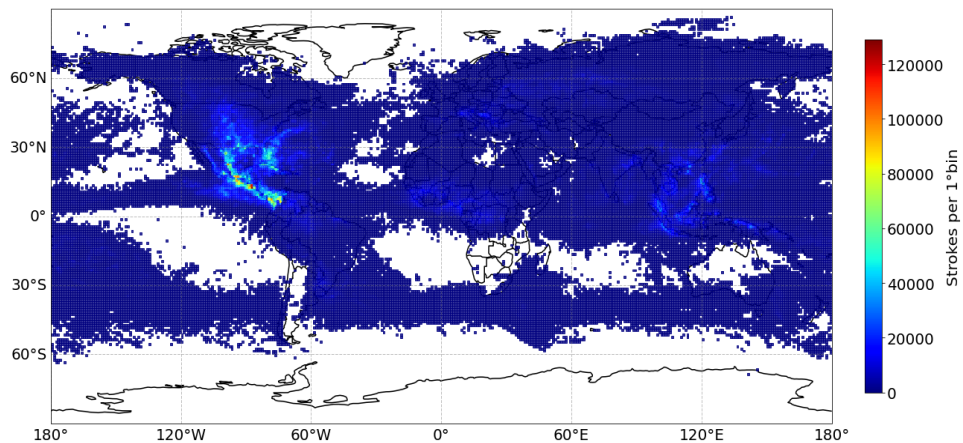


Fig. 4.8: WWLLN seasonal lightning strokes during summer (4th May to 3rd August).

4.5 Daily Lightning Cycle

To examine regional differences in the WWLLN strokes, the data are separated into the six global continental regions. Data from regions (a) Asia, (b) Europe, (c) Africa, (d) Australia, (e) North America, and (f) South America are shown in Table 4.1. The contribution of each region makes to the position of the local time peak in lightning strokes count are shown in Fig. 4.9.

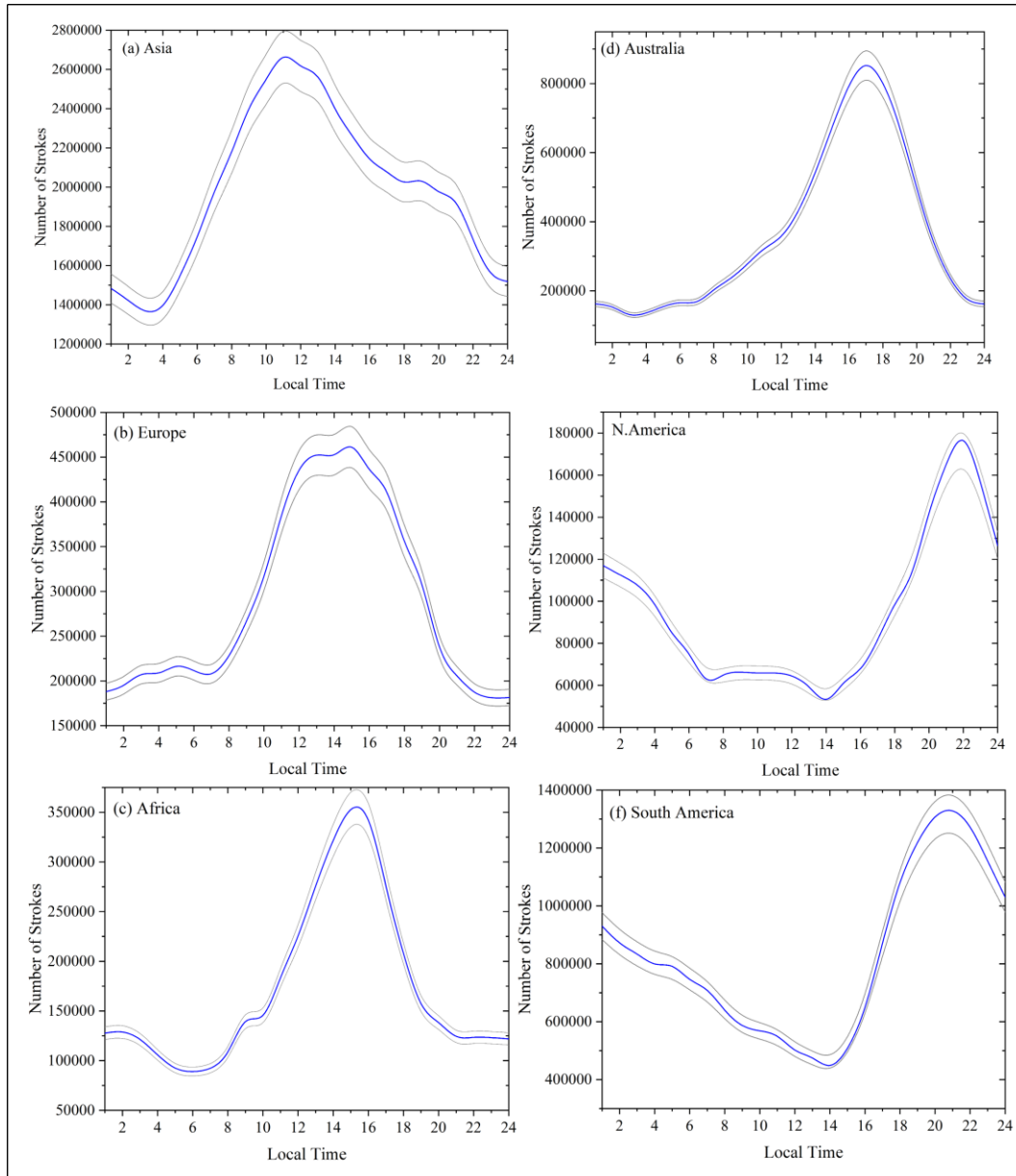


Fig. 4.9: Daily lightning cycle depicting the WLLN lightning stroke count in every 24 hours (Local Time). Data from regions (a) Asia, (b) Europe, (c) Africa, (d) Australia, (e) North America, and (f) South America. Poisson statistics define error bars on the order of the width of the line (gray line).

The diurnal amplitude variation of land strokes peak in the local evening, around 20:00 LT in North America and South America. The Europe, Africa and Australia show the pick in the local afternoon, around 16:00 LT. But the in Asia the pick is little deferent, around 14:00 LT. Similar diurnal patterns are seen in each region. Similar observation was found in [79]. The statistical error bars (Poisson statistics) are not plotted as they would be on the order, or smaller than, the line width.

It is to be noted that, WWLLN has a higher threshold but overall since WWLLN sees the whole world all the time, it actually locates orders of magnitude more total strokes than any of the low altitude lightning sensors. On the other hand ISS-LIS cannot covers the globe at a time, only see a small region (~400 km across) just below the satellite for about 1 minute or so, and then do not return to that location for 2 to 3 days. Therefore, the diurnal patterns of lightning flash will not pick the same time as WWLLN strokes.

4.6 Lightning over Bangladesh

Lightning over Bangladesh has been a topic of increasing concern due to its significant impact on human lives, property, and the environment. The country experiences a high frequency of lightning events, particularly during the pre-monsoon and monsoon seasons (April to October) which has already discussed in section 2.8.2. These events pose severe threats to the densely populated regions, especially in rural areas where people often lack proper lightning protection infrastructure and awareness. An investigation of 3 years (2017-2019) ISS-LIS data provides a lightning risk analysis for Nepal and Bangladesh, based on a combination of LIS flash rates and socioeconomic factors [44]. The addition of the Dhaka station to the WWLLN network, as discussed in the previous sections (Chapter-3), has significantly improved the DE of lightning strokes over Asia. Also described in section 2.8.3, the any station sees strokes over at least 6,000 to 12,000 km from the center [1]. So, the presumed improvement in WWLLN by adding Dhaka station will have a nearly global impact at some level, not just in Bangladesh. This study has investigated the lightning activities over Bangladesh's landmass during 2020. The strokes detected by WWLLN is the stations were activated during the investigated period (see in Fig. 4.4). Fig. 4.10 shows the border of Bangladesh is located between 88.05° E to 92.74° E longitudes and 20.45° to 26.63° N latitudes.

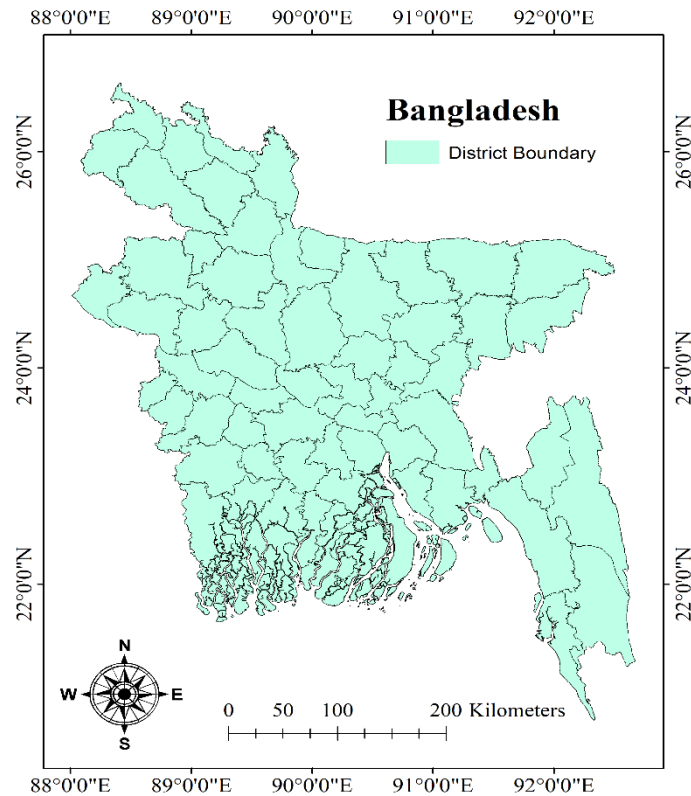


Fig. 4.10: The study area of Bangladesh’s landmass (20°34' to 26°38' north latitude and 88°01' to 92°41' east longitude).

In 2020, WWLLN recorded a total of 478,042 lightning strokes over Bangladesh. The analysis of spatial variation in lightning activity across the country revealed that the primary hotspots were situated in the northwestern and northeastern regions (Fig. 4.11). Specifically, the highest concentration of lightning events was found between latitudes 25.00° to 26.00° N and longitudes 89.75° to 92.50° E, where the mean stroke density reached 8 strokes per km² per year. Smaller lightning activity occurred between latitudes 22.00° to 24.00° N and longitudes 90.00° to 92.00° E, with a similar mean stroke density of 8 strokes per km² per year. The central region and the hilly areas in southeastern Bangladesh experienced moderate lightning activity during the study period, with a stroke density of 4-7 strokes per km² per year. The similar observation has found in [67], [82].

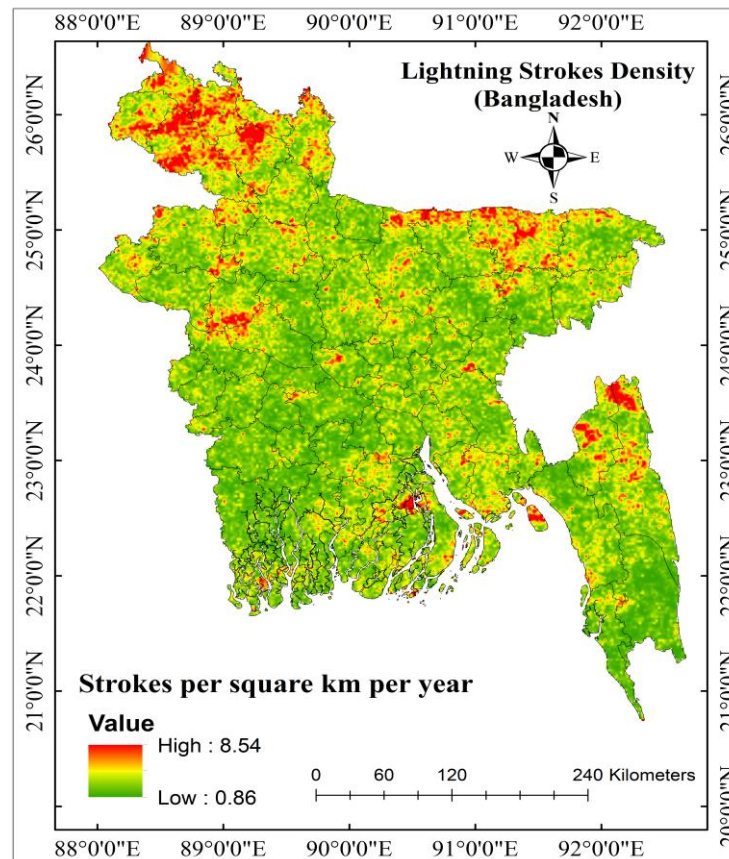


Fig. 4.11: Spatial variation of lightning strokes density over Bangladesh’s landmass detected by WWLLN during 2020.

Figure 4.12 displays the monthly distribution of lightning strokes detected by WWLLN over Bangladesh's landmass from January 2020 to December 2020. The majority of lightning events took place between April and October, with the highest occurrence observed in April 2020. In contrast, the lowest occurrences were recorded during December and January.

The summer months (April, May, June) experienced the most lightning activity in Bangladesh, while the winter season (December, January, February) saw significantly lower levels of lightning. This pattern highlights the seasonal variation of lightning events and the increased risk during the warmer months of the year.

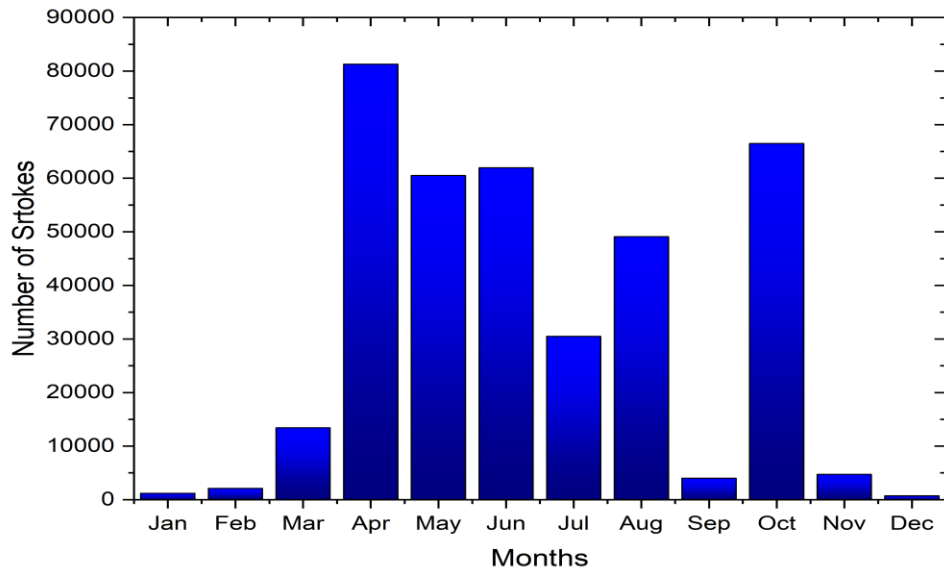


Fig. 4.12: Monthly distribution of WWLLN lightning strokes over Bangladesh's landmass during January 2020 to December 2020.

Fig. 4.13 depicts the diurnal cycle of lightning over Bangladesh, exhibiting a bimodal distribution that mirrors the annual diurnal cycle. Consistent with the annual pattern, two distinct maxima appear in the 01:00 local time and evening 20:00 local time. This bimodal distribution underscores the temporal fluctuations in lightning occurrences, indicating specific times of day when lightning activity is more prevalent in Bangladesh.

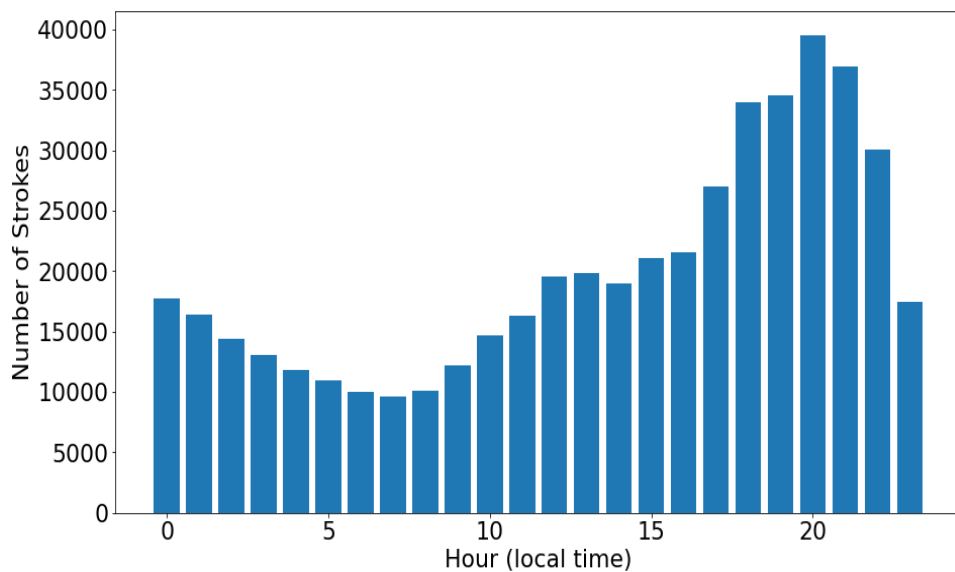


Fig. 4.13: Diurnal variation of lightning strokes over Bangladesh's landmass detected by WWLLN during 2020.

4.7 Summary

In this chapter, a detailed analysis of the climatological characteristics of global lightning phenomena is presented, utilizing data derived from both WWLLN lightning strokes and ISS-LIS flashes. Firstly, the annual-mean lightning climatology of ISS-LIS is scrutinized and compared with that of WWLLN, offering insights into the similarities and differences between the two datasets. Furthermore, the regional distribution of lightning occurrences is thoroughly described, shedding light on the spatial patterns of lightning activity. The seasonal variations in lightning activity, examining the fluctuations in WWLLN lightning strokes and ISS-LIS lightning flashes over time. Additionally, the diurnal variation of lightning is explored across six distinct continents, considering the Local Time for each region. The lightning activities over Bangladesh has also investigated in this chapter. This investigation provides valuable information on how lightning activity varies throughout the day in different geographical areas. In the subsequent chapter, attention will be given to the development of a proposed lightning prediction model. This innovative model leverages time series analysis techniques to accurately forecast lightning events, offering a valuable tool for meteorologists and researchers in the field.

CHAPTER 5

PROPOSED LIGHTNING PREDICTION MODEL

5.1 Introduction

The proposed lightning prediction model has been developed by applying time series analysis. One year of ISS-LIS Lightning flash data (2020) and one year's of WWLLN energy data (2020) are used in this analysis. The objective is to extract meaningful inferences from both the dataset and pick an appropriate model in order to predict the data for both of short time long time period in absence of real time data. A time series is a sequentially indexed succession of data items separated by defined time periods. The parameters may be estimated and the quality of fit be evaluated after selecting the Auto Regressive Integrated Moving Average (ARIMA) model [92].

The ARIMA time series model is a reliable method frequently used to forecast times series data and as a result, the acceleration of fatality functions can be used to produce ARIMA models for forecasting purposes [92]. ARIMA models are used for non-stationary data and is made up of the Auto Regression model AR (p), which uses the dependent relationship between $y(t)$ and p number of lagged [92]. The model also includes the Integrated (I) aspect, which is the differencing of raw observations, d times to allow for the time series to become stationary. Making the time series data stationary is necessary since stationary series are relatively easier to predict.

5.2 Method of Performing Time Series Analysis

For performing time series analysis, WWLLN strokes energy data (AE file) are used at 40° to 141° east longitude and 5° to 50° north latitude (10000×5000 km² region of Asia) during 2020. Side by side the flash radiance data from ISS-LIS are used for performing the time series analysis in global scale in the same duration. This study assigning a weight to each energy measurement detected by WWLLN based on the uncertainty in the energy measurement. In this case, the weight is equal to 50% of the energy error, which represents the uncertainty or error associated with the energy measurement. For example, if an energy measurement has an error of 10 units, the weight assigned to that measurement would be 5 units (i.e., 50% of the energy error). So, any WWLLN energy data where the energy error is equal to or greater than 50% of the energy was not used in this study. Also, the strokes in which energy is equal to zero were eliminated in this study. Fig. 5.1 depict the number of WWLLN stations that were on, off or weak during 2020.

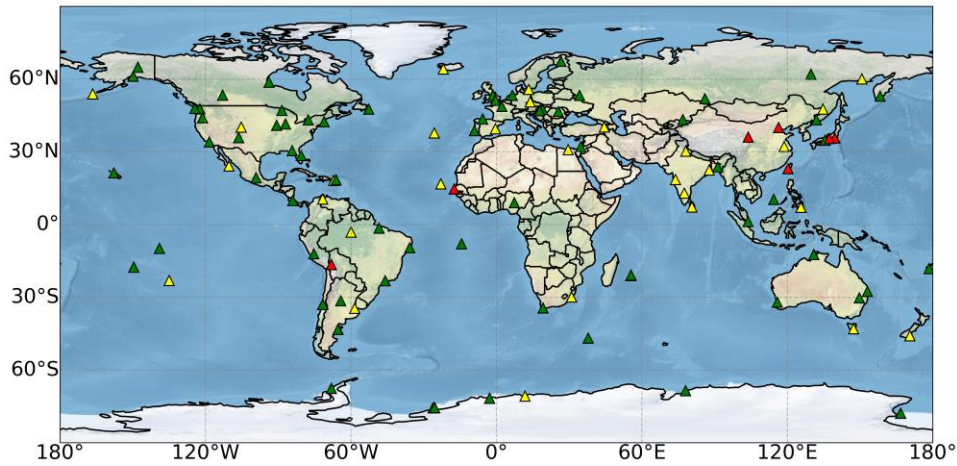


Fig. 5.1: Locations and hosts of the 111 VLF receiving stations operating in the VLF WWLLN stations as of 2020. The green triangles indicate the stations were functional, while the yellow triangles indicate the stations were weak, and the red triangles indicate the stations were not functional during the period of investigation.

There were seven stations such as Tainan (22.99° N, 120.21° E), Lanzhou (36.04° N, 103.85° E), Beijing (39.97° N, 116.38° E), Chofu (35.65° N, 139.54° E), Dakar (14.68° N, 17.46° W), UOsaka (35.43° N, 137.37° E) and LaPaz (16.53° S, 68.06° W) were not functional and also there other 29 stations were remain weak during the period of investigation.

To applying time series, firstly both data are converted into an hourly spaced time series. If more occurrences were found in a particular hour, the data has averaged. After applying the average raw lightning counts, the hourly data is obtained and the annual number of detections is 8760. Thereafter, the median of every averaged data point of a particular hour within a month is determined. Finally, the total 24×12 of data points is obtained. The Box-Jenkins method [92] is used to fit Auto Regressive Integrated Moving Average (ARIMA) models via the processes of identification, estimate, and validation. Fig. 5.2 shows the flow diagram for stages of the work done.

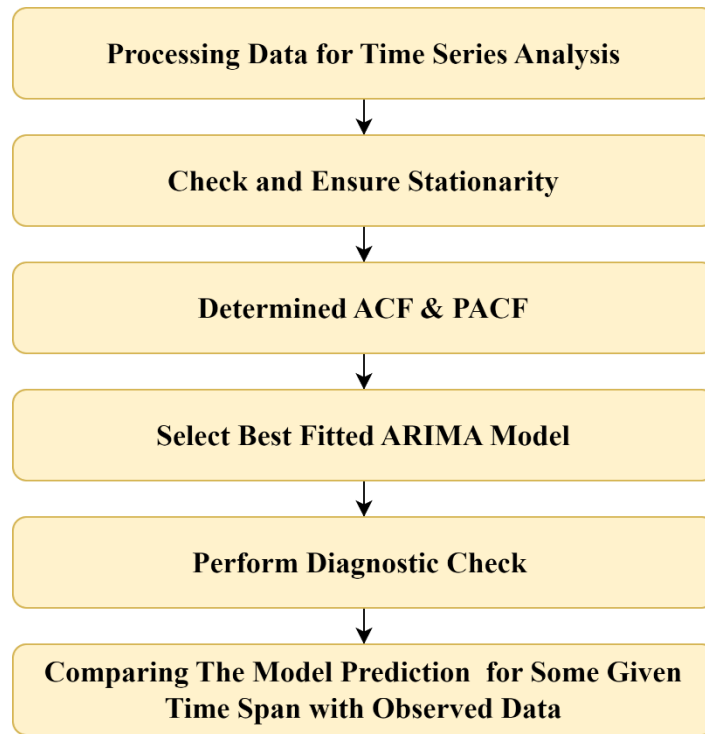


Fig. 5.2: Flow diagram for performing time series analysis.

5.3 Time Series Analysis of WWLLN Strokes Energy

The time plots of fluctuation in electrostatic energy during the year 2020 at 40° to 141° east longitude and 5° to 50° north latitude (10000×5000 km² region of Asia) are shown in Fig. 5.3. The statistical error bars (Poisson statistics) are not plotted as they would be on the order, or smaller than, the line width. In this graph, it can be seen that the levels of the energy change repeatedly, indicating that the changes are not stable across time intervals. More formally, the energy of lightning strokes is getting a sudden raise at the month of March and getting a sudden drop from the month of July during the year. The Strokes energy also raises in the month of November and December.

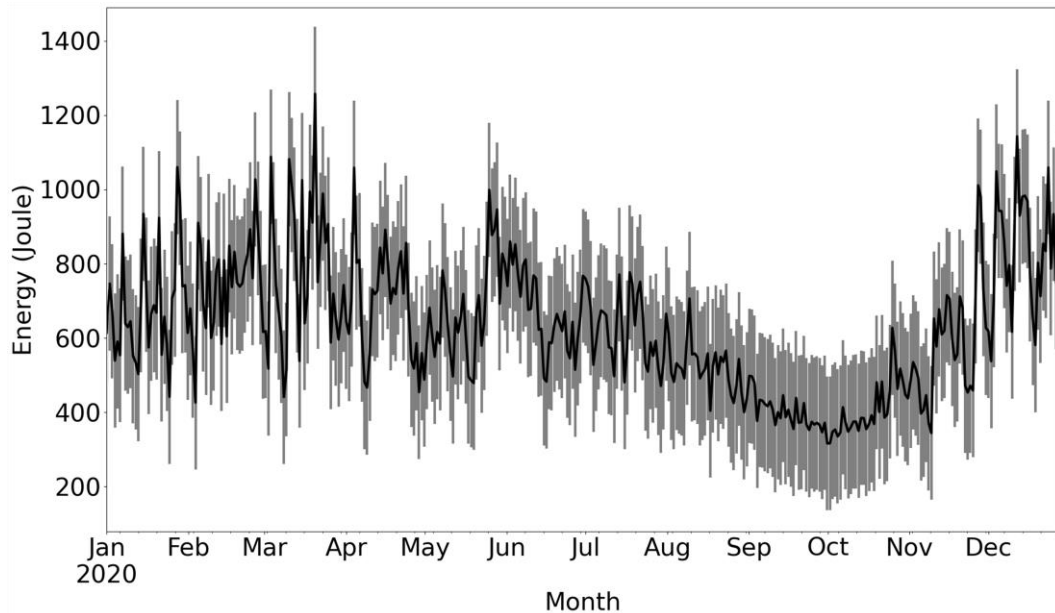


Fig. 5.3: The time plots of fluctuation in WWLLN strokes energy during the year 2020 at 40° to 141° east longitude and 5° to 50° north latitude (10000×5000 km^2 region of Asia). The grey lines are statistical count errors.

A stationary time series is needed for forecasting with the ARIMA model [92]. In general, the stationary time series are unaffected by trend, seasonality, and noise. If the data is remaining non-stationary, the forecasting of the ARIMA model is poor. In this case, there have two options: either make it stationary or use different model (SARIMAX [92]). The Augmented Dickey-Fuller Test (ADF Test) [93] can be applied on the time series analysis to check the stationarity of the data. This test examine the null hypothesis of an ARIMA against stationary and alternatively. In ADF test [93], if the p-value (critical value) is lower 0.05 or 5%, the time series will be stationary, and if the p-value is larger than 0.05 or 5%, the time series will be non-stationary.

By applying the ADF test the p-value for this dataset is greater than 5% (0.0914 or 9%), indicating that the time series is non-stationary. The time series can be made stationary by using differencing methods. In this scenario, rolling mean differencing approaches is formulated [94]. The first preparation of data to make it stationary is referred to as identification. To make the series a second-order stationary series, the linear trends and periodic effects is eliminated by preprocessed the dataset.

The first preparation of data to make it stationary is referred to as identification. As part of the preprocessing, we removed the dataset's linear trends and periodic effects to make the series as a second-order stationary. A process X_t is called second-order stationary [94] if:

- 1) The first moment $\mu_t = E[X_t]$ is independent of time t ;
- 2) The auto covariance $\gamma(t, t + y) = E[(X_t - \mu_t)(X_{t+y} - \mu_{t+y})]$ is independent of time t but dependent on time difference y , called lag. A stationary process X_t is said to be an ARMA(p, q) process [94] if for every t ,

$$X_t - \phi_1 X_{t-1} - \dots - \phi_p X_{t-p} = Z_t + \theta_p Z_{t-1} + \dots + \theta_q Z_{t-q} \quad 5.1$$

Where, $Z_t \sim WN(0, \sigma^2)$ is uncorrelated white noise that has zero mean and variance σ^2 and follows a normal distribution. Equation 7.1 can be written symbolically:

$$\phi_p(B)X_t = \theta_q(B)Z_t \quad ; t = 0 \pm 1 \pm 2 \dots \quad 5.2$$

Where, B is the Back-shift Operator,

$$B^j X_t = X_{t-j} \quad ; t = 0 \pm 1 \pm 2 \dots \quad 5.3$$

And ϕ_p and θ_q are respectively the p order of Auto Regressive (AR) and the q order of Moving Average (MA). In ARIMA model, where "I" stands for "integrated" that represents how many times are differentiated to make the data stationary. Fig. 5.4 shows the seasonal first difference plot. This graph shows the seasonality after the differencing. By applying ADF test, the p-value is less than 5% (0.010 or 1%), as a result, the data is stationary.

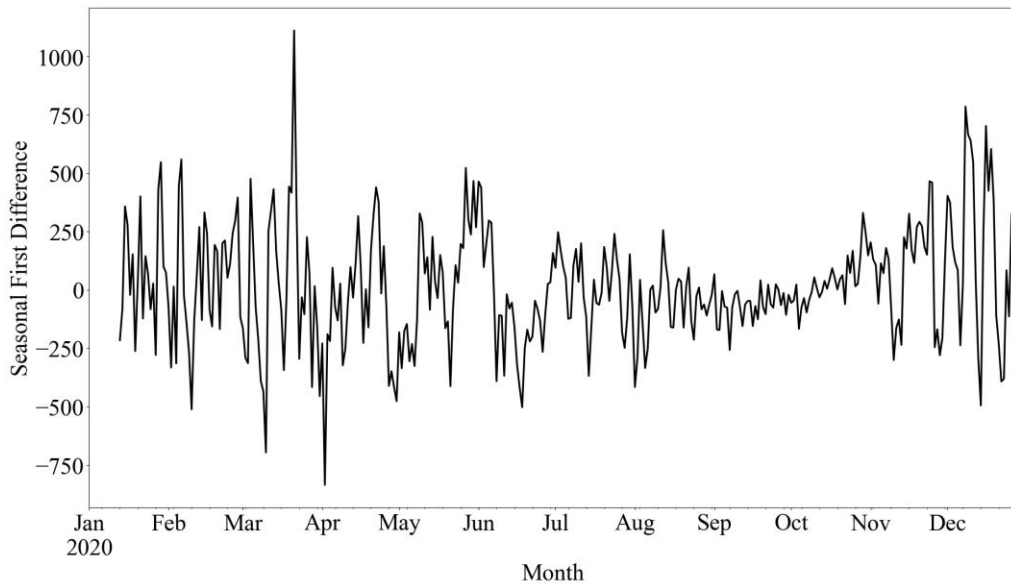


Fig. 5.4: Seasonal first difference plot.

If there are no obvious departures from stationarity and the auto-covariance function is fast decreasing, an ARMA model is attempted to fit the mean corrected data [92]. Otherwise, it seeks for a data transformation that produces a novel series with stationarity and a quickly declining auto-covariance function before considering a fitted ARIMA model. In practice, the seasonal component may be included in the seasonal ARIMA model, which was developed in [92].

5.3.1 Analysis of WWLLN Strokes Energy Using Time Series Models

To match the appropriate model, the AR and MA terms must be determined. For this, the Auto Correlation Function (ACF) and the Partial Auto Correlation Function (PACF) are determined. A stationary ACF is defined by the following equation [92]:

$$\rho_k = \frac{E\{(X_t - \mu_t)\{X_{t+h} - \mu_{t+h}\}\}}{\sqrt{E\{(X_t - \mu_t)^2(X_{t+h} - \mu_{t+h})^2\}}} = \frac{\gamma_h}{\gamma_0} \quad 5.4$$

The PACF of a stationary time series is defined by [92] as follows:

$$\alpha_{(1)} = cor[X_1, X_2] = \gamma_{(1)} \quad 5.5$$

$$\alpha_{(k)} = cor[X_{k+1} - P_{sp(1, X_2, \dots, X_k)} X_1, X_{k+1} - P_{sp(1, X_2, \dots, X_k)} X_1] \quad 5.6$$

Where, $k \geq 2$ and $X_{k+1} - P_{sp\{1, X_2, \dots, X_k\}} X_1$ is a project operation that projects X on $1, X_2, \dots, X_k$.

The PACF, like the ACF, conveys critical information about the correlation of a stationary process. The differenced series of ACF and PACF are shown in Fig. 5.5.

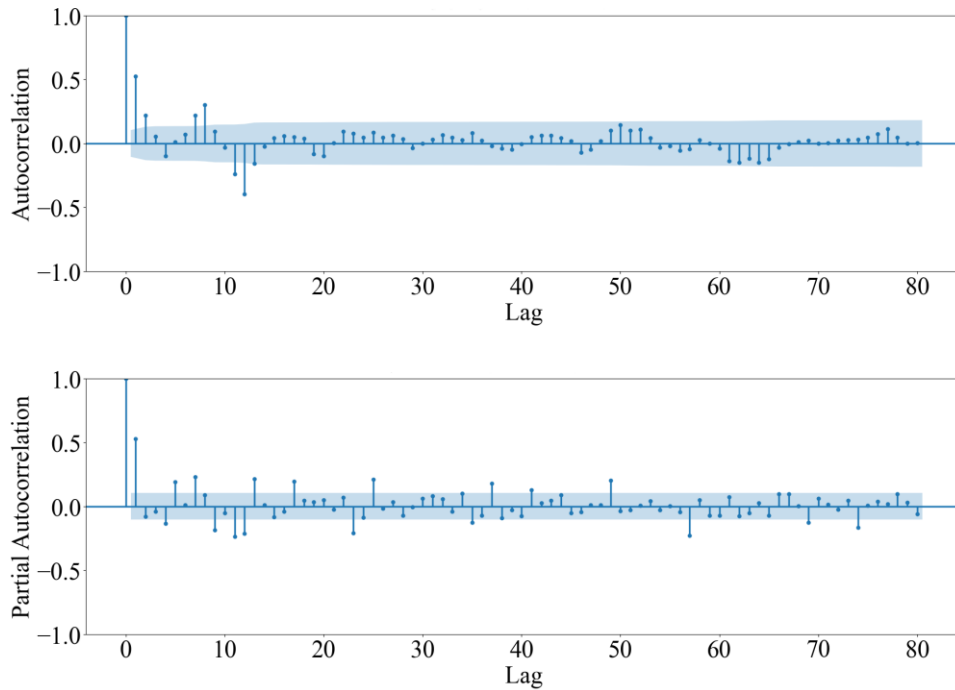


Fig. 5.5: Auto Correlation Function (ACF) and the Partial Auto Correlation Function (PACF) of the differenced series.

The ACF decays gradually, however the PACF has two spikes at short delays, indicating the AR (p) model in the order of 2. The significant negative autocorrelation coefficient observed in ACF plot indicating the seasonal period 12 proposes that a seasonal MA term $Q = 1$ be added to the model. Similarly, surges in the PACFs at multiples of seasonality, $S = 12, 24, 36, 48, 60, 72, \dots$, it is indicating that the term $P = 1$ for seasonal AR. It is crucial to choose appropriate parameter values for the seasonal ARIMA $(p, d, q) \times (P, D, Q)_S$ model.

Another strategy for selecting an appropriate model with the maximum possibility given the data is The Akaike's Information Criterion (AIC), which may be used to pick predictors for regression [95]. It can be written as:

$$AIC = -2\log(L) + 2(p+q+k+1) \quad 5.7$$

Where, L is defined as the likelihood of the data. Table 5.1 displays the results of a portion of the parameter enumeration as well as their AIC values. From those, ARIMA $(3, 1, 1) \times (2, 1, 0)_{12}$ is found to be the best-fitted model. The estimated parameters are listed in Table 5.2.

Table 5.1: AIC values of different models for WWLLN strokes energy

p,d,q	P,D,Q	AIC
0,1,0	0,1,0	4826.373
1,1,0	1,1,0	4740.133
1,1,0	0,1,0	4817.551
1,1,0	2,1,0	4702.758
0,1,0	2,1,0	4722.107
2,1,0	2,1,0	4695.438
2,1,0	1,1,0	4729.392
3,1,0	2,1,0	4693.026
3,1,0	1,1,0	4725.252
3,1,1	2,1,0	4639.244
3,1,1	1,1,0	4670.914
2,1,1	2,1,0	4639.500
3,1,2	2,1,0	4641.876
2,1,2	2,1,0	4641.446
3,1,1	2,1,0	4641.135

Table 5.2: Estimated parameters of the fitted models for WWLLN strokes energy

Variable	Coefficient	Standard error	Z	Log Likelihood	AIC	BIC
ar.L1	0.4539	0.057	8.020	-2312.62	4639.244	4666.25
ar.L2	-0.0045	0.054	-0.083			
ar.L3	-0.0861	0.059	-1.448			
ma.L1	-0.9238	0.029	-32.137			
ar.S.L12	-0.6090	0.044	-13.926			
ar.S.L24	-0.3387	0.050	-6.775			
σ^2	3.148e+04	1754.569	17.944			

5.3.2 Diagnostic Check of the Fitted ARIMA Model for WWLLN Strokes Energy

To determine how well a statistical model fits the data, it is necessary to compare the measured values to the corresponding fitted values. In this manner, the first priority is to guarantee that the chosen model's residuals are uncorrelated and regularly distributed. Clearly, further work must be performed on the seasonal ARIMA model if it fails to meet these conditions. In Fig. 5.6 shows the diagnostic plot of the fitted ARIMA model.

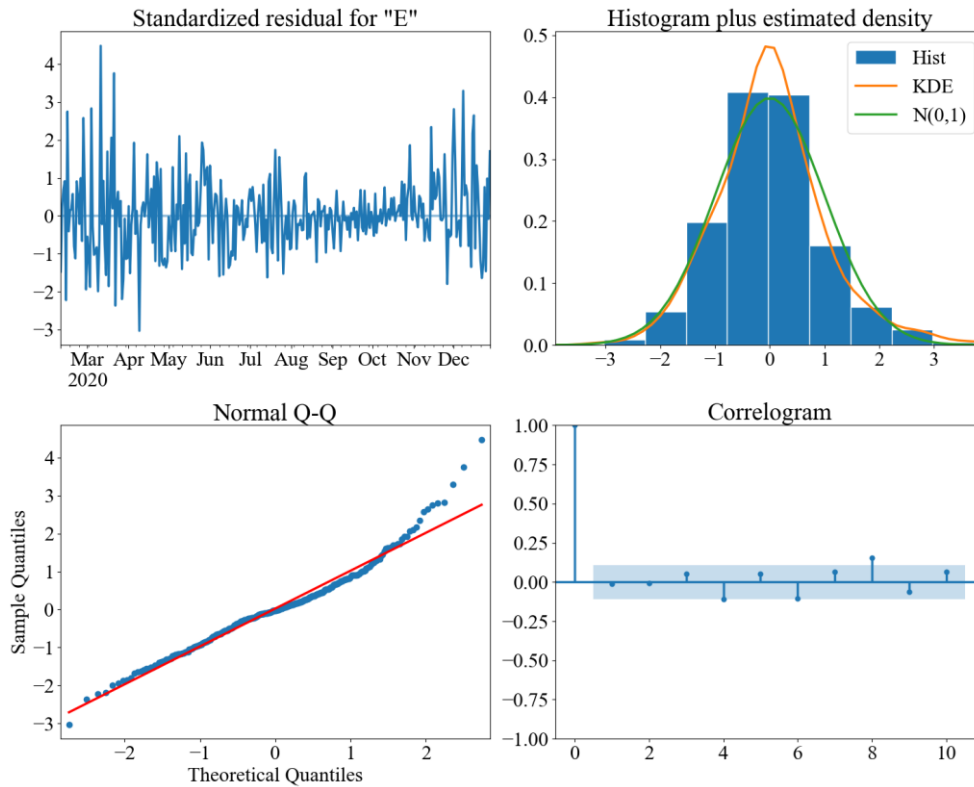


Fig. 5.6: Standardized residuals, histogram plus density, theoretical quantiles and ACF of the residuals of strokes energy data.

The following evidence suggests that the residuals of the chosen model follow a normal distribution, as determined by the model diagnostics:

- In the top-right figure, the red KDE line closely matches the $N(0, 1)$ line, which represents a normal distribution with a mean of 0 and a standard deviation of 1. This indicates that the residuals are distributed consistently.
- The QQ-plot in the lower-left corner demonstrates how the linear trend of samples drawn from a standard normal distribution follows the ordered residual distribution (blue dots). Once more, this strongly indicates that the residuals are distributed in a linear pattern.
- The residuals over time (top left panel) seem to be white noise rather than seasonal. The autocorrelation diagram in the bottom right supports this, demonstrating that the residuals of the time series have minimal correlation with their lags.

These findings indicate that the chosen model provides a good match that comprehends the time series data and estimates future values.

5.3.3 Forecasting the ARIMA Model of WLLN Strokes Energy

The predicted time series from January 2020 to December 2021 are shown in Fig. 5.7, and Fig. 5.8 shows the fitted model of prediction, which have an excellent match. The residuals would behave as expected if the suggested model were accurate. The discrepancy between the measured and fitted values is known as the residuals.

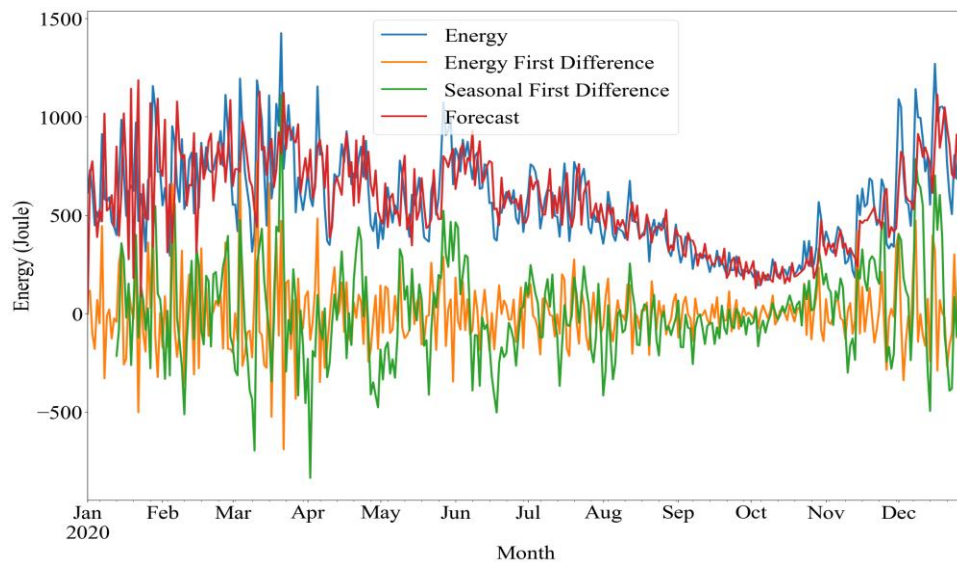


Fig. 5.7: Model of prediction for some given time span with observed data from January 2020 to December 2020, estimated by the suggested ARIMA model.

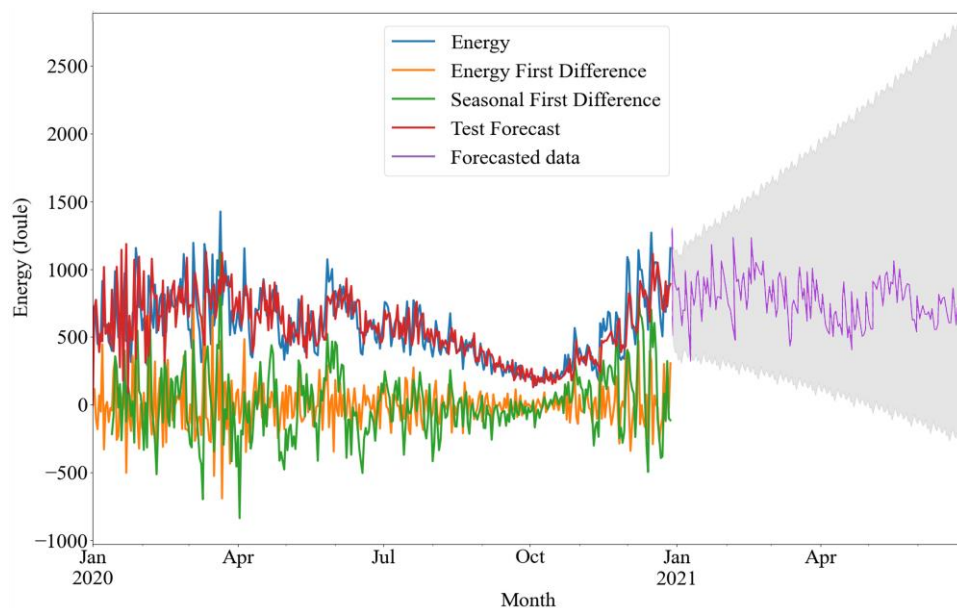


Fig. 5.8: Measured and fitted model of prediction from January 2021 to June 2021, estimated by the suggested ARIMA model.

5.4 Time Series Analysis of ISS-LIS Lightning Flashes Radiance

The time plots of fluctuation in lightning flashes during the year 2020 around the globe, are shown in Fig. 5.9. The statistical error bars (Poisson statistics) are not plotted as they would be on the order, or smaller than, the line width.

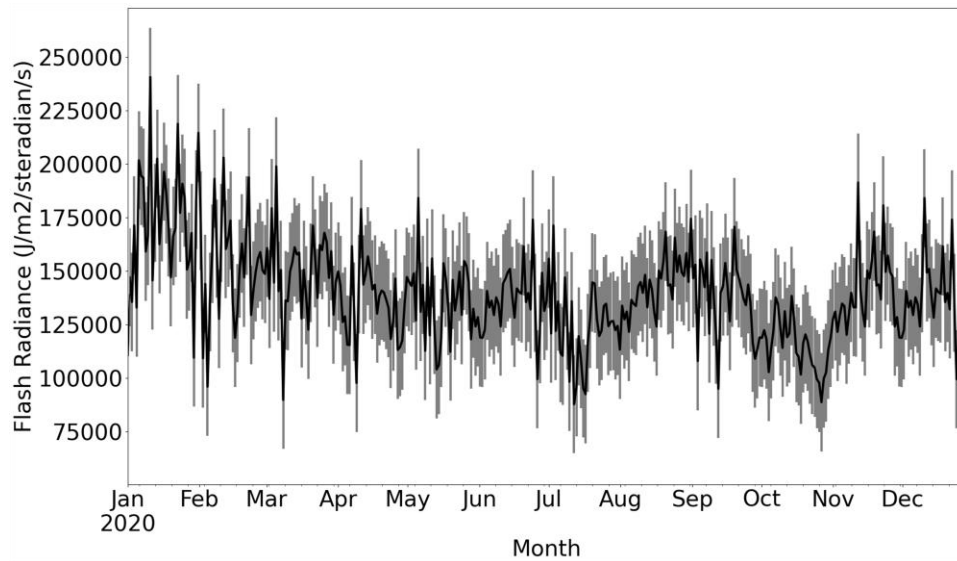


Fig. 5.9: The time plots of fluctuation in lightning flashes radiance during the year 2020 around the globe. The grey lines are statistical count errors.

It is observed that the levels of the flashes radiance ($\text{J/m}^2/\text{steradian/s}$) change repeatedly, indicating that the changes are not stable across time intervals. In the starting month of the year, a sudden raise in the flashes radiance and in the month of March-June, a drop is observed. The flashes radiance also raises in the month of August-September and drop in December. By applying ADF test [93], the p-value (critical value) is less than 5% (0.006 or 0.6%), as a result, the data is stationary.

5.4.1 Analysis of ISS-LIS Flash Radiance Using Time Series Model

In order to match the appropriate model, the AR and MA terms must be determined. For this, ACF and the PACF has determined. A stationary ACF and stationary PACF are defined by above equation 5.4 and 5.5.

The ACF and PACF of the differenced series are shown in Fig. 5.10. The ACF decays gradually, however the PACF has two spikes at short delays, indicating the AR (p) model in the order of 2. The significant negative autocorrelation coefficient observed in ACF plot indicating the seasonal period 12 proposes that a seasonal MA term $Q = 1$ be added to the

model. Similarly, surges in the PACFs at multiples of seasonality, $S = 12, 24, 36, 48, 60, 72, \dots$, indicating that a seasonal AR term $P = 1$ may be included in the model. It is vital to select the suitable values for the parameters in the seasonal ARIMA $(p, d, q) \times (P, D, Q)_S$ model.

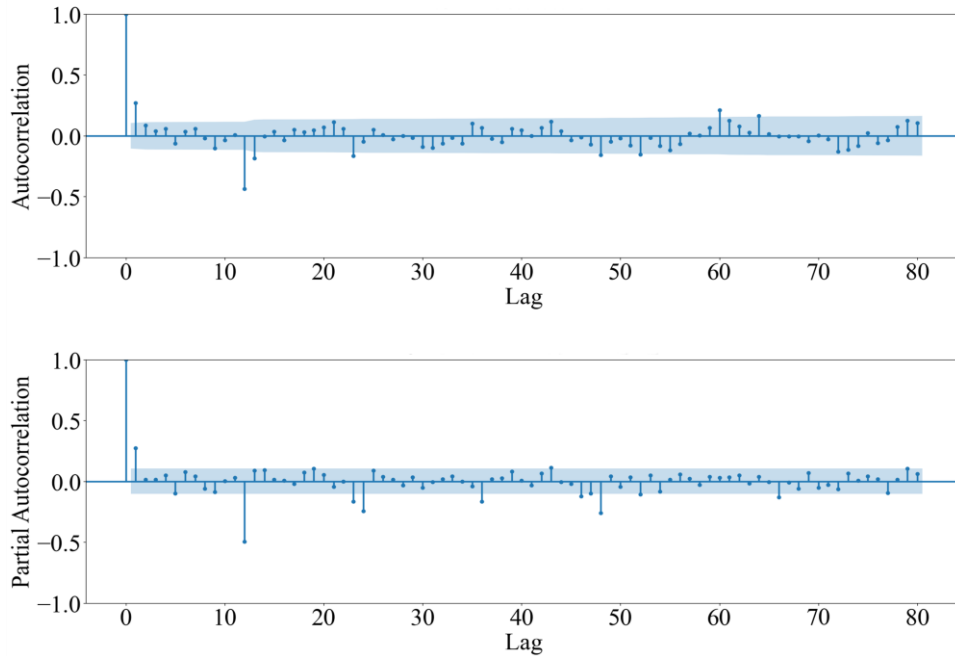


Fig. 5.10: Auto Correlation Function (ACF) and the Partial Auto Correlation Function (PACF) of the differenced series.

The AIC may be used to pick predictors for regression [95], can also be used to determine the values of p and q , not for determining the right order of differencing (d) of a model. It can be written by following above equation 5.7. Table 5.3 displays the results of a portion of the parameter enumeration as well as their AIC values. From those, ARIMA $(2, 1, 2) \times (0, 1, 1)_{12}$ is found to be the best-fitted model. The estimated parameters are listed in Table 5.4.

Table 5.3: AIC values of different models for ISS-LIS flash radiance

p,d,q	P,D,Q	AIC
1,1,1	0,1,1	8201.316
0,1,0	1,0,1	8450.684
1,1,0	1,1,0	8317.645
0,1,1	0,1,1	8203.692
1,1,1	0,1,0	8351.332
1,1,1	1,1,1	8203.037
1,1,1	0,1,2	8202.970
1,1,1	1,1,0	8269.461
2,1,1	0,1,1	8203.173
1,1,2	0,1,1	8193.386
1,1,2	1,1,1	8195.564
1,1,2	0,1,2	8195.383
1,1,2	1,1,0	8266.506
0,1,2	0,1,1	8193.540
2,1,2	0,1,1	8188.263
2,1,2	0,1,0	8355.623
2,1,2	1,1,1	8189.640
2,1,2	0,1,2	8189.471
2,1,2	1,1,0	8264.167
2,1,2	0,1,1	8188.263
3,1,2	0,1,1	8188.642
2,1,3	0,1,1	8190.317
1,1,3	0,1,1	8191.187
3,1,1	0,1,1	8204.506
3,1,3	0,1,1	8191.244

Table 5.4: Estimated parameters of the fitted models for ISS-LIS flash radiance

Variable	Coefficient	Standard error	Z	Log Likelihood	AIC	BIC
ar.L1	-0.7222	0.347	-2.081	-4088.132	8188.263	8211.411
ar.L2	0.1661	0.134	1.236			
ma.L1	0.1387	0.332	0.418			
Ma.L2	-0.6170	0.198	-3.115			
ma.S.L12	-0.8763	0.075	-11.620			
σ^2	1.218e ⁺¹⁰	2.17e ⁻¹⁰	5.61e ⁺¹⁸			

5.4.2 Diagnostic Check of the Fitted ARIMA Model ISS-LIS Flashes Radiance

To determine how well a statistical model fits the data, it is necessary to compare the measured values to the corresponding fitted values. In this manner, the first priority is to guarantee that the chosen model's residuals are uncorrelated and regularly distributed. The diagnostic plot of the fitted ARIMA model are shown in Fig. 5.11.

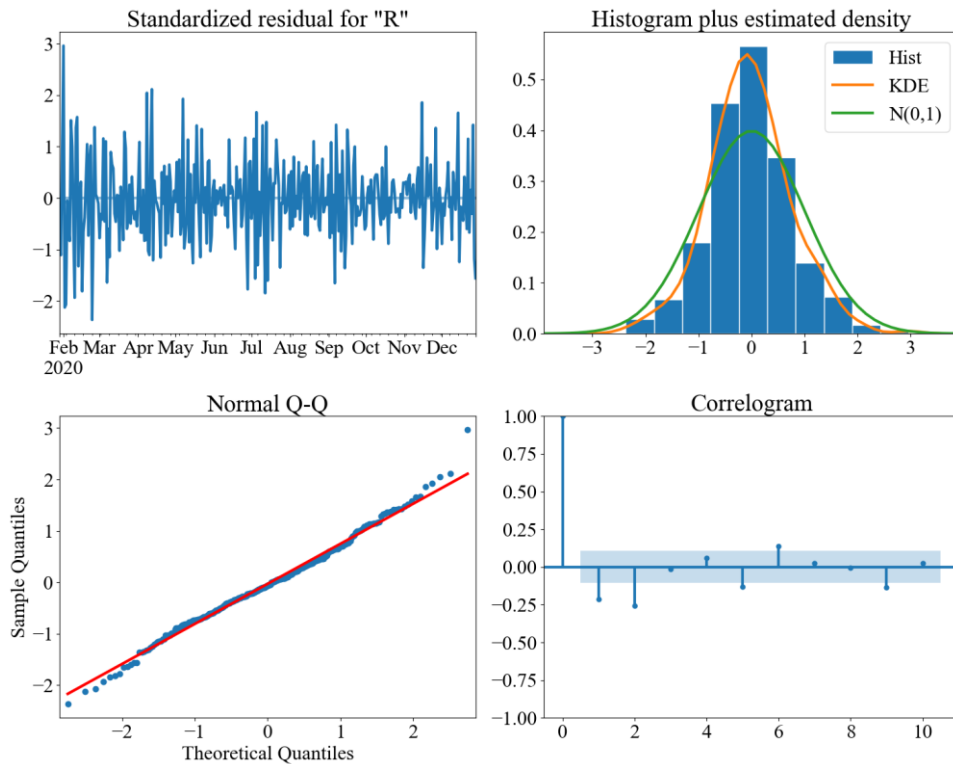


Fig. 5.11: Standardized residuals, histogram plus density, theoretical quantiles and ACF of the residuals of lightning flashes radiance data.

The model diagnostics shows that the residuals of this model are normally distributed based on the following observations:

- In the top right figure, the red KDE line closely matches the $N(0,1)$ line, which represents a normal distribution with a mean of 0 and a standard deviation of 1. This indicates that the residuals are distributed consistently.
- The QQ-plot on the bottom left shows how the linear trend of the samples taken from a standard normal distribution follows the ordered residual distribution (blue dots). Once more, this strongly indicates that the residuals are distributed in a linear pattern.

(c) The residuals over time (top left panel) seem to be white noise rather than seasonal.

The autocorrelation diagram in the bottom right supports this, demonstrating that the residuals of the time series have minimal correlation with their lags.

These findings indicate that our model provides a good match that enables us to comprehend the time series data and estimate future values.

5.4.3 Forecasting the ARIMA Model of ISS-LIS Flashes Radiance

The predicted time series from January 2020 to December 2020 are shown in Fig. 5.12 and Fig. 5.13 shows the fitted model of prediction from January 2021 to June 2021, which have an excellent match. The residuals would behave as expected if the suggested model were accurate. The discrepancy between the measured and fitted values is known as the residuals.

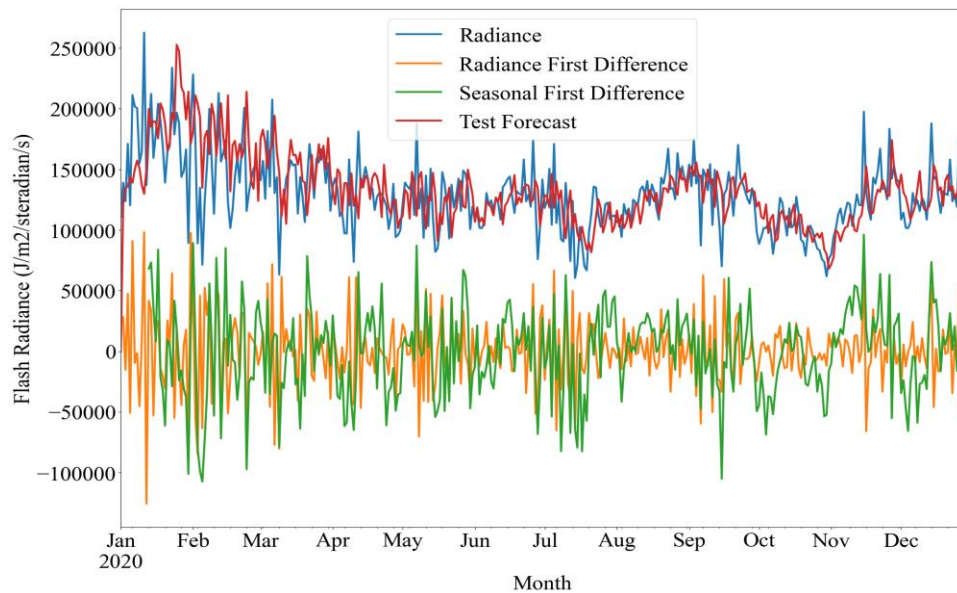


Fig. 5.12: Model of prediction for some given time span with observed data from January 2020 to December 2020, estimated by the suggested ARIMA model.

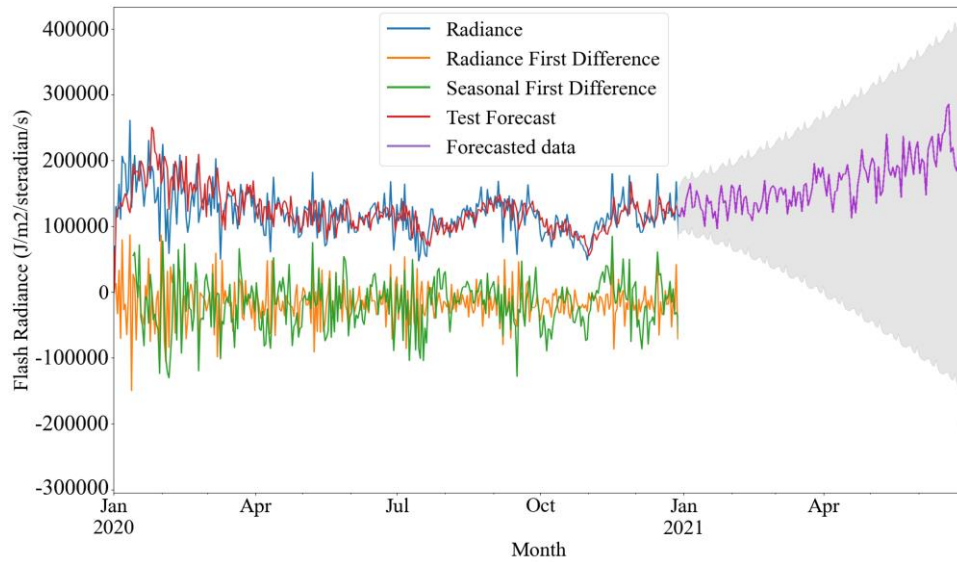


Fig. 5.13: Measured and fitted model of prediction from January 2021 to June 2021, estimated by the suggested ARIMA model.

5.5 Summary

This chapter offers a concise overview of the measurement systems and techniques used in time series modeling for forecasting lightning events. It details the time series analysis using the second derivative stationary method and the development of a time series prediction model for WWLLN stroke energy. The construction of a time series prediction model for ISS-LIS flash radiance is also discussed, along with various diagnostic tests for the fitted model and an explanation of the selected model. The final chapter of the thesis will draw conclusions, emphasize the importance of the research, and suggest future avenues of study in this field.

CHAPTER 6

CONCLUSION AND FUTURE RECOMMENDATIONS

6.1 Conclusion

This study examines the DE of WWLLN using two distinct methods: a comparison between WWLLN and ENTLN data within 50 km and 100 microseconds and an analysis using WWLLN APfiles data. To determine WWLLN DE relative to ENTLN, matching criteria are applied to strokes detected by both networks. The investigation also explores the diurnal and seasonal variations of lightning strokes from WWLLN and flashes from ISS-LIS in 2020. The global maps, plotted in 1° by 1° grid boxes, highlight lightning concentrations across tropical regions, with pronounced gradients near coastlines. The analysis uncovers the spatial distribution and temporal patterns of lightning strokes in Bangladesh, revealing both monthly and daily fluctuations. A regional representation of seasonal lightning variation is also provided, offering valuable insights into the diurnal lightning cycle. For the first time, time series analysis is employed to model ISS-LIS flash radiance and WWLLN stroke energy in order to predict the data for both of short time long time period, introducing a novel approach to lightning research. This study is expected to enhance our understanding of global lightning activity and contribute to knowledge in our target regions.

6.2 Significance of the Research

The research conducted in this study has yielded the following outcomes:

- a) Determining the detection efficiency of WWLLN enhances our comprehension of the network's capabilities and accuracy, which is crucial for scientists and researchers using WWLLN data to study lightning patterns and their impact on the environment. Also, the results of this analysis can help find places where the lightning detection system isn't working well and where more lightning detection stations or other changes may be needed to make the system more accurate.
- b) Assessing the percentage of strokes in the global dataset that would not have been detected without the WWLLN Dhaka station highlights the importance of individual stations within the network. This information can help decision-makers priorities the establishment and maintenance of such stations to optimize the WWLLN's overall performance and better understand regional lightning phenomena.
- c) A global lightning climatology that covers a time period that hasn't been looked at by other researchers has been made.

- d) By comparing the data collected by ISS-LIS and the data collected by WWLLN after 2020, this analysis has given new information about how well both systems can detect lightning. This has improved the quality of the lightning data collected by these systems.
- e) The time series prediction models developed for WWLLN stroke energy and ISS flash radiance may serve as a basis for predicting lightning energy and flash radiance.

6.3 Contribution of the Thesis

The contribution to this lightning thesis is significant and has the potential to make a positive impact in several areas related to lightning research. The study on lightning presented here is highly informative, covering various aspects related to lightning detection, distribution, and modeling.

- a) One of the significant contributions of this thesis is determining the Detection Efficiency of WWLLN, as it could lead to the development of more accurate lightning detection and warning systems in the region.
- b) The updated assessment of global lightning climatology using different ground-based and space-based lightning detection equipment provides valuable insights into lightning patterns and behavior, which can be used to inform future research and safety measures.
- c) Finally, developing a model that can predict lightning events in the absence of real-time lightning data is an important step towards enhancing our understanding of lightning and improving safety measures.

Overall, the contribution to this lightning thesis is impressive and has the potential to advance our understanding of lightning and its impact on Earth's climatology.

6.4 Future Scope

The work in this thesis has improved the characterization of WWLLN DE significantly, but a concrete global estimate of WWLLN DE remains to be accomplished.

- a) To validate the LIS/WWLLN comparison, it is necessary to investigate the day/night dynamics and the effect of power/internet loss on the DE measurement with varying station count and trigger levels.

- b) Precise calibration of WWLLN VLF stations and a better understanding of daily ionospheric changes could improve estimates of radiated stroke energy and provide insight into the lightning mechanisms that produce elves/TGFs. Accurate WWLLN data can be used to predict lightning-produced energetic effects.
- c) The time series analysis of lightning phenomena presented in this thesis can be extended by investigating other regions over longer periods using ground-based regional networks.
- d) WWLLN's lightning observations offer an opportunity to explore fundamental lightning processes and build lightning parameterization techniques using machine learning. ML-based lightning schemes can improve the accuracy of lightning forecasts by incorporating more input variables and data from observations and weather models.
- e) Although the global electric circuit was not investigated in this research, improving the characterization of WWLLN is crucial for real-time studies of global lightning fluctuations and fair weather return current.

6.5 Summary

In the concluding chapter of my thesis, I have synthesized the main findings and arguments to provide a comprehensive summary of the research. This overview emphasizes the importance of the study, outlining its contributions to the existing body of knowledge and the validity of the results obtained. Furthermore, I have candidly addressed the limitations and challenges faced during the research process, demonstrating transparency and offering a balanced perspective on the study's outcomes.

Recognizing that research is an ongoing endeavor, I have also discussed potential directions for future investigations in this area. By identifying promising avenues for further exploration, I aim to inspire and guide other researchers who are interested in building upon the findings and insights presented in this thesis. This forward-looking perspective aims to foster continued progress and deepen our understanding of the subject matter, contributing to the advancement of the field.

LIST OF PUBLICATION

- [1] **M. H. Rafi** and M. G. Mostafa, "Global Lightning Phenomena and Time Series Model of Lightning Flash Radiance," *2022 International Conference on Energy and Power Engineering (ICEPE)*, Dhaka, Bangladesh, 2022, pp. 1-6, doi: 10.1109/ICEPE56629.2022.10044878.

- [2] **M. H. Rafi** and M. G. Mostafa, "Time Series Models for Radiated Electromagnetic Energy of Lightning Stroke Detected by World Wide Lightning Location Network," *Recent Advances in Wireless Communications & Emerging Technologies (RAWCET 2022)*, India.

Reference

- [1] C. J. Rodger *et al.*, “Detection efficiency of the VLF World-Wide Lightning Location Network (WWLLN): initial case study,” *Ann. Geophys.*, vol. 24, pp. 3197–3214, Dec. 2006, doi: 10.5194/angeo-24-3197-2006.
- [2] Abarca, Kristen L., “An evaluation of the Worldwide Lightning Location Network (WWLLN) using the National Lightning Detection Network (NLDN) as ground truth,” *J. Geophys. Res. Atmospheres*, vol. 115, no. D18, 2010, doi: 10.1029/2009JD013411.
- [3] D. Abreu, D. Chandan, R. H. Holzworth, and K. Strong, “A performance assessment of the World Wide Lightning Location Network (WWLLN) via comparison with the Canadian Lightning Detection Network (CLDN),” *Atmospheric Meas. Tech.*, vol. 3, no. 4, pp. 1143–1153, Aug. 2010, doi: 10.5194/amt-3-1143-2010.
- [4] K. S. Virts, J. M. Wallace, M. L. Hutchins, and R. H. Holzworth, “Highlights of a New Ground-Based, Hourly Global Lightning Climatology,” *Bull. Am. Meteorol. Soc.*, vol. 94, no. 9, pp. 1381–1391, Sep. 2013, doi: 10.1175/BAMS-D-12-00082.1.
- [5] Robert H. Holzworth and Michael L. Hutchins, “Far-Field Power of Lightning Strokes as Measured by the World Wide Lightning Location Network in: Journal of Atmospheric and Oceanic Technology Volume 29 Issue 8 (2012),” 2012. https://journals.ametsoc.org/view/journals/atot/29/8/jtech-d-11-00174_1.xml (accessed Aug. 23, 2022).
- [6] Y. Zhu *et al.*, “Evaluation of ENTLN Performance Characteristics Based on the Ground Truth Natural and Rocket-Triggered Lightning Data Acquired in Florida,” *J. Geophys. Res. Atmospheres*, vol. 122, no. 18, pp. 9858–9866, 2017, doi: 10.1002/2017JD027270.
- [7] D. J. Cecil, D. E. Buechler, and R. J. Blakeslee, “Gridded lightning climatology from TRMM-LIS and OTD: Dataset description,” *Atmospheric Res.*, vol. 135–136, pp. 404–414, Jan. 2014, doi: 10.1016/j.atmosres.2012.06.028.
- [8] S. W. Nesbitt, E. J. Zipser, and D. J. Cecil, “A Census of Precipitation Features in the Tropics Using TRMM: Radar, Ice Scattering, and Lightning Observations,” *J. Clim.*, vol. 13, no. 23, pp. 4087–4106, Dec. 2000, doi: 10.1175/1520-0442(2000)013<4087:ACOPFI>2.0.CO;2.
- [9] H. J. Christian *et al.*, “Global frequency and distribution of lightning as observed from space by the Optical Transient Detector,” *J. Geophys. Res. Atmospheres*, vol. 108, no. D1, p. ACL 4-1-ACL 4-15, 2003, doi: 10.1029/2002JD002347.

- [10] L. T. Murray, D. J. Jacob, J. A. Logan, R. C. Hudman, and W. J. Koshak, “Optimized regional and interannual variability of lightning in a global chemical transport model constrained by LIS/OTD satellite data,” *J. Geophys. Res. Atmospheres*, vol. 117, no. D20, 2012, doi: 10.1029/2012JD017934.
- [11] S. W. Nesbitt, R. Zhang, and R. E. Orville, “Seasonal and global NO_x production by lightning estimated from the Optical Transient Detector (OTD),” *Tellus B Chem. Phys. Meteorol.*, vol. 52, no. 5, pp. 1206–1215, Jan. 2000, doi: 10.3402/tellusb.v52i5.17098.
- [12] “Estimation of detection efficiency of the world wide lightning location network in the democratic republic of congo basin using lightning imaging sensor (LIS) as reference,” *Phys. Astron. Int. J.*, vol. Volume 2, no. Issue 2, Mar. 2018, doi: 10.15406/paij.2018.02.00071.
- [13] H. Fukunishi, Y. Takahashi, M. Kubota, K. Sakanoi, U. S. Inan, and W. A. Lyons, “Elves: Lightning-induced transient luminous events in the lower ionosphere,” *Geophys. Res. Lett.*, vol. 23, no. 16, pp. 2157–2160, 1996, doi: 10.1029/96GL01979.
- [14] X.-M. Shao, T. Hamlin, and D. M. Smith, “A closer examination of terrestrial gamma-ray flash-related lightning processes,” *J. Geophys. Res. Space Phys.*, vol. 115, no. A6, 2010, doi: 10.1029/2009JA014835.
- [15] C. J. Rodger, J. B. Brundell, and R. L. Dowden, “Location accuracy of VLF World-Wide Lightning Location (WWLL) network: Post-algorithm upgrade,” *Ann. Geophys.*, vol. 23, no. 2, pp. 277–290, Feb. 2005, doi: 10.5194/angeo-23-277-2005.
- [16] M. L. Hutchins, R. H. Holzworth, J. B. Brundell, and C. J. Rodger, “Relative detection efficiency of the World Wide Lightning Location Network,” *Radio Sci.*, vol. 47, no. 6, 2012, doi: 10.1029/2012RS005049.
- [17] R. H. Holzworth and M. P. McCarthy, “Global Distribution of Superbolts - Holzworth - 2019 - Journal of Geophysical Research: Atmospheres - Wiley Online Library.” <https://agupubs.onlinelibrary.wiley.com/doi/10.1029/2019JD030975> (accessed Aug. 20, 2022).
- [18] D. R. MacGorman, J. M. Straka, and C. L. Ziegler, “A Lightning Parameterization for Numerical Cloud Models,” *J. Appl. Meteorol. Climatol.*, vol. 40, no. 3, pp. 459–478, Mar. 2001, doi: 10.1175/1520-0450(2001)040<0459:ALPFNC>2.0.CO;2.
- [19] M. B. Baker and J. G. Dash, “Mechanism of charge transfer between colliding ice particles in thunderstorms,” *J. Geophys. Res. Atmospheres*, vol. 99, no. D5, pp. 10621–10626, 1994, doi: 10.1029/93JD01633.

- [20] H. Asakawa, G. Sazaki, K. Nagashima, S. Nakatsubo, and Y. Furukawa, “Two types of quasi-liquid layers on ice crystals are formed kinetically,” *Proc. Natl. Acad. Sci.*, vol. 113, no. 7, pp. 1749–1753, Feb. 2016, doi: 10.1073/pnas.1521607113.
- [21] Y. He, B. Gu, D. Zhang, W. Lu, C. W. Yu, and Z. Gu, “Towards the Understanding of Ice Crystal-graupel Collision Charging in Thunderstorm Electrification.” Preprints, Nov. 13, 2018. doi: 10.20944/preprints201811.0320.v1.
- [22] E. Lay, “Investigating lightning-to-ionosphere energy coupling based on VLF lightning propagation characterization,” Jan. 2008.
- [23] V. A. Rakov and M. A. Uman, *Lightning: Physics and Effects*. Cambridge University Press, 2003.
- [24] Martin A. Uman., “Lightning: The Lightning Discharge. Academic Press, San Diego, CA, 1987. xii, 377 pp., illus. \$49. International Geophysics Series, vol. 39. | Science.” <https://www.science.org/doi/10.1126/science.242.4886.1713> (accessed Mar. 15, 2023).
- [25] X. M. Shao and P. R. Krehbiel, “The spatial and temporal development of intracloud lightning,” *J. Geophys. Res. Atmospheres*, vol. 101, no. D21, pp. 26641–26668, 1996, doi: 10.1029/96JD01803.
- [26] V. P. Pasko, “Recent advances in theory of transient luminous events,” *J. Geophys. Res. Space Phys.*, vol. 115, no. A6, 2010, doi: 10.1029/2009JA014860.
- [27] J. L. Chern *et al.*, “Global survey of upper atmospheric transient luminous events on the ROCSAT-2 satellite,” *J. Atmospheric Sol.-Terr. Phys.*, vol. 65, no. 5, pp. 647–659, Mar. 2003, doi: 10.1016/S1364-6826(02)00317-6.
- [28] D. D. Sentman, E. M. Wescott, D. L. Osborne, D. L. Hampton, M. J. Heavner, “Preliminary results from the Sprites94 Aircraft Campaign: 1. Red sprites - Sentman - 1995 - Geophysical Research Letters - Wiley Online Library.” <https://agupubs.onlinelibrary.wiley.com/doi/abs/10.1029/95GL00583> (accessed Dec. 13, 2022).
- [29] M. J. Taylor *et al.*, “Rare measurements of a sprite with halo event driven by a negative lightning discharge over Argentina,” *Geophys. Res. Lett.*, vol. 35, no. 14, 2008, doi: 10.1029/2008GL033984.
- [30] E. M. Wescott, D. Sentman, D. Osborne, D. Hampton, and M. Heavner, “Preliminary results from the Sprites94 Aircraft Campaign: 2. Blue jets,” *Geophys. Res. Lett.*, vol. 22, no. 10, pp. 1209–1212, 1995, doi: 10.1029/95GL00582.

- [31] G. J. Fishman, P. N. Bhat, R. Mallozzi, J. M. Horack, T. Koshut, C. Kouveliotou, G. N. Pendleton, C. A. Meegan, R. B. Wilson, “Discovery of Intense Gamma-Ray Flashes of Atmospheric Origin | Science.” <https://www.science.org/doi/abs/10.1126/science.264.5163.1313> (accessed Dec. 13, 2022).
- [32] N. Demetriades, M. Murphy, and J. A. Cramer, “Validation of Vaisala’s Global Lightning Dataset (GLD360) over the continental United States,” Jan. 2010.
- [33] R. Said and M. Murphy, “GLD 360 Upgrade: Performance Analysis and Applications,” 2016. Accessed: Jan. 15, 2023. [Online]. Available: <https://www.semanticscholar.org/paper/GLD-360-Upgrade-%3A-Performance-Analysis-and-Said-Murphy/1ea3732f5db17e3392f9dfff122ea4605fd3b54d>
- [34] M. B. Cohen, U. S. Inan, and E. W. Paschal, “Sensitive Broadband ELF/VLF Radio Reception With the AWESOME Instrument,” *IEEE Trans. Geosci. Remote Sens.*, vol. 48, no. 1, pp. 3–17, Jan. 2010, doi: 10.1109/TGRS.2009.2028334.
- [35] R. K. Said, U. S. Inan, and K. L. Cummins, “Long-range lightning geolocation using a VLF radio atmospheric waveform bank,” *J. Geophys. Res. Atmospheres*, vol. 115, no. D23, 2010, doi: 10.1029/2010JD013863.
- [36] V. Bui, L.-C. Chang, and S. Heckman, “A Performance Study of Earth Networks Total Lightning Network (ENTLN) and Worldwide Lightning Location Network (WWLLN),” in *2015 International Conference on Computational Science and Computational Intelligence (CSCI)*, Dec. 2015, pp. 386–391. doi: 10.1109/CSCI.2015.120.
- [37] Stan Heckman and C. Liu, “The application of total lightning detection and cell tracking for severe weather prediction | Request PDF,” 10 2011. https://www.researchgate.net/publication/262187111_The_application_of_total_lightning_detection_and_cell_tracking_for_severe_weather_prediction (accessed Dec. 15, 2022).
- [38] S. Mallick *et al.*, “Performance characteristics of the ENTLN evaluated using rocket-triggered lightning data,” *Electr. Power Syst. Res.*, vol. 118, pp. 15–28, Jan. 2015, doi: 10.1016/j.epsr.2014.06.007.
- [39] M. Marchand, K. Hilburn, and S. D. Miller, “Geostationary Lightning Mapper and Earth Networks Lightning Detection Over the Contiguous United States and Dependence on Flash Characteristics,” *J. Geophys. Res. Atmospheres*, vol. 124, no. 21, pp. 11552–11567, 2019, doi: 10.1029/2019JD031039.

- [40] R. L. Dowden, J. B. Brundell, and C. J. Rodger, “VLF lightning location by time of group arrival (TOGA) at multiple sites,” *J. Atmospheric Sol.-Terr. Phys.*, vol. 64, no. 7, pp. 817–830, May 2002, doi: 10.1016/S1364-6826(02)00085-8.
- [41] Martin Füllekrug and Steven Constable, “Global triangulation of intense lightning discharges - Füllekrug - 2000 - Geophysical Research Letters - Wiley Online Library.” <https://agupubs.onlinelibrary.wiley.com/doi/abs/10.1029/1999GL003684> (accessed Dec. 06, 2022).
- [42] D. Crombie, “Periodic fading of VLF signals received over long paths during sunrise and sunset.,” Published 1964, doi: DOI:10.6028/JRES.068D.012.
- [43] C. Kummerow, W. Barnes, T. Kozu, J. Shiue, and J. Simpson, “The Tropical Rainfall Measuring Mission (TRMM) Sensor Package,” *J. Atmospheric Ocean. Technol.*, vol. 15, no. 3, pp. 809–817, Jun. 1998, doi: 10.1175/1520-0426(1998)015<0809:TTRMMT>2.0.CO;2.
- [44] R. J. Blakeslee *et al.*, “Three Years of the Lightning Imaging Sensor Onboard the International Space Station: Expanded Global Coverage and Enhanced Applications,” *J. Geophys. Res. Atmospheres*, vol. 125, no. 16, p. e2020JD032918, 2020, doi: 10.1029/2020JD032918.
- [45] P. Jenniskens *et al.*, “Detection of meteoroid impacts by the Geostationary Lightning Mapper on the GOES-16 satellite,” *Meteorit. Planet. Sci.*, vol. 53, no. 12, pp. 2445–2469, 2018, doi: 10.1111/maps.13137.
- [46] D. Cao, F. Lu, X. Zhang, and J. Yang, “Lightning Activity Observed by the FengYun-4A Lightning Mapping Imager,” *Remote Sens.*, vol. 13, no. 15, Art. no. 15, Jan. 2021, doi: 10.3390/rs13153013.
- [47] Themistoklis Chronis and William J. Koshak, “Diurnal Variation of TRMM/LIS Lightning Flash Radiances in: Bulletin of the American Meteorological Society Volume 98 Issue 7 (2017),” Jul. 01, 2017. <https://journals.ametsoc.org/view/journals/bams/98/7/bams-d-16-0041.1.xml> (accessed Sep. 09, 2022).
- [48] D. Boccippio *et al.*, “The Optical Transient Detector (OTD): Instrument Characteristics and Cross-Sensor Validation,” *J. Atmospheric Ocean. Technol. - J ATMOS OCEAN TECHNOL*, vol. 17, pp. 441–458, Apr. 2000, doi: 10.1175/1520-0426(2000)017<0441:TOTDOI>2.0.CO;2.

- [49] Blakeslee, R., “Optical Transient Detector (OTD) Lightning.” NASA Global Hydrometeorology Resource Center DAAC, 1996. doi: 10.5067/LIS/OTD/DATA101.
- [50] P. Krehbiel, T. Hamlin, Y. Zhang, J. Harlin, R. Thomas, and W. Rison, “Three-dimensional total lightning observations with the lightning mapping array,” presented at the Preprints. Int. Lightning Detection Conf, 2002, pp. 16–18.
- [51] L. Maier, C. Lennon, T. Britt, and S. Schaefer, “LDAR system performance and analysis,” presented at the Proceedings of the International Conference on Cloud Physics, Am. Meteorol. Soc. Boston, Mass., Dallas, Tex., 1995.
- [52] W. Rison, R. J. Thomas, P. R. Krehbiel, T. Hamlin, and J. Harlin, “A GPS-based three-dimensional lightning mapping system: Initial observations in central New Mexico,” *Geophys. Res. Lett.*, vol. 26, no. 23, pp. 3573–3576, 1999.
- [53] R. J. Thomas *et al.*, “Comparison of ground-based 3-dimensional lightning mapping observations with satellite-based LIS observations in Oklahoma,” *Geophys. Res. Lett.*, vol. 27, no. 12, pp. 1703–1706, 2000, doi: 10.1029/1999GL010845.
- [54] D. Mach, H. Christian, R. Blakeslee, D. Boccippio, S. Goodman, and W. Boeck, “Performance assessment of the Optical Transient Detector and Lightning Imaging Sensor,” *J. Geophys. Res. Atmospheres*, vol. 112, p. 9210, May 2007, doi: 10.1029/2006JD007787.
- [55] R. E. Bürgesser, “Assessment of the World Wide Lightning Location Network (WWLLN) detection efficiency by comparison to the Lightning Imaging Sensor (LIS),” *Q. J. R. Meteorol. Soc.*, vol. 143, no. 708, pp. 2809–2817, 2017, doi: 10.1002/qj.3129.
- [56] Jed O. Kaplan and Katie Hong-Kiu Lau, “The WGLC global gridded lightning climatology and time series, 2022 update,” Jun. 21, 2022. <https://essd.copernicus.org/preprints/essd-2022-88/> (accessed Sep. 16, 2022).
- [57] C. Bovalo, C. Barthe, and N. Bègue, “A lightning climatology of the South-West Indian Ocean,” *Nat. Hazards Earth Syst. Sci.*, vol. 12, no. 8, pp. 2659–2670, Aug. 2012, doi: 10.5194/nhess-12-2659-2012.
- [58] I. Kolmašová, O. Santolík, and K. Rosická, “Lightning activity in northern Europe during a stormy winter: disruptions of weather patterns originating in global climate phenomena,” *Atmospheric Chem. Phys.*, vol. 22, no. 5, pp. 3379–3389, Mar. 2022, doi: 10.5194/acp-22-3379-2022.

- [59] K. Kikuchi and B. Wang, “Diurnal Precipitation Regimes in the Global Tropics,” *J. Clim. - J Clim.*, vol. 21, pp. 2680–2696, Jun. 2008, doi: 10.1175/2007JCLI2051.1.
- [60] B. Kucieńska, G. B. Raga, and O. Rodríguez, “Cloud-to-ground lightning over Mexico and adjacent oceanic regions: a preliminary climatology using the WWLLN dataset,” *Ann. Geophys.*, vol. 28, no. 11, pp. 2047–2057, Nov. 2010, doi: 10.5194/angeo-28-2047-2010.
- [61] Michael P and Douglas M, “A Global LIS/OTD Climatology of Lightning Flash Extent Density - Peterson - 2021 - Journal of Geophysical Research: Atmospheres - Wiley Online Library,” Mar. 17, 2021. <https://agupubs.onlinelibrary.wiley.com/doi/full/10.1029/2020JD033885> (accessed Jan. 27, 2022).
- [62] S. Soula, J. K. Kasereka, J. F. Georgis, and C. Barthe, “Lightning climatology in the Congo Basin,” *Atmospheric Res.*, vol. 178–179, pp. 304–319, Sep. 2016, doi: 10.1016/j.atmosres.2016.04.006.
- [63] A. Dewan, M. F. Hossain, M. M. Rahman, Y. Yamane, and R. L. Holle, “Recent Lightning-Related Fatalities and Injuries in Bangladesh,” *Weather Clim. Soc.*, vol. 9, no. 3, pp. 575–589, Jul. 2017, doi: 10.1175/WCAS-D-16-0128.1.
- [64] Chandima Gomes, Firoza Hussain, M Ahmed, and K R Abeysinghe, “Lightning accidents and awareness in South Asia: Experience in Sri Lanka and Bangladesh,” Sep. 28, 2006.
- [65] N. Umakanth, G. Ch. Satyanarayana, B. Simon, M. C. Rao, and N. R. Babu, “Analysis of lightning flashes over Bangladesh,” *AIP Conf. Proc.*, vol. 2220, no. 1, p. 140041, May 2020, doi: 10.1063/5.0001294.
- [66] Ashraf Dewan, Emmanuel T, M. Rafiuddin, and Md. Masudur Rahman, “Lightning activity associated with precipitation and CAPE over Bangladesh - Dewan - 2018 - International Journal of Climatology - Wiley Online Library,” Sep. 27, 2017. <https://rmets.onlinelibrary.wiley.com/doi/abs/10.1002/joc.5286> (accessed Jan. 04, 2023).
- [67] A. Dewan, E. T. Ongee, Md. M. Rahman, R. Mahmood, and Y. Yamane, “Spatial and temporal analysis of a 17-year lightning climatology over Bangladesh with LIS data,” *Theor. Appl. Climatol.*, vol. 134, no. 1, pp. 347–362, Oct. 2018, doi: 10.1007/s00704-017-2278-3.

- [68] S. Uddin and R. Suravi, *THE RISE OF A NEW DISASTER IN BANGLADESH: ANALYSIS OF CHARACTERISTICS AND VULNERABILITIES OF LIGHTNING DURING MARCH TO SEPTEMBER 2018*. 2019.
- [69] S. Rudlosky and D. Shea, “Evaluating WWLLN performance relative to TRMM/LIS,” *Geophys. Res. Lett.*, vol. 40, pp. 2344–2348, May 2013, doi: 10.1002/grl.50428.
- [70] Michael L. Hutchins, Robert H. Holzworth, and Rodger, “WWLLN Absolute Detection Efficiencies and the Global Lightning Source Function,” *Eur. Geophys. Union*, 2012.
- [71] C. J. Rodger *et al.*, “Growing Detection Efficiency of the World Wide Lightning Location Network,” in *AIP Conference Proceedings*, Corte (France): AIP, 2009, pp. 15–20. doi: 10.1063/1.3137706.
- [72] K. B. Thompson, M. G. Bateman, and L. D. Carey, “A Comparison of Two Ground-Based Lightning Detection Networks against the Satellite-Based Lightning Imaging Sensor (LIS),” *J. Atmospheric Ocean. Technol.*, vol. 31, no. 10, pp. 2191–2205, Oct. 2014, doi: 10.1175/JTECH-D-13-00186.1.
- [73] M. L. Hutchins and R. H. Holzworth, “Radiated VLF energy differences of land and oceanic lightning - Hutchins - 2013 - Geophysical Research Letters - Wiley Online Library.” <https://agupubs.onlinelibrary.wiley.com/doi/full/10.1002/grl.50406> (accessed Dec. 07, 2022).
- [74] Eugene W. McCaul Jr., Steven J. Goodman, Daniel J. Cecil, and Katherine M. LaCasse, “Forecasting Lightning Threat Using Cloud-Resolving Model Simulations in: Weather and Forecasting Volume 24 Issue 3 (2009).” https://journals.ametsoc.org/view/journals/wefo/24/3/2008waf2222152_1.xml?tab_body=fulltext-display (accessed Dec. 23, 2022).
- [75] Yoav Yair, Barry Lynn, and Colin Price, “Predicting the potential for lightning activity in Mediterranean storms based on the Weather Research and Forecasting (WRF) model dynamic and microphysical fields - Yair - 2010 - Journal of Geophysical Research: Atmospheres - Wiley Online Library.” <https://agupubs.onlinelibrary.wiley.com/doi/full/10.1029/2008JD010868> (accessed Dec. 23, 2022).
- [76] B. Lynn and Y. Yair, “Prediction of lightning flash density with the WRF model,” in *Advances in Geosciences*, Copernicus GmbH, Feb. 2010, pp. 11–16. doi: 10.5194/adgeo-23-11-2010.

- [77] M. Gharaylou, M. M. Farahani, A. Mahmoudian, and M. Hosseini, “Prediction of lightning activity using WRF-ELEC model: Impact of initial and boundary conditions,” *J. Atmospheric Sol.-Terr. Phys.*, vol. 210, p. 105438, Nov. 2020, doi: 10.1016/j.jastp.2020.105438.
- [78] Philippe Lopez, “A Lightning Parameterization for the ECMWF Integrated Forecasting System in: Monthly Weather Review Volume 144 Issue 9 (2016).” [https://journals.ametsoc.org/configurable/content/journals\\$002fmwre\\$002f144\\$002f9\\$002fmwr-d-16-0026.1.xml?t:ac=journals%24002fmwre%24002f144%24002f9%24002fmwr-d-16-0026.1.xml](https://journals.ametsoc.org/configurable/content/journals$002fmwre$002f144$002f9$002fmwr-d-16-0026.1.xml?t:ac=journals%24002fmwre%24002f144%24002f9%24002fmwr-d-16-0026.1.xml) (accessed Dec. 23, 2022).
- [79] E. H. Lay, A. R. Jacobson, R. H. Holzworth, C. J. Rodger, and R. L. Dowden, “Local time variation in land/ocean lightning flash density as measured by the World Wide Lightning Location Network,” *J. Geophys. Res. Atmospheres*, vol. 112, no. D13, 2007, doi: 10.1029/2006JD007944.
- [80] S. D. Rudlosky and H. E. Fuelberg, “Pre-and postupgrade distributions of NLDN reported cloud-to-ground lightning characteristics in the contiguous United States,” *Mon. Weather Rev.*, vol. 138, no. 9, pp. 3623–3633, 2010.
- [81] R. Albrecht *et al.*, “The 13 years of TRMM Lightning Imaging Sensor: From individual flash characteristics to decadal tendencies,” presented at the XIV ICAE: International Conference on Atmospheric Electricity, 2011.
- [82] A. Dewan *et al.*, “Spatial pattern and land surface features associated with cloud-to-ground lightning in Bangladesh: an exploratory study,” *Earth Syst. Environ.*, vol. 6, no. 2, pp. 437–451, 2022.
- [83] E. H. Lay, R. H. Holzworth, C. J. Rodger, J. N. Thomas, O. Pinto Jr, and R. L. Dowden, “WWLL global lightning detection system: Regional validation study in Brazil,” *Geophys. Res. Lett.*, vol. 31, no. 3, 2004.
- [84] C. Rodger, J. Brundell, R. Dowden, and N. Thomson, “Location accuracy of long distance VLF lightning locationnetwork,” presented at the Annales Geophysicae, Copernicus Publications Göttingen, Germany, 2004, pp. 747–758.
- [85] A. R. Jacobson, R. Holzworth, J. Harlin, R. Dowden, and E. Lay, “Performance Assessment of the World Wide Lightning Location Network (WWLLN), Using the Los Alamos Sferic Array (LASA) as Ground Truth,” *J. Atmospheric Ocean. Technol.*, vol. 23, no. 8, pp. 1082–1092, Aug. 2006, doi: 10.1175/JTECH1902.1.

- [86] B. N. Turman, "Detection of lightning superbolts," *J. Geophys. Res.* 1896-1977, vol. 82, no. 18, pp. 2566–2568, 1977, doi: 10.1029/JC082i018p02566.
- [87] Marcia B. Baker, John Latham, and Hugh J. Christian, "A computational study of the relationships linking lightning frequency and other thundercloud parameters - Baker - 1995 - Quarterly Journal of the Royal Meteorological Society - Wiley Online Library." <https://rmets.onlinelibrary.wiley.com/doi/abs/10.1002/qj.49712152703> (accessed Dec. 22, 2022).
- [88] S. J. Goodman, "Predicting thunderstorm evolution using ground-based lightning detection networks," *NAS* 1.15:103521, Nov. 1990. Accessed: Dec. 22, 2022. [Online]. Available: <https://ntrs.nasa.gov/citations/19910006347>
- [89] N. Reeve and R. Toumi, "Lightning activity as an indicator of climate change," *Q. J. R. Meteorol. Soc.*, vol. 125, no. 555, pp. 893–903, 1999, doi: 10.1002/qj.49712555507.
- [90] K. Dixon, C. F. Mass, G. J. Hakim, and R. H. Holzworth, "The impact of lightning data assimilation on deterministic and ensemble forecasts of convective events," *J. Atmospheric Ocean. Technol.*, vol. 33, no. 9, pp. 1801–1823, 2016.
- [91] D. Smith *et al.*, "The Los Alamos Sferic Array: A research tool for lightning investigations," *J. Geophys. Res. Atmospheres*, vol. 107, no. D13, p. ACL-5, 2002.
- [92] George E. P. Box, G. M. Jenkins, and Gregory C. Reinsel, *Time Series Analysis: Forecasting and Control.*, Fourth Edition. A John Wiley & Sons, Inc., Publication, 2008. [Online]. Available: <https://doi.org/10.1002/9781118619193>
- [93] R. Mushtaq, "Augmented Dickey Fuller Test." Rochester, NY, Aug. 17, 2011. doi: 10.2139/ssrn.1911068.
- [94] Peter J. Brockwell, and Richard A. Davis, *Time Series: Theory and Methods*, Second Edition. Publisher: Springer-Verlag New York, 1991. [Online]. Available: <http://library.lol/main/6558FDD17CD37F9101A94C72AE65C90F>
- [95] S. I. Vrieze, "Model selection and psychological theory: A discussion of the differences between the Akaike information criterion (AIC) and the Bayesian information criterion (BIC)," *Psychol. Methods*, vol. 17, pp. 228–243, 2012, doi: 10.1037/a0027127.